SSD

SCIENCE FOR A SUSTAINABLE DEVELOPMENT

CONSTRAINING LONG-TERM CLIMATE AND SEA-LEVEL PROJECTIONS USING THE LAST INTERGLACIAL

«ICLIPS»

P. HUYBRECHTS, H. GOELZER, M.-F. LOUTRE, T. FICHEFET

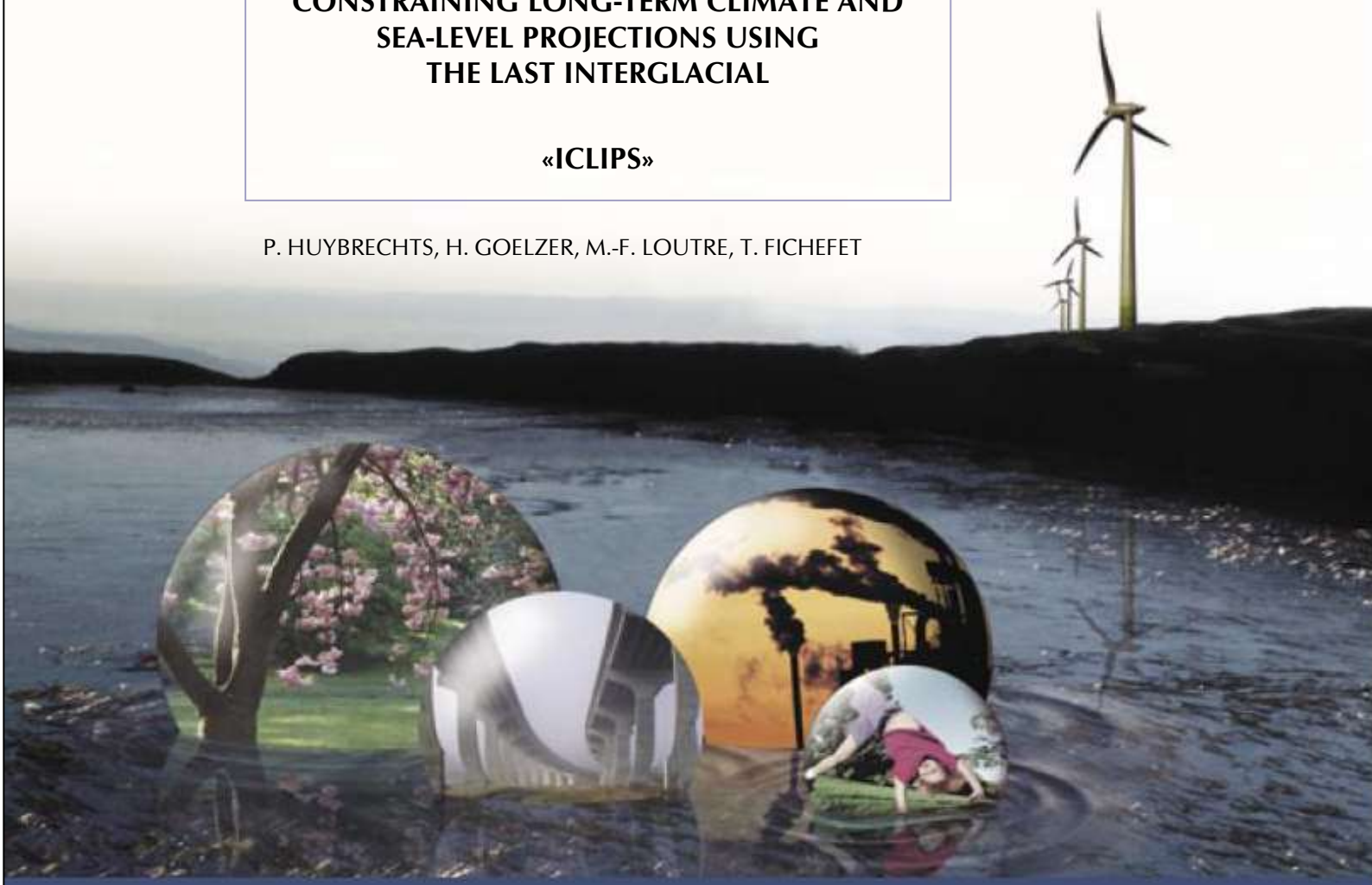

ENERGY

TRANSPORT AND MOBILITY

AGRO-FOOD

HEALTH AND ENVIRONMENT

CLIMATE

BIODIVERSITY

ATMOSPHERE AND TERRESTRIAL AND MARINE ECOSYSTEMS

TRANSVERSAL ACTIONS

.be

SCIENCE FOR A SUSTAINABLE DEVELOPMENT
(SSD)

Climate

FINAL REPORT

CONSTRAINING LONG-TERM CLIMATE AND SEA-LEVEL PROJECTIONS USING THE LAST INTERGLACIAL «ICLIPS»

SD/CS/06A

Promoters

Philippe Huybrechts
Vrije Universiteit Brussel
Earth System Sciences & Departement Geografie (VUB-ESSC)
Pleinlaan, 2
B-1050 Brussels

Thierry Fichefet
Université Catholique de Louvain,
Earth and Life Institute,
Georges Lemaître Centre for Earth and Climate Research (UCL-TECLIM)
Chemin du Cyclotron, 2
B-1348 Louvain-la-Neuve

Authors

P. Huybrechts, H. Goelzer
(VUB-ESSC)
M.-F. Loutre, T. Fichefet
(UCL-TECLIM)

Vrije Universiteit Brussel

UCL Université catholique de Louvain

EARTH & LIFE INSTITUTE

Published in 2017 by the Belgian Science Policy
Avenue Louise 231
Louizalaan 231
B-1050 Brussels
Belgium
Tel: +32 (0)2 238 34 11 – Fax: +32 (0)2 230 59 12
http://www.belspo.be

Contact person: Martine Vanderstraeten
+32 (0)2 238 3610

Huybrechts, P., H. Goelzer, M.-F. Loutre, T. Fichefet - ***Constraining long-term climate and sea-level projections using the Last Interglacial «iCLIPS» (SD/CS/06A)***. Brussels: Belgian Science Policy 2017 – 111 p. (Research Programme Science for a Sustainable Development: Final Report)

TABLE OF CONTENT

SUMMARY

A. Context

Uncertainties in future climate and sea-level projections are of major concern for policy makers, facing the need for concrete decisions on mitigation and adaptation strategies. Aside from the inherent uncertainties of future anthropogenic emissions of greenhouse gases and aerosols, the wide range of possible scenarios of long-term climate and sea-level evolution arises from uncertainties in the modelling of key processes in the Earth system. iCLIPS intended to constrain these uncertainties by using information from the Last Interglacial (130-115 kyr BP), a period warmer than today which is probably the best analogue for future climate change for which increasingly better proxy data have become available.

B. Objectives

The overall objective of iCLIPS was to improve projections of climate and sea-level changes over the current century and this millennium, to identify the likelihood of abrupt changes, and to better understand their causes and mechanisms. The focus lied on the evolution of the two polar regions, the North Atlantic and Europe. We used LOVECLIM, a global three-dimensional Earth System model of intermediate complexity. The computational efficiency of this model was exploited for a large number of transient experiments over the Last Interglacial using several parameter sets. The model was run with fixed-prescribed ice sheets or with an interactively coupled Greenland and Antarctic ice sheet model. Informed by these palaeoclimatic simulations, the best performing parameter sets were used in experiments driven by the four IPCC Representative Concentration Pathway (RCP) scenarios, extended over the third millennium.

C. Conclusions

The major outcome of iCLIPS was an improved version of LOVECLIM yielding an improved range of future long-term climate and sea-level change projections with reduced parameter uncertainty.
Modifications to the atmospheric and oceanic models were made addressing oceanic heat uptake, the polar amplification, cloud feedbacks, and katabatic winds over Antarctica. The ice sheet models were upgraded with new geometric boundary conditions, new treatments for fast physics of outlet glaciers and Antarctic grounding-

line dynamics, and better interfaces between the ocean and floating ice shelves, and between the atmosphere and the ice sheet surface.

The climate simulations carried out over the Last Interglacial provided useful information to help answering some of the key questions regarding the evolution of the climate system during that warm interglacial period. The meltwater fluxes from the retreating Northern Hemisphere ice sheet were found to play a key role at the onset of the Last Interglacial in the strength of the North Atlantic Ocean meridional circulation and the evolution of the surface temperature of both hemispheres. Changes in the configuration (extent and albedo) of the Northern Hemisphere ice sheets however impacted only slightly on the simulated climate. By means of the interhemispheric see-saw effect, variations in the Atlantic meridional overturning circulation also gave rise to temperature changes in the Southern Hemisphere, which were additionally modulated by the direct impact of Antarctic meltwater fluxes into the Southern Ocean. Freshwater fluxes from the melting Antarctic ice sheet led to a millennial timescale oceanic cold event in the Southern Ocean with expanded sea ice as evidenced in some ocean sediment cores. The mechanism involving surface freshening, increased stratification, and sea ice cover and consequently reduced ocean heat loss to the atmosphere, with temporary heat build-up in the mid-depth ocean, could well be relevant for future warmer climates. The importance of additional freshwater input from the Greenland ice sheet was found to be small compared to the much larger fluxes from the other Northern Hemisphere ice sheets and became more important only later during the Last Interglacial, when it became the only remaining ice sheet contributing freshwater fluxes to the North Atlantic.

The project also yielded the first coupled transient simulation of the entire Last Interglacial period with interactive Greenland and Antarctic ice sheet components. We found both ice sheets to contribute to the sea-level high stand during the Last Interglacial, but subject to different forcing and response mechanisms. Surface mass balance change governed by changes in surface meltwater runoff was the dominant forcing for the Greenland ice sheet, which showed a peak sea-level contribution of 1.4 m at 123 kyr BP. Southern Hemisphere polar and sub-polar ocean warming was limited throughout the Last Interglacial and surface and sub-shelf melting exerted only a minor control on the Antarctic sea-level contribution with a peak of 4.4 m at 125 kyr BP. Retreat of the Antarctic ice sheet at the onset of the Last Interglacial was mainly forced by rising sea-level and to a lesser extent by reduced ice shelf viscosity as the surface temperature increased. Global sea level showed a peak of 5.3 m at 124.5 kyr BP, which included a minor contribution of 0.35 m from oceanic thermal expansion. Taken together, the modelled global sea-level evolution was consistent with reconstructions of the sea-level high stand during the Last Interglacial using the optimal parameter set.

Neither the individual contributions nor the total modelled sea-level stand showed fast multi-millennial time scale variations as indicated by some reconstructions.
The new version of LOVECLIM, with four parameter sets validated in the context of Last Interglacial simulations, was then used to perform simulations over the third millennium. For these projections, IPCC AR5 scenarios (RCP2.6, RCP4.5, RCP 6.0 and RCP8.5) were used until 2100 AD. Extended Concentration Pathways (ECPs) were used until 2300 AD, with greenhouse gas concentrations held constraint at their 2300 AD values until 3000 AD. According to these simulations, the global mean temperature increased by 0.5°C to 5.2°C after 1000 years for all scenarios and all parameter sets. All the simulations showed an initial reduction in the intensity of the thermohaline circulation, which recovered almost completely after 2200 AD. Equally all simulations experienced a reduction in the summer sea ice of the Arctic, but with complete melting by 2200 AD only in the highest RCP8.5 scenario. The polar amplification was found to be between 1.7 and 3.9 in both polar regions, partly compensating for the somewhat lower global climate sensitivity of between 2.0°C and 3.6°C to give reasonable climate scenarios over the polar ice sheets. The maximum warming was found to be 12.0°C and 14.2°C for all scenarios and all four parameter sets over the Greenland and Antarctic ice sheets, respectively.
The future sea-level response has contributions from mountain glaciers and small ice caps, the Greenland ice sheet, the Antarctic ice sheet, and oceanic thermal expansion. The Greenland ice sheet was found to lose up to 80% of its mass in the highest scenario with the most sensitive parameter set, corresponding to a sea level contribution of 5.8 m after 1000 years of climate warming. Almost all of the melting occurs by surface ablation, whereas iceberg calving quickly decreases as the ice sheet recedes from the coast. None of the scenarios predicts a complete melting of the Greenland ice sheet before 3000 AD. For Antarctica, volume changes varied between slight growth for RCP2.6 and a volume loss corresponding to an 8 m sea level rise for RCP8.5 and the most sensitive parameter set. On the millennial time scale, changes in the Antarctic ice sheet are mainly driven by changes in accumulation and ice shelf melt, with a significant contribution from marginal ablation for the experiments producing the largest warming. For all scenarios and all parameter sets, virtually all of the ice contained in mountain glaciers and small ice caps has disappeared after 1000 years of climatic warming. For the same range of experiments, sea level rise from oceanic thermal expansion was found to vary between 0.1 and 3.2 m. We conclude from these experiments that a global eustatic sea level rise of at least 1.2 m is very likely to occur before the end of the third millennium, and that it may be as high as 15 m for RCP8.6 considering the most sensitive parameter set.

D. Contribution of the project in a context of scientific support to a sustainable development policy

The work made under iCLIPS is a contribution to the ongoing international scientific effort to better understand climate change and to quantify more accurately the uncertainties related with climate and sea level projections. This is needed in order to provide a sound basis for policies designed to address the challenge of climate change. Identifying and reducing the uncertainties is deeply in line with the recommendation of the scientific community.

E. Keywords

Sea level, ice sheets, ocean circulation, polar regions, Last Interglacial, future climate change.

1. INTRODUCTION

Future climate change is a major global concern due to necessary mitigation and adaptation strategies that urgently have to be decided upon by policy makers. Aside from uncertainties in future anthropogenic emissions of greenhouse gases (GHGs) and aerosols, the wide range of possible scenarios of long-term climate evolution arises from large uncertainties in the modelling of key processes in the Earth system.

The ocean circulation plays an important role in supplying heat from the equatorial region to the polar regions and regulates e.g. the amount of sea ice in these regions. Changes in the ocean circulation, which could be related to melting of ice sheets, changes in ocean temperature or modifications in the hydrological cycle, have significant impacts on the Earth's energy budget and consequently on the global and regional climate. There is a large uncertainty on the probability and intensity of such changes in the future.

Current methods for sea-level projections, including those of the UN Intergovernmental Panel on Climate Change (IPCC) Fifth Assessment Report (AR5), can give no firm constraints on the ice-dynamical contribution of the polar ice sheets to future ice loss, which contribution dominates the uncertainty of the projections. Especially the upper bound of possible future sea-level rise is not well constrained, with vast planning and financial implications for coastal protection and adaptation. This also includes uncertainties about the expected rate of change, which is of crucial importance for the timing of planning coastal defences.

It is therefore of great importance to limit uncertainties and better understand the processes and mechanisms of changes in the climate system and the ice sheet response for the 21st century and beyond.

The Last Interglacial (LIG) is probably the best (although not perfect) analogue for future climate change for which increasingly better proxy data have become available. The LIG is the most recent warm period before the current interglacial when global mean annual surface temperature was up to 2°C higher than today (e.g. Capron et al., 2014). Due to polar amplification, high-latitude surface temperatures were up to 5°C higher over the ice sheets (EPICA community members, 2004; NEEM community members, 2013). At the same time, global sea-level was at least 5.5 m higher than today, with some studies giving numbers up to 9 m above present (Kopp et al., 2009; Masson-Delmotte et al., 2013).

Here we report on transient model simulations of the LIG period. The objective to perform such simulations is twofold. On the one hand, the model results can be compared with proxy data for that period to better constrain model parameter sets in warmer climates relevant for long-term future projections. On the other hand, process studies of the LIG period can help to better understand the key physical mechanisms in

the Earth system, in particular those that have the potential to produce large amplitude oscillations, instabilities and abrupt changes.

We utilize the fully coupled Earth system model of intermediate complexity LOVECLIM v1.3, a further development of v.2 described in Goosse et al. (2010). LOVECLIM is an ideal tool for this study, since it incorporates all important components and ice-climate interactions necessary to simulate climate and sea-level changes on centennial to millennial time scales. Moreover, compared to coupled general circulation models (CGCMs), LOVECLIM has the advantage of greatly reduced computer requirements, so that much longer simulations can be conducted. LOVECLIM is therefore invaluable to explore uncertainties in long-term climate and sea level change projections. First, some components of the model are improved. Then an evaluation of model performance is made in sensitivity tests to doubling the atmospheric CO_2 concentration and freshwater hosing in the North Atlantic. Subsequent experiments with the improved version of LOVECLIM employ several parameter sets. We study the climate simulated over the Last Interglacial, using a version with fully interactively coupled ice sheets. Such simulations validate the parameter sets in LOVECLIM regarding climate variability, likely rates of long-term climate and sea-level changes, bipolar interactions, and the possible existence of thresholds and irreversible behaviour in the climate system, with applications to the future. Finally, based on the best performing parameter sets, climate projections over the third millennium are made using four extended RCP scenarios.

2. METHODOLOGY AND RESULTS

2.1. MODEL DESCRIPTION

LOVECLIM consists of four major components representing the atmosphere (ECBilt), the ocean and sea ice (CLIO), the terrestrial biosphere (VECODE) and the Greenland and Antarctic ice sheets (AGISM). For a full list of references on climate change studies carried out with the model please refer to:
http://www.elic.ucl.ac.be/modx/elic/index.php?id=288

2.1.1. ECBilt

ECBilt is a three-dimensional, spectral, quasi-geostrophic model of the atmosphere developed at the Koninklijk Nederlands Meteorologisch Instituut, De Bilt (Opsteegh et al., 1998). It has a T21 horizontal resolution and 3 levels located at 800, 500 and 200 hPa. The model includes an explicit representation of the hydrological cycle and a dynamically passive stratospheric layer. Cloudiness is prescribed according to present-day climatology. The shortwave radiation scheme accounts for the absorption of solar radiation by atmospheric gases and clouds. Absorption is parameterised as a prescribed fraction of the incoming solar radiation. Reflection of solar radiation takes place at the top of the atmosphere and at the surface. The reflected sunlight from the surface is completely reemitted to space. The longwave radiation scheme follows the approach proposed by Chou and Neelin (1996). To take into consideration clouds, we combine the perturbed fluxes for clear sky conditions with those for cloudy conditions using the actual cloud cover per grid cell.

2.1.2. CLIO

CLIO (Coupled Large-scale Ice–Ocean model) is a three-dimensional ocean–sea ice model built at the Université catholique de Louvain (Goosse and Fichefet, 1999).
The oceanic component is a primitive-equation, free-surface ocean general circulation model (Deleersnijder and Campin, 1995; Campin and Goosse, 1999). It contains a sophisticated formulation of the subgrid-scale vertical mixing (Goosse et al., 1999) and a parameterisation of density-driven downslope flows (Campin and Goosse, 1999). An isopycnal diffusion scheme, the Gent and McWilliams' (1990) parameterisation of the tracer transport due to meso-scale eddies, a parameterisation of the large-scale interactions between Antarctic ice shelves and the ocean (Beckmann and Goosse, 2003) and a physically-based representation of the upper boundary condition for the salinity balance (Tartinville et al., 2001) are implemented in this model. Furthermore, a module that computes the contribution of the oceanic thermal expansion and/or haline contraction to global and regional sea level changes is included.

The sea ice component (Fichefet and Morales Maqueda, 1997) accounts for the heat capacity of the snow-ice system, the storage of latent heat in brine pockets trapped inside the ice, the effect of the subgrid-scale snow and ice thickness distributions on sea ice thermodynamics, the formation of snow ice under excessive snow loading and the existence of leads within the ice pack. Ice dynamics are calculated by assuming that sea ice behaves as a two-dimensional viscous-plastic continuum.
The horizontal resolution of CLIO is 3° × 3°, and there are 20 unequally spaced levels in the ocean. The only flux correction applied to CLIO when coupled to ECBilt is an artificial reduction of precipitation over the Atlantic and Arctic Oceans, and a homogeneous distribution of the removed amount of freshwater over the North Pacific Ocean (Goosse et al., 2001).

2.1.3. VECODE

VECODE (VEgetation COntinuous DEscription model) is a reduced-form model of the vegetation dynamics and of the terrestrial carbon cycle (Brovkin et al., 2002).
This model simulates at the same resolution as the one of ECBilt the dynamics of two main terrestrial plant functional types: trees and grassland. The equilibrium tree fraction in a given grid cell is taken as a function of climatic parameters (the positive degree-day (PDD) index and the annual mean precipitation). The equilibrium fraction of desert (i.e. bare soil), either cold or warm, is also obtained from climatic parameters using empirical formulas. The equilibrium grassland fraction is defined as the land covered neither by tree nor by desert. If climate changes, the model simulates vegetation transition from the equilibrium for the previous climate towards equilibrium for the new climate.
Four carbon compartments are considered in the carbon cycle component of the model. They all have different turnover times: a fast pool of green biomass (leaves), a slow pool of structural biomass (stems, roots), a fast pool of organic matter (litter) and a slow pool of organic matter (woody stems and roots). Carbon isotopes ^{13}C and ^{14}C as well as fractionation processes during their transfer are also modelled. The simulated vegetation changes only affect the land surface albedo in ECBilt and have no influence on other processes such as, for instance, evapotranspiration.

2.1.4. AGISM

AGISM (Antarctic and Greenland Ice Sheet Model) consists of two three-dimensional thermomechanical ice dynamics models for each of the polar ice sheets. Both models are based on the same physics and formulations. They are composed of a three-dimensional thermomechanical model of ice sheet flow, a visco-elastic bedrock model and a model of the mass balance at the ice-atmosphere and ice-ocean interfaces (Huybrechts, 2002). For the Greenland ice sheet, calculations are made on a 10 km ×10 km resolution grid and for the Antarctic model on either 10 km ×10 km or 20 km ×20

km with 31 vertical layers in the ice and another 9 layers in the bedrock for the calculation of heat conduction in the crust. The only difference between both ice sheet models is that AISM includes coupled ice shelf flow to enable grounding-line migration, whereas GISM assumes iceberg calving when the ice sheet reaches the prescribed coastline or according to a calving parameterisation when sea-level is below present-day levels. Interaction with atmosphere and ocean is effectuated by prescribing the climatic input, consisting of the surface mass balance (accumulation minus ablation), surface temperature and the basal melting rate below the ice shelves surrounding the Antarctic continent.

The atmospheric variables needed as an input for AGISM are surface temperature and precipitation. Because the details of the Greenland and Antarctica surface climates are not well captured on the ECBilt coarse grid, these boundary conditions consist of present-day observations as represented on the much finer AGISM grid onto which climate change anomalies from ECBilt are superimposed. Monthly temperature differences and annual precipitation ratios, computed against a reference climate corresponding to the period 1970-2000 AD, are interpolated from the ECBilt grid onto the AGISM grid and added to and multiplied by the observed surface temperatures and precipitation rates, respectively. The mid-depth ocean temperature in proximity to Antarctic ice shelves is used to parameterise spatially explicit sub-shelf melt rates following Beckmann and Goosse (2003). After performing mass balance and ice dynamics computations, AGISM transmits the calculated changes in land fraction covered by ice and orography to ECBilt and VECODE. In addition, AGISM provides CLIO with the geographical distribution of the annual mean freshwater flux resulting from ice sheet runoff, iceberg calving, runoff from ice-free land and basal ice melting. All of these sources of freshwater are added to the surface layer of coastal oceanic grid boxes. Some adjustments are regionally applied to the heat and freshwater fluxes to ensure conservation in the coupled system (see Driesschaert (2005) for details).

2.1.5. Global glacier melt algorithm

The response of mountain glaciers and ice caps is accounted for by a global glacier melt algorithm (Raper and Braithwaite, 2006). The algorithm is run in off-line mode and consists of a mass balance and a geometric glacier model. A separation is made between melt contributions from mountain glaciers and ice caps, as these have distinctly different geometric characteristics. The algorithm also has an improved treatment of volume shrinkage to take into consideration simultaneous changes in glacier area. This allows glaciers to reach a new equilibrium under a climate warming, contrary to older models which use a time-constant sensitivity for mass balance, so that glaciers would melt away for any warming rather than approaching a new equilibrium (e.g., Gregory and Oerlemans, 1998; van de Wal and Wild, 2001). The algorithm is forced by applying

annual temperature anomalies with respect to the 1961-1990 period. Precipitation changes are not considered in line with conclusions from several studies showing this to be of secondary importance (Braithwaite et al., 2002; van de Wal and Wild, 2001).

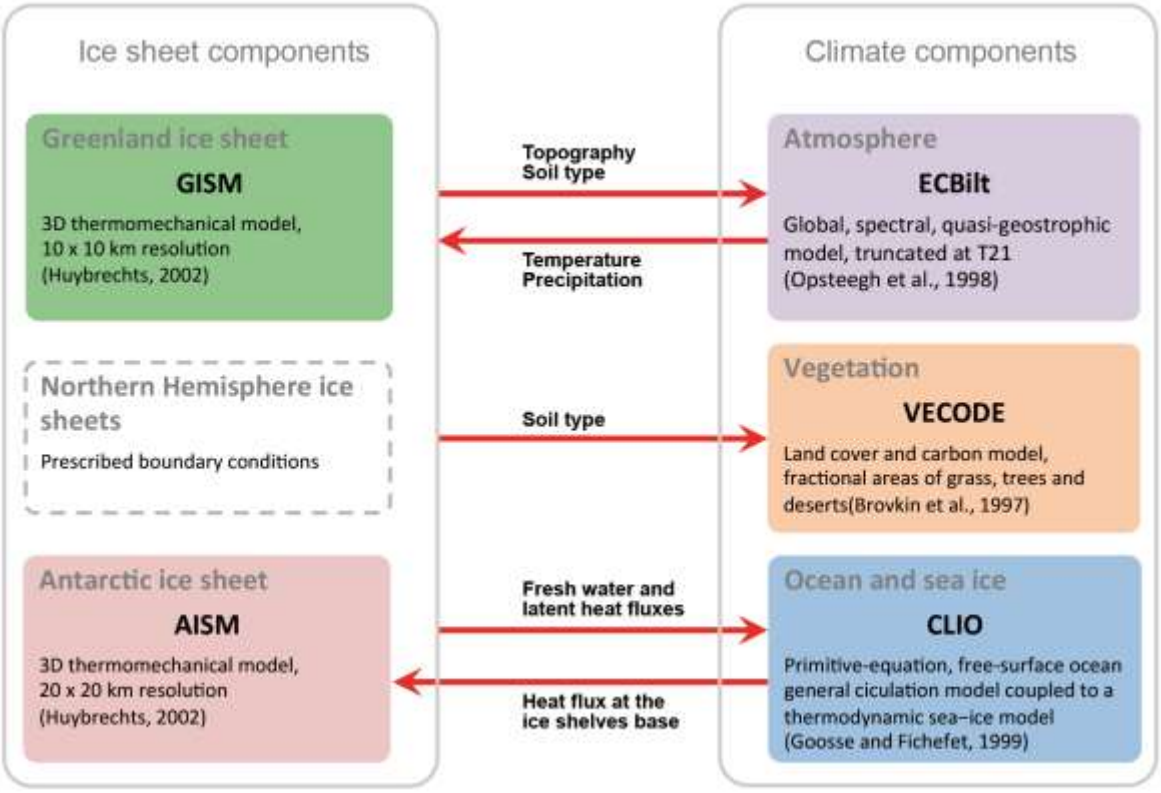

Figure 1: LOVECLIM model configuration including dynamic components for the Greenland and Antarctic ice sheets and prescribed Northern Hemisphere ice sheet boundary conditions.

2.2. MODEL IMPROVEMENT

2.2.1. The climate component

Improvements made to the climate component of LOVECLIM1.2 are described in the following sections and are made publically available in a recent release of the model called LOVECLIM1.3 (http://www.elic.ucl.ac.be/repomodx/elic/index.php?id=289).

2.2.1.1. TOBI

An empirical topography-catalysed diapycnal mixing scheme has been incorporated into the oceanic component of LOVECLIM according to A. Timmermann (personal communication). The adopted parameterisation (hereafter referred to as TOBI) induces a large annual mean surface temperature increase in the Southern Ocean area (not shown). The warming is of 1.9°C on average at 63°S and it reaches up to 3.1°C at 22.5°E. In the Northern Hemisphere, the Arctic Ocean is colder than in the reference simulation (without TOBI parameterisation) (the cooling is about 0.4°C, on average, north of 80°N), but the northern North Atlantic (0.8°C in a region 50°N-75°N 65°W-0°W) and North Pacific (0.4°C in a region 0°N-63°N 150°E-110°W) are experiencing

higher temperatures with TOBI than in the reference. In the Northern Hemisphere, the maximum sea ice extent is reduced mostly in the Denmark Strait and the Bering Sea (not shown). In the Southern Hemisphere, the reduction in sea ice extent occurs all around Antarctica. This leads to values in closer agreement with observation, for both the Southern and Northern Hemisphere. The minimum sea ice extents are reduced mostly in the Laptev Sea and all around Antarctica. This improves the simulated values although they remain too large compared to observations. A. Timmermann (personal communication) showed that this parameterisation significantly improved ocean ventilation, and that water mass ages and oxygen concentrations are in better agreement with observations.

2.2.1.2. ABEL

The polar amplification, which is defined as the ratio of the warming at high latitudes to its global mean, is higher in LOVECLIM than in most CGCMs. To partly remedy this problem, it was proposed to implement an improved representation of tropical dynamics (hereafter called ABEL) in LOVECLIM. More precisely, a modified atmospheric balance equation is used (A. Timmermann, personal communication). In LOVECLIM1.2, the term describing the effect of divergent winds on the stream function was neglected. In the extratropics, this is a valid assumption. However, in equatorial regions this omission leads to a misrepresentation of the trade winds and a damping of the equatorial Kelvin waves. The polar latitudes (both in the Northern and Southern Hemisphere), except northern Europe, are warmer with ABEL than with LOVECLIM1.2 (not shown). In the Northern Hemisphere, this warming pattern extents over the North Pacific and North-East Asia (Siberia and China) (+0.2°C in a region 45°N-90°N 110°E-110°W). The surface temperature is lower in ABEL than in the reference almost everywhere in the equatorial to mid-latitudes (in both hemispheres). The cooling is generally larger over the continent although some regions in North Africa and Arabia experience a warming. In other words, ABEL reduces the meridional temperature contrast. The increase in polar temperature due to an increase in atmospheric CO_2 concentration is smaller with ABEL than with LOVECLIM1.2, while there are only very small changes in the tropical area. Thus, ABEL improves the representation of the cold bias of the model. In the Northern Hemisphere, in spring, the sea ice extent is reduced in the Denmark Sea. In autumn, it is reduced in the Beaufort, Chukchi and Kara Seas, while it is larger in the Barents Sea (compared to the reference simulation).

2.2.1.3. CLOU

The cloud cover in LOVECLIM1.2 depends on location and season, the cloudiness is prescribed based on the ISCCP D2 dataset (see Rossow et al., 1996), which prevents the representation of any cloud feedback. An empirical cloud scheme (hereafter called CLOU) was implemented in LOVECLIM to circumvent this limitation (A. Timmermann, personal communication). The major feature of the simulated pre-industrial climate with

CLOU compared to LOVECLIM1.2 is a cooling of the Arctic (-0.2°C north of 63°N, on average), while the other regions do not experience temperature change except for a slight warming over some parts of Antarctica. Large areas of the Northern high latitudes, mostly the region of deep-water formation, experience larger warming with CLOU compared to LOVECLIM1.2 in response to an increase in atmospheric CO_2 concentration. This will not improve the problem of the cold bias of the model, in particular for the representation of temperatures over the Greenland ice sheet.

2.2.1.4. KATA

In Antarctica, katabatic winds flowing from the top of the ice sheet are a major component of the atmospheric surface circulation. They push sea ice away from the coast and create open water areas, where sea ice will rapidly form because of the cold air masses. This production of sea ice is accompanied by salt rejection and can therefore increase the vertical mixing, resulting in changes in ocean circulation. A parameterisation of katabatic winds was implemented in LOVECLIM (hereafter called KATA). The impact of those winds on the Antarctic sea ice is represented through constant corrections applied to the ice transport in the vicinity of the coast (Barthélemy et al., 2012). Annual wind stress simulated by LOVECLIM is corrected according to results from a simulation with a regional climate model (MAR). The correction is applied to both the meridional and zonal wind components.

The largest warming (annual mean surface temperature) occurs along the coast of Antarctica and the Amundsen Sea, the Ross Sea and the Indian sector of the Southern Ocean (+0.6°C in a region 55°E-80°W 85°S-63°S). There is also a slight warming over the North Pacific and in East Siberia (+0.2°C in a region 140°E-165°W 50°N-75°N). The Arctic Ocean is cooler compared to the reference (the cooling is about 0.3°C, on average, north of 80N).

The changes in sea ice extent remain small in the Northern Hemisphere (both the minimal and maximum extents). In the Southern Hemisphere the most significant variations occur within the ice pack and along the ice edge, reaching $\pm$ 50 % in some areas. The decrease in the summer extent is important in the Ross Sea sector. There is also a decrease in the maximum extent in the same sector. However, the increase in the Atlantic-Indian sector is very pronounced during winter only. In general this improves the agreement between the model results and observations for this region. Sea ice thickness experiences a much stronger response along Antarctica, reflecting the transport of ice by katabatic winds. The largest changes tend to occur in regions undergoing the most intense winds. The thinning exceeds 1 m in several regions and reaches around 1.5 m close to 130°W, for instance. On the other hand, the ice thickness is higher in the open ocean, where sea ice is advected.

2.2.1.5. CFC

The heat uptake simulated in LOVECLIM1.2 is too high compared to observations (Loutre et al., 2011). In order to investigate if this feature is due to too intense mixing and/or deep-water formation in the ocean, we implemented the uptake of chlorofluorocarbons (CFC-11 and CFC-12, in particular) in LOVECLIM. Indeed, their uptake is simply linked with ocean dynamics. Therefore, thanks to simulation of the CFC-11 and CFC-12 over the 20th century, we will determine if any overestimation of the uptake can be attributed to a global problem, e.g. the turbulence closure scheme used in the model, or if it is mainly located in areas of intermediate and deep-water formation. CFC-11 and CFC-12 are implemented in LOVECLIM according to the standard OCMIP-2 protocol (Orr et al., 1999).

The LOVECLIM1.2 model simulates the vertically integrated CFC-11 quite well, except in the North Pacific and in the Pacific sector of the Southern Ocean, along the coast of Antarctica. At 47°N, the CFC-11 concentration is slightly too high at the surface in the model. Moreover the model simulates an excessive penetration of this tracer in the ocean (not shown). The depth sections (not shown) confirm the general good agreement of the model (LOVECLIM1.2) with observations. Despite these differences, the general good agreement between simulation and observation suggests that the model simulates fairly accurately the ocean circulation, and therefore that this model component is not involved in the too large estimate of the heat uptake.

2.2.2. The ice sheet models (AGISM)

Major model improvements for AGISM have been achieved in part through VUB-ESSC's participation in the EU-FP7 project ice2sea and through further development within iCLIPS itself.

2.2.2.1. Improved boundary conditions

We have upgraded GISM to include new geometric data sets for surface elevation, ice thickness and bedrock elevation (Bamber et al., 2013). Some modifications were necessary to make the data appropriate for ice sheet modelling. These include the application of a geoid correction, masking of unwanted bedrock features and interpolation to the 10 km GISM grid. The major improvement to the older data set is that the new dataset is derived from an internally consistent set of bedrock elevation (including well resolved bathymetry of most fjords and continental shelves), surface elevation and ice thickness data. Differences to the old data set are nevertheless small and have an influence only on small-scale features but not on the overall model behaviour. An improved Antarctic dataset (Bedmap2, Fretwell et al., 2013) intended for high resolution numerical ice sheet models was adapted for use in AISM. It consists of bedrock, surface elevation and ice thickness data. This data set has been interpolated to the AISM model grid and resolution and adjusted to match the model's density

parameters that determine the floatation criterion. We have created a new present-day reference data set for GISM for precipitation minus evaporation (P-E), based on measurements from shallow ice cores (Bales et al., 2009). The new P-E map shows larger values especially over the ice sheet margins in the North and in the South-East of Greenland and includes a large amount of new measurements with extended coverage compared to the previous data set. Another boundary condition that has been improved is the geothermal heat flux. Instead of using a constant value throughout, the geothermal heat flux is now based on data derived by Shapiro and Ritzwoller (2004) for GISM and by Fox Maule et al. (2005) for AISM. For GISM the original map has been modified to match modelled and measured ice temperature close to the bedrock in proximity to ice core sites.

2.2.2.2. Updated calving parameterisation

A new marine calving parameterisation (Simpson et al., 2009) was included in GISM that produces a later and more rapid deglaciation of the GrIS after the LGM, more in line with reconstructions inferred from relative sea-level records. This has important implications for the small present-day background trend of the ice sheet, which is partly determined by the long-term isostatic response and ice temperature evolution.

2.2.2.3. Basal lubrication parameterisation

A new parameterisation has been included in GISM that simulates the lubricating effect of melt water penetration to the bed, which is a mechanisms widely speculated to enhance the response of the GrIS to continued atmospheric warming (Zwally et al., 2002). For the parameterisation, we have assumed that all runoff from the ice sheet is reaching the bed and modifies the sliding according to observed relations between runoff and speedup (e.g. Sundal et al., 2011). However, results for a future simulation over 200 years under the prolonged forcing scenario A1B indicate a negligible effect on the evolution of total ice volume compared to SMB changes (Shannon et al., 2013). The effect is limited by three important factors. First, much of the perimeter of the Greenland ice sheet is land-based and here accelerated flow only generates a displacement but not a loss of ice. This limits the potential effect on sea-level change mainly to marine-terminated margins. Second, marginal regions where runoff is large are mostly already in an accelerated state today. And third, regions further inland that will have increased runoff in the future have generally lower velocities, limiting the potential speedup considerably.

2.2.2.4. Higher-order model

We have developed a new finite difference implementation of a three-dimensional higher-order ice sheet model (Fürst et al., 2011) that can be used in an updated version of GISM. In comparison to a conventional centred difference discretisation, it enhances both numerical stability and convergence. In order to achieve these benefits the discretisation of the governing force balance equation makes extensive use of

information on staggered grid points. Comparison with the traditional shallow ice approximation model shows a similar large-scale response between the models (Fürst et al., 2013a). The higher-order model is therefore not used for the millennial to multi-millennial time scale simulations of iCLIPS.

2.2.2.5. Sea-level control on grounded ice sheet extent

In their stand-alone set-up, both GISM and AISM are forced with a recently updated global sea-level record (Grant et al., 2012) to take into account glacial retreat over the continental shelves. The sea-level stand controls the maximum ice sheet extent (GISM) and the grounding-line position (AISM). Both models have been upgraded to respond to sea-level changes also in fully coupled mode.

2.2.3. Coupling interface between ECBilt-CLIO-VECODE and AGISM

The following sections describe improvements of the coupling interface between the climate and ice sheet model components relevant for LIG and future simulations.

2.2.3.1. Coupling interface with GISM

The coupling interface between the climate component of LOVECLIM and the Greenland ice sheet model has been revised to address two problems that have been identified in earlier experiments with LOVECLIM. In previous work it was shown that regrowth of the GrIS after (partial) deglaciation was largely inhibited (Ms thesis Goublomme and Decerf, 2007). The interpolation method used to translate temperature anomalies from the atmospheric grid to the ice sheet model grid was the main reason for this. When the ice sheet is retreating, bare land is exposed and replaced by tundra close to the ice sheet, the albedo is reduced and relatively higher temperatures are smoothed out over the margins. The reason for this behaviour is the coarse resolution of the climate model and the fact that different surface types are averaged according to their relative share within one combined atmospheric grid cell. The same is incidentally true for ocean temperature changes that are imprinted on coastal land points (with partial ice sheet cover). From the climate model perspective, this behaviour makes sense and should be preserved. Note, this problem is largely absent for the AIS, which still covers most of the underlying bedrock even when the volume is considerably reduced. In reality, a glacier surface (here the Greenland ice sheet) can preserve a relatively sharp boundary with lower temperatures above the ice and in close proximity due to development of a local katabatic wind system.

The second problem that was identified is that LOVECLIM assumes surface temperatures to be limited by the melting point when snow or ice is at the surface. For the climate model this again makes sense, since it is a physical constraint to the lower boundary condition. However, the limit applies also to the surface temperature on the ice sheet and implies that the derived temperature anomalies used to force the ice sheet model are not correctly calculated, i.e. low biased, especially for large forcing scenarios. So far this

effect had been largely overprinted by large warming at the ice sheet margins, but needs to be corrected as part of the modified interface.

The implemented solution to both problems is the use of a diagnostic forcing temperature, which is loosely coupled to the climatic land temperature evolution over the ice sheets. This is realised in three steps.

1. As basis for all calculations the land surface type temperature (T_{land}) is used instead of the combined (ocean, sea-ice, land) surface type temperature in order to avoid mixing with other surface types.

2. The diagnostic temperature T_{wg} (white grass) evolves as a function of calculated heat fluxes similar to T_{land}, but without melting point limit and ignoring heat fluxes in relation to the melting. The diagnostic temperature is loosely coupled to T_{land} in order to prevent runaway feedbacks. This is done by introducing a correction heat flux term HFLX correction = beta (T_{wg} - T_{land}), proportional to the temperature difference between land temperature and diagnostic forcing temperature. The proportionality scaling factor beta controls the strength of the coupling, where beta ~ 0.1 appears as a best guess to allow temperature T_{wg} to exceed the melting point, but not show unwanted overshoot behaviour (Figure 2)

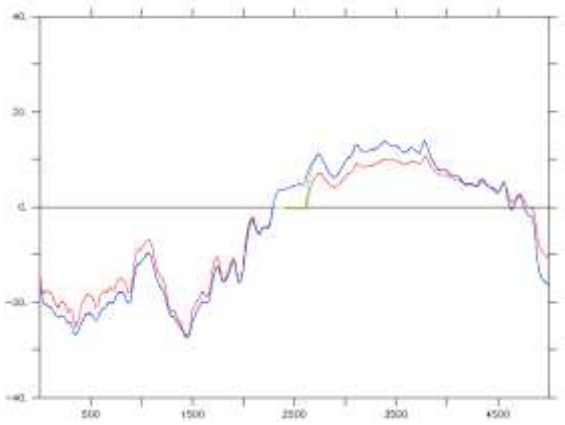

Figure 2: Temperature evolution over one year of a tundra point off the Greenland ice sheet. As long as snow is on the surface, the land temperature (green) is limited to the melting point, while the diagnostic temperature T_{wg} evolves further. The combined type temperature (red) is low biased in summer and high biased in winter due to the moderating effect of the partial ocean cover in this atmospheric grid box.

3. In a final step, T_{wg} is further modified by calculating modified outgoing (sw and lw) heat fluxes in function of T_{wg} itself and by assuming the surface always exhibits surface albedo equal to full snow cover. This step only affects the ice-free land and limits the contamination of the nearby ice sheet surface by tundra warming. The scaling factor beta now has the role of a tuning factor that controls the amount of tundra warming affecting the ice sheet periphery (Figure 3).

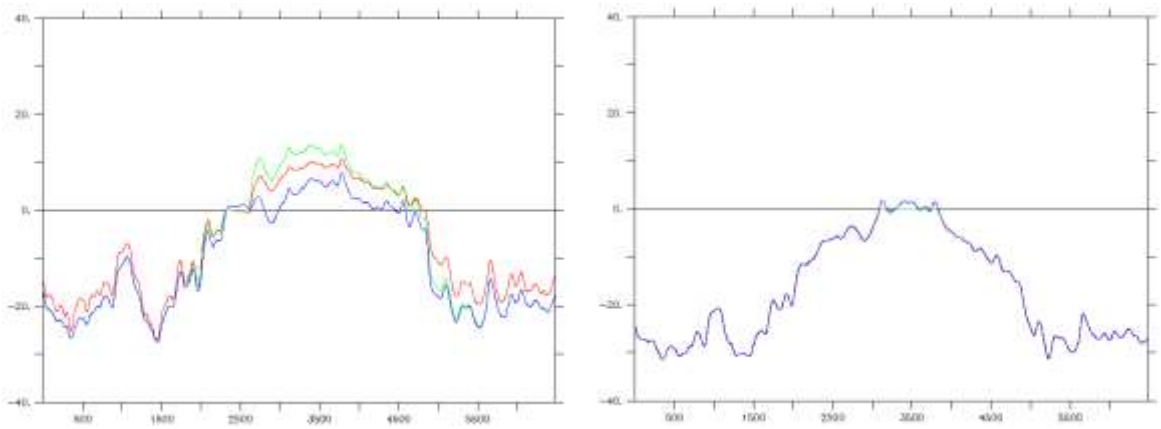

Figure 3: Final forcing temperature T_{wg} (blue) without melting point limit and a heat balance based on prevailing snow albedo over the whole time for a tundra point (left) and on the ice sheet (right). In both cases a beta coefficient of 0.08 was used. The diagnostic forcing temperature T_{wg} is higher than the land temperature (red) and mixed temperature (green) while snow is melting at the surface and lower after the albedo change happens for both.

For beta ~ 1.0, T_{wg} is similar to T_{land}, reproducing the original model closely (except for ocean influence). The melting point limit is approximately fulfilled and tundra warming fully affects the ice sheet margin.
For beta ~ 0.1, T_{wg} is unlimited by the melting point, shows similar variations as T_{land}, but is colder in summer and shows reduced anomalies over ice free land, limiting the tundra contamination considerably.

2.2.3.2. Antarctic shelf melt parameterisation

Compared to earlier versions of the model (Goosse et al., 2010) which used spatial constant ice-shelf basal melt rates, ocean temperatures surrounding the Antarctica ice sheet are now used directly to parameterise spatially explicit ice-shelf basal melt rates, defining the flux boundary condition at the lower surface of the Antarctic ice sheet in contact with the ocean. The sub-shelf basal melt rate M_{shelf} is parameterised as a function of local mid-depth (485-700 m) ocean-water temperature T_{oc} above the freezing point T_f (Beckmann and Goosse, 2003):

$$M_{shelf} = r_w c_p g_T F_{melt} (T_{oc} - T_f) / L r_i,$$

where $r_i = 910$ kg m^{-3} and $r_w = 1028$ kg m^{-3} are ice and seawater density, $c_p = 3974$ J kg^{-1} °C^{-1} is the specific heat capacity of ocean water, $g_T = 10^{-4}$ is the thermal exchange velocity and $L = 3.35 \times 10^5$ J kg^{-1} is the latent heat of fusion. The local freezing point is given (Beckmann and Goosse, 2003) as:

$$T_f = 0.0939 - 0.057 \times S_0 + 7.64 \acute{} \ 10^{-4} z_b,$$

with a mean value of ocean salinity $S_0 = 35$ PSU and the bottom of the ice shelf below sea level z_b. A distinction is made between protected ice shelves (Ross and Ronne-

Filchner) with a melt factor of $F_{melt} = 1.6x10^{-3}m\ s^{-1}$ and all other ice shelves with a melt factor of $F_{melt} = 7.4x10^{-3}m\ s^{-1}$. The parameters are chosen to reproduce observed average melt rates (Depoorter et al., 2013) under the Ross, Ronne-Filchner and Amery ice shelf for the pre-industrial LOVECLIM ocean temperature and Bedmap2 (Fretwell et al., 2013) shelf geometry. For ice shelves located inland from the fixed land-sea mask of CLIO, ocean temperature from the nearest deep-ocean grid point in the same embayment is used for the parameterisation.

In addition, surface melting of the ice shelves has been taken into account, compared to earlier model versions where all surface meltwater was assumed to refreeze at the end of summer. The surface mass balance of sheet and shelf are now treated consistently with the same positive-degree-day model including capillary water and refreezing terms. The same melting schemes for basal and surface melt have been used for the Antarctic ice sheet model version that participated in the PlioMIP intercomparison exercise of de Boer et al. (2015).

2.2.3.3. Icebergs

The dynamic-thermodynamic iceberg model of Jongma et al. (2009), leading to a spatio-temporal redistribution of freshwater and heat fluxes directly related to iceberg calving, was also included in LOVECLIM1.3.

The dynamics and thermodynamics of the iceberg-module are based on the iceberg-drift model proposed by Smith (Loset, 1993; Smith, 1993; Smith and Banke, 1983) and further developed by Bigg et al. (1996; 1997). Empirical parameters include drag coefficients, reflecting the exchange of momentum between the icebergs and the ocean, the atmosphere and the sea-ice, and melt coefficients, which determine the relative importance of basal melt, side melt and wave erosion and ultimately dictate the melting speed of the icebergs. This model predicts the path of a melting iceberg. Icebergs of various size classes are produced at appropriate calving sites, with a fixed yearly production rate. The calving sites are based on observations of glacier and ice sheet calving, complemented with ad hoc iceberg sources where observations are scarce (Jongma et al., 2009).

Jongma et al. (2009) have shown that this model is able to reproduce a reasonable iceberg distribution in both hemispheres when compared to recent data (Figure 4). In the Southern Hemisphere the general pattern of distribution agrees well with modelling results (Gladstone et al., 2001). They even confirm the 'tongue' of icebergs in South Atlantic Ocean. In the Northern Hemisphere, although the general pattern of distribution is quite well reproduced (Bigg et al., 1996), some smaller discrepancies can be identified, e.g. in the southern and eastern drift of the icebergs. The major consequence of the iceberg melting is a cooling (in the annual mean) of the southern oceans, the Denmark Strait as well as most of the northern North Atlantic.

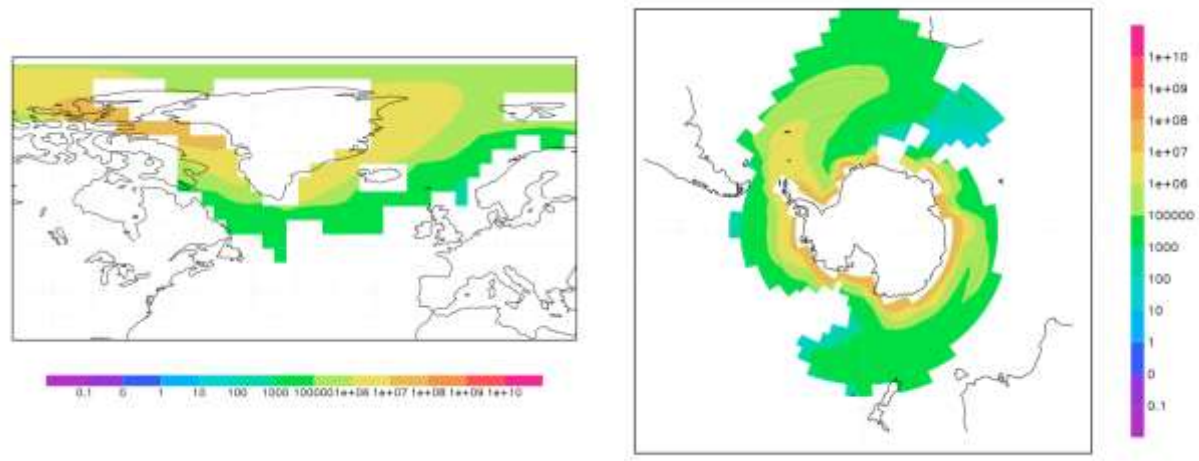

Figure 4: Pre-industrial distribution of the simulated iceberg melt (m^3) in the North Atlantic Ocean (left) and in the Southern Ocean (right).

The Denmark Strait is also less salty while the Barents Sea is slightly saltier. Consequently, convection sites experience slight changes. Convection is deeper along the Greenland coast and shallower north of Scandinavia (Figure 5).

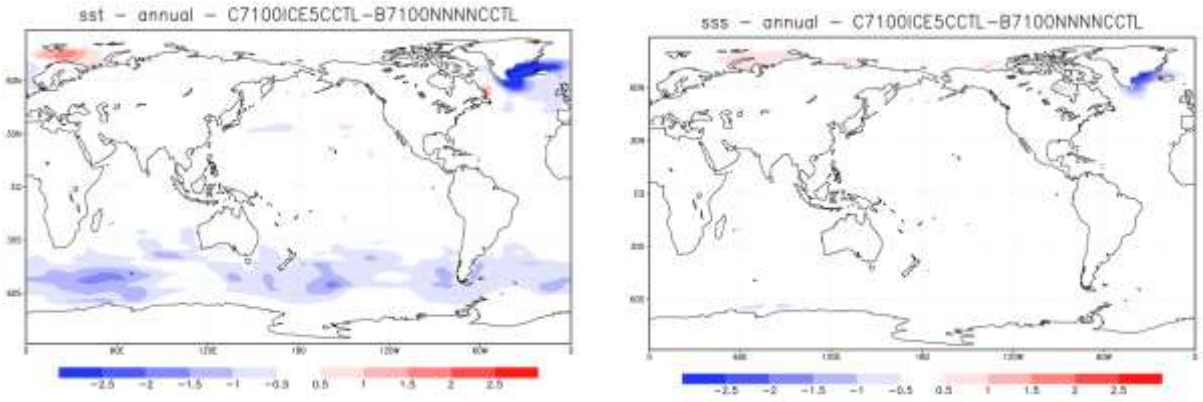

Figure 5: Change in sea surface temperature (C) and sea surface salinity (PSU) induced by the drifting and melting of icebergs for pre-industrial climate.

2.3. EVALUATION OF MODEL PERFORMANCE

2.3.1. The simulations

We tested the performance of LOVECLIM in response to the different climate modules described in the previous section. The reference state for each simulation refers to the simulations conducted without any additional module (i.e. with LOVECLIM1.2), with the parameter set published in Goosse et al. (2010). Three simulations were performed for each of the model configuration (including one or several modules) and are discussed in the three following sections (2.3.1.1-2.3.1.3). The climate of the last century and the impact of the parameter sets are then discussed in section 2.3.1.4.

2.3.1.1. Pre-industrial equilibrium (CCTL)

First, we checked that the different modules are able to simulate properly the pre-industrial climate. Several variables were specifically looked at. The sea ice area in the Northern Hemisphere does not vary much amongst the simulations while the differences are more significant in the Southern Hemisphere for some configurations. Only KATA improves the simulated upper level temperature compared to LOVECLIM1.2. As far as the deep ocean is concerned, there is no large difference between the configurations, some performing slightly better, such as the simulations performed with ABEL and KATA modules.

2.3.1.2. Sensitivity tests: doubling atmospheric CO_2 concentration

In these simulations, the atmospheric CO_2 concentration increases by 1% per year during 70 years from the pre-industrial value (277.5 ppm) until twice the pre-industrial value (555 ppm). The simulation is then continued with this constant value. The model sensitivity to a doubling of the atmospheric CO_2 concentration, measured as the global annual mean temperature increase after 1000 years of this simulation, is not deeply modified. Indeed, according the different modules, it varies between 1.9 and 2.0°C.

We concentrated on two configurations, i.e. AK01 in which ABEL and KATA are activated and AK02 in which ABEL, KATA and CLOU are activated. Moreover, the mixing length used in the parameterisation of vertical mixing used in CLIO (*lotur*, Goosse et al., 1999), is set to 25 m in AK01 and to 20 m in AK02, and the isopycnal mixing coefficient (Redi, 1982) and the thickness diffusion linked to the eddy-induced advection parameter (*iso*, Gent and Mc Williams,1990) is set to 400 m^2s^{-1} in both AK01 and AK02.

The distribution of annual mean surface temperature change (Figure 6) for AK01 and AK02 shows that the temperature increase is less important over the Arctic Ocean in AK01 and AK02 than in the control simulation. However, the North Atlantic and the North Pacific are warming more in AK01 and AK02 than in the control simulation. The equatorial region, in particular over the Pacific Ocean, is also warming more with AK01 and AK02 than with the control simulation. The high southern latitudes are experiencing either stronger or weaker warming depending on the longitude.

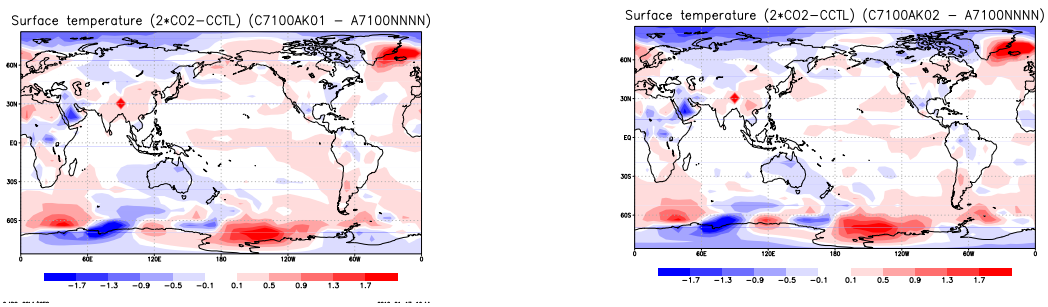

Figure 6: Change in annual mean surface temperature (°C) between the control simulation and the AK01 (left) and AK02 (right) simulations.

2.3.1.3. Sensitivity tests: freshwater fluxes

In these simulations**,** the amount of freshwater added in the North Atlantic (30-60°N) increases linearly by 0.1 Sv in 500 yr (i.e. a rate of 0.0002 Sv/yr). Most of the configurations show a smaller sensitivity to the input of freshwater in the North Atlantic than the control. In other words, in most of the cases, the reduction in the maximum value of the North Atlantic meridional overturning streamfunction due to the freshwater added in the North Atlantic is up to 15 points of percentage smaller with TOBI than in LOVECLIM1.2.

2.3.1.4. The climate of the last century

For the last century experiments, we consider the mean over an ensemble of five members in order to reduce the impact of internal variability. Each member consists of a simulation of the last century climate (1900–2010). Each simulation starts in 1900 from the state of the corresponding simulation of the last millennium at that time. We compared the simulated and observed trends of several variables over the time interval for which observation are available.

From this analysis, we cannot conclude that one single module or one group of modules significantly and simultaneously improve the trends in the last century simulated climate. However, configurations AK01 and AK02 allow improvements of the representation of the atmospheric dynamics in the tropics, of surface features along the coast of Antarctica and of the cloud feedbacks. Therefore, it was decided to select AK01 for further simulations, in particular to check that it performs also well for other parameter sets and for other forcings.

2.3.2. The parameter sets

Several parameter sets (numbered 11, 21, 22, 31, 32, 41, 51 and 71) were identified in Loutre et al. (2011) and used in Goelzer et al. (2011). They provided modified model response to increase in atmospheric CO_2 concentration and to a freshwater hosing and are used here to test the response of LOVECLIM1.3 with the AK01 configuration. The AGISM component is not activated in these simulations. Three experiments are performed with each parameter set, i.e. CCTL, 2CO2 and HYST, like in the previous section.

The global climate sensitivity varies between 1.5 °C and 3.6 °C. The standard parameter set (71) provided with the new model release leads to a sensitivity of 2.0°C. This value is between the one obtained with parameter set 11, on the one hand, and parameter sets 21 and 22, on the other hand. The sensitivity to the freshwater hosing also varies between -16% and -47%. Once again parameter set 71 leads to a value between the one obtained with parameter sets 11, on the one hand, and 21 and 22, on the other hand. The northern polar latitude sensitivity is stronger than the southern one with parameter set 71, while it is of the same order of magnitude for the other parameter sets.

2.3.3. Fully coupled ice sheet sensitivity

We have performed simulations under 4xCO_2 forcing as above, but now with the fully-coupled ice sheet-climate model to evaluate the new coupling interface and its effect on model sensitivity. Since the new interface prevents tundra warming adjacent to the GrIS to contaminate the temperature boundary condition used to force the ice sheet model, the ice sheet sensitivity is reduced (when beta is well below 1.0). The decisive difference is the limited albedo-temperature feedback, which renders the temperature anomalies used for ISM melt calculations lower. The temperature contrast between ice sheet and the tundra replacing it after retreat is equally reduced. Figure 7 shows that in the new interface (cyan) the parameter beta can be tuned (magenta) to approximately reproduce the original sensitivity (black). A comparison between green and blue lines for a preliminary version of the new interface shows that the model is robust to changing the restart interval of the temperature calculations from 1 (blue) to every 100 years (green).

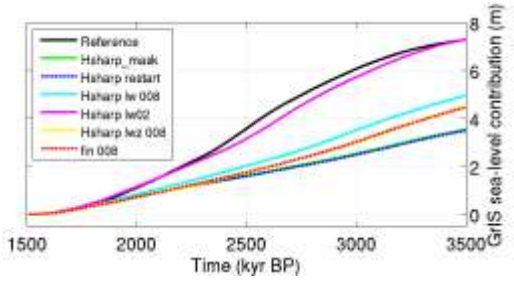

Figure 7: GrIS sea-level contribution under 4xCO_2 forcing for the original (ASTER, MILMO) interface (black) and for the new interface with beta = 0.08 (cyan) and beta = 0.02 (magenta).

With the new interface, linear regrow rates are between 24 kyr and 130 kyr (280 ppm) as visualised in Figure 8. The experiments have been repeated with glacial CO_2 forcing (200 ppm), which exhibits a similar regrow patterns (not shown) but at a faster rate. The regrow rates found by Goublomme and Decerf (2007) were of 350 kyr (200 ppm) and 1000 kyr (280 ppm). Regrowth is faster for beta = 0.08 (black and green) compared to beta = 0.2 (red and blue) and faster when fully rebounded (blue, green) despite lower initial ice volume.

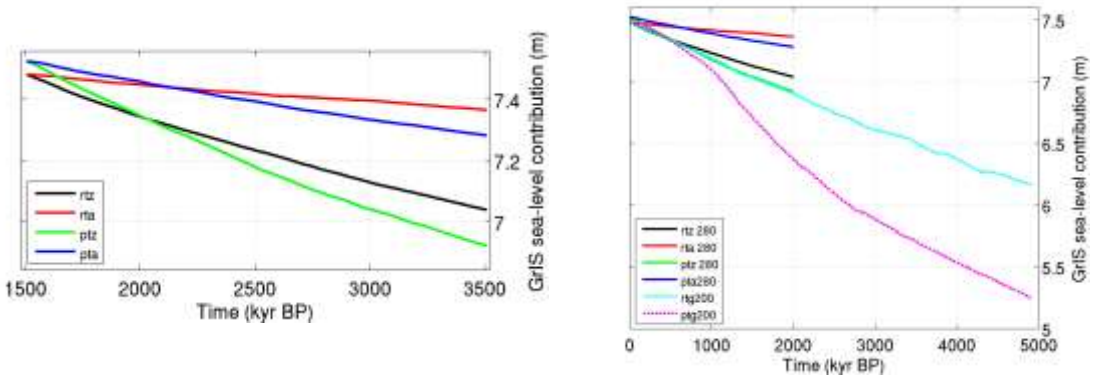

Figure 8: Left: regrow of the GrIS under pre-industrial CO_2 forcing (280 ppm) after full deglaciation with a 4xCO_2 forcing for 3000 years (black, red) and full deglaciation with complete bedrock rebound for 12000 years (blue, green). Right: Additional lines for regrowth of the GrIS under glacial CO_2 forcing (200 ppm) after full deglaciation with a 4xCO_2 forcing for 3000 years (cyan) and with full rebound for 12000 years (magenta).

2.4. THE LAST INTERGLACIAL PERIOD

Understanding the climate and ice sheet evolution during past warm periods in the history of the Earth may provide important insights for projections of future climate and sea-level changes. The growing amount of paleo-reconstructions for the Last Interglacial period (e.g. Govin et al., 2012; Capron et al., 2014) in combination with improved model simulations of this most recent warm period (e.g. Bakker et al., 2013; Lunt et al., 2013, Langebroek and Nisancioglu, 2014) make it an interesting target for studying the coupled climate-ice sheet system. Different configurations of the time evolution of the NH ice sheets are used and the sensitivity of the model response to two parameter sets is tested.

2.4.1. Climate simulations

The simulations were performed with LOVECLIM1.3 using the AK01 configuration. All the transient simulations performed in this study start at 135 kyr BP from an equilibrium state at that time and are run for 20 kyr, until 115 kyr BP. They are all forced by time-dependent changes in insolation and greenhouse gas (GHG) concentrations.

2.4.1.1. Insolation and greenhouse gas forcing

The changes in the distribution of insolation received by the Earth are computed from the changes in orbital configuration (Berger, 1978). June insolation at all latitudes (except polar latitudes in the SH) reaches a maximum at about 127 kyr BP. Then it decreases to a minimum at 116 kyr BP. December insolation follows an almost opposite pattern for all latitudes (except northern polar latitudes). It increases starting from 127 kyr BP until ~116 kyr BP. The June insolation is more than 10% larger than the present-day value for most of the latitudes, while the December insolation is more than 10% smaller than the present-day value for most of the latitudes. The largest anomalies occur in the polar regions during their local summer. The timing of the insolation changes is mostly driven by the changes in the climatic precession and its amplitude is large due to large values of the eccentricity. The obliquity also plays a role in the large changes in the amplitude of the insolation in particular in the polar regions.

The GHG forcing (Figure 9) (Petit et al., 1999; Pépin et al., 2001; Raynaud et al., 2005; Loulergue et al., 2008; Spahni et al., 2005) is prescribed and the concentrations of the different gases are time-dependent. The atmospheric CO_2, CH_4 and N_2O concentrations of the PMIP3 protocol (https://pmip3.lsce.ipsl.fr) is used from 132 kyr BP to 115 kyr BP. Before 130 kyr BP, the atmospheric CO_2 concentration experiences a fast increase by more than 50 ppm in 5 kyr. Then, it remains between 260 and 280 ppm until 115 kyr BP, except during a short time interval (128.9 to 128.3 kyr BP), when its values are higher than 280 ppm. The N_2O concentration displays a similar behaviour, with a rapid increase from 135 to 130 kyr BP, followed by almost stable values, with a low variability. By contrast, the CH_4 concentration shows a different behaviour. It reaches a

clear maximum at about 128 kyr BP. This maximum is preceded by a fast increase and followed by a slow decline. The maximum atmospheric concentrations of these GHGs during the LIG are similar to the pre-industrial ones.

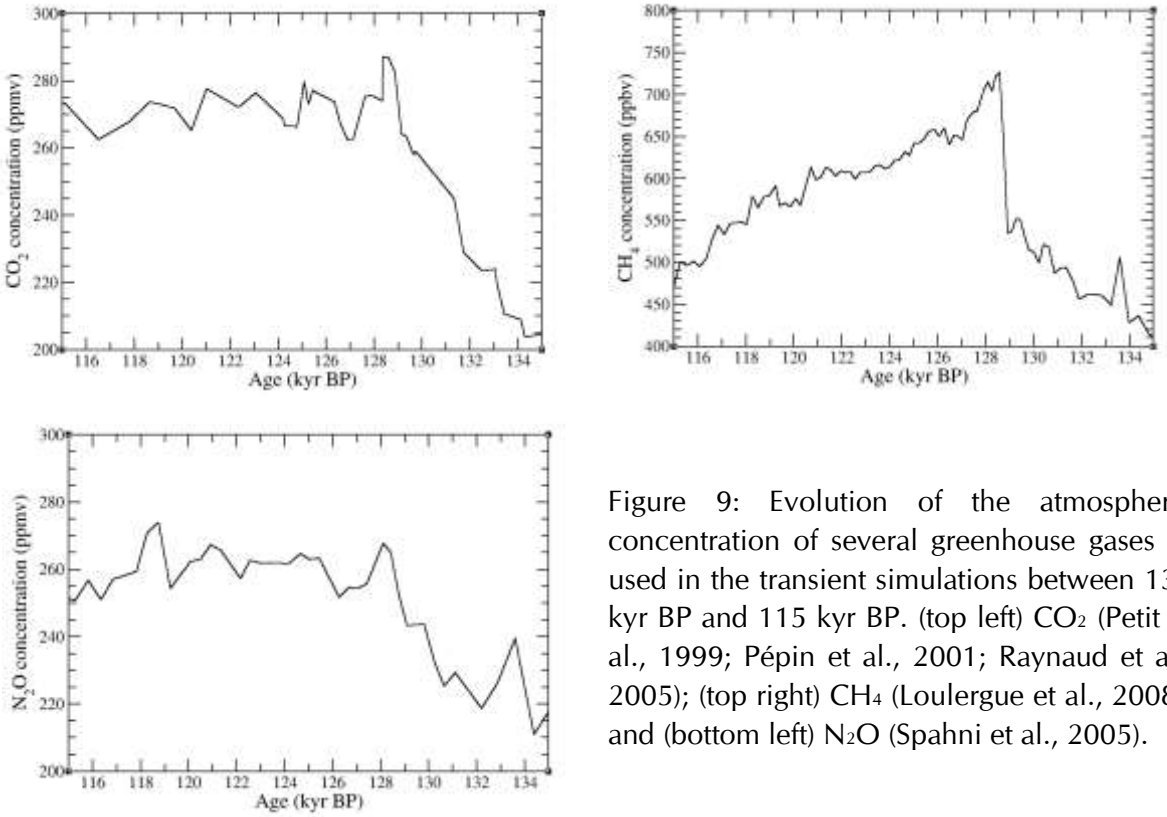

Figure 9: Evolution of the atmospheric concentration of several greenhouse gases as used in the transient simulations between 135 kyr BP and 115 kyr BP. (top left) CO_2 (Petit et al., 1999; Pépin et al., 2001; Raynaud et al., 2005); (top right) CH_4 (Loulergue et al., 2008); and (bottom left) N_2O (Spahni et al., 2005).

2.4.1.2. Surface boundary conditions

The Antarctic ice sheet is kept fixed to its pre-industrial state and there is no additional freshwater flux in the SH. Instead, the time evolution of the NH ice sheets is prescribed to several different configurations. In a first set of simulations, the Greenland ice sheet extent and surface elevation are fixed to their pre-industrial values through the whole simulation, and without any other ice sheet in the NH (PI ice sheet in Table 1). The presence of remnant NH ice sheets at the onset of the transient experiments at 135 kyr BP makes it necessary to complement these boundary conditions. For instance, as ice sheet constraints on the penultimate glacial termination (Termination II) are sparse, the NH ice sheet retreat from the last deglaciation has been remapped based on other available information for Termination II. It is assumed that, if the global sea level at a time during termination II is similar to that at a given moment of termination I, then the NH ice sheet configuration is the same for both times. This method (used e.g. by Ritz et al., 2011) has been extended by relying on a recently updated sea level record (Grant et al., 2012) and by using an alternative NH ice sheet reconstruction. For the latter, a large number of geomorphological constraints on ice sheet extent have been digitized from the literature and ice sheet surface elevation has been reconstructed by assuming a

plastic flow relation for the ice sheets. The resulting boundary conditions consist of a chronology of ice mask and surface elevation over the entire LIG period (called GR in Table 1), later referred to as the NH ice sheet configuration. Ice sheet albedo is also applied in this simulation. According to this reconstruction, the Fennoscandian ice sheet is fully melted at 132.1 kyr BP, while the North American ice sheet persists until 131.3 kyr BP. At the end of the interglacial, the regrowth of the ice sheet starts at 120.2 kyr BP over North America and at 117.4 kyr BP over northern Europe.

Table 1: Description of the transient simulations. All the simulations are forced by changes in insolation and atmospheric GHG concentrations (see text). Parameter set std is defined and used in Goosse et al (2010), while parameter set 22 is defined and used in Loutre et al. (2011) and Goosse et al. (2007). PI stands for pre-industrial; GR (respectively LR) means that the LIG ice sheet configuration and/or freshwater flux is reconstructed based on Grant et al. (2012) (respectively, Lisiecki and Raymo (2005)).

Name	Parameter set	Ice sheets	Freshwater flux
allGR	*std*	GR	GR
IGonly	*std*	PI	–
topoGR	*std*	GR	–
fwfGR	*std*	PI	GR
allLR	*std*	LR	LR
parGR	22	GR	GR
parLR	22	LR	LR

NH ice sheet melting is accompanied by an increased flow of freshwater (FW) into the surrounding oceans, which could potentially alter the strength of the AMOC, and hence the global climate. The NH FW forcing was estimated based on the same remapping as used for the elevation and ice mask reconstructions. The spatial distribution of produced melt water is estimated from the reconstructed elevation changes and a continental runoff routing model (Goelzer et al. 2012b) is used to identify the location and magnitude of meltwater fluxes to the ocean. The FW flux to four regions is distinguished: Pacific (PAC), Arctic Ocean (ARC), North Atlantic (NAT) and North Sea (NOS). In order to avoid too large FW input into the coastal ocean model grid points, the freshwater flux is integrated over each region and equally redistributed to the points that show a magnitude higher than 0.01 Sv any time over the period 135 kyr BP - 125 kyr BP. The total freshwater flux magnitude is scaled to be in line with the total sea level contribution of the NH ice sheets (Figure 10; GR in Table 1). The glacial-interglacial contrast in NH sea-level contribution between penultimate glaciation and LIG is assumed to be the same as between LGM and present day, for which a value of 110 m SLE is taken, in line with the reference model results of Zweck and Huybrechts (2005).

Alternatively, the changes in the NH ice sheet configuration and in the additional freshwater flux in the NH are computed from the sea level record estimated from Lisiecki and Raymo (2005) (LR in Table 1). Sea level reconstruction from LR lags behind the one from GR by about 2.8 kyr during the LIG. Therefore, both reconstructed melting and glacial inception are delayed in LR compared to GR. Indeed, in LR scenario, the Fennoscandian ice sheet is fully melted at 131 kyr BP and the North American ice sheet persists until 127.5 kyr BP, while glacial inception starts at 116.5 kyr BP over North America and even later over northern Europe in LR. Moreover, the FW flux magnitude has been smoothed in time so that peaks in the FW flux are not so high in the LR reconstruction.

a b

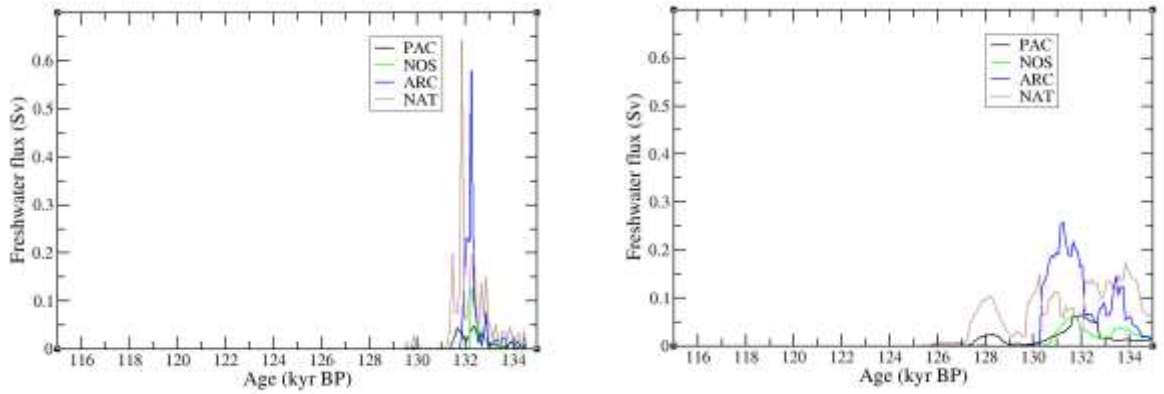

Figure 10: Freshwater flux from melting ice sheets entering the ocean for four regions: the Pacific (PAC), Arctic Ocean (ARC), North Atlantic (NAT) and North Sea (NOS). FW flux is estimated based on sea level change reconstructions from (a) Grant et al. (2012) and (b) Lisiecki and Raymo (2005).

2.4.1.3. Parameter sets

Loutre et al. (2011) and Goosse et al. (2007) identified several parameter sets that provide modified model responses to increased atmospheric CO_2 concentration and to freshwater hosing. Amongst the parameters involved in these parameter sets, there are the albedos of the ocean and sea ice, and parameters involved in the equation of the quasi-geostrophic potential vorticity, in the formulation of the longwave radiative scheme, in the representation of the vertical diffusivity of the ocean and in the computation of the Coriolis term in the equation of motion. A detailed description of the different parameter sets is available in Loutre et al. (2011). In addition to the reference parameter set (*std*), we also use parameter set 22 (as defined and used in Loutre et al. (2011), Goelzer et al. (2011) and Goosse et al. (2007); see also supplementary material) to test the response of LOVECLIM1.3.

The global climate sensitivity with both parameter sets is 2.1°C. It is computed as the global annual mean surface temperature increase after 1000 years from the pre-industrial

value in a simulation for which the atmospheric CO_2 concentration is increased by 1% per year from the pre-industrial value until doubling is reached (after 70 years) and held constant thereafter. The northern polar latitude sensitivity is stronger than the southern one with parameter set *std*, while they are almost the same for parameter set 22. The polar latitude sensitivity is computed as the annual mean surface temperature increase poleward of 75° in either hemisphere after 1000 years from the pre-industrial value in the same simulation as for the computation of the global climate sensitivity.
The AMOC sensitivity to a freshwater hosing is -24% for parameter set *std* and -41% for parameter set 22. The AMOC sensitivity index is computed as the percentage of decrease in the maximum value of the meridional overturning streamfunction below the Ekman layer in the Atlantic Ocean after 1000 years in a water hosing experiment. In this experiment, freshwater is added in the North Atlantic (20 ° -50 ° N) with a linearly increasing rate of 2×10^{-4} Sv yr^{-1}.

2.4.1.4. The reference simulation

The reference simulation (allGR) is forced by orbital and GHG changes and takes into account changes of the NH ice sheets from both their configuration and additional freshwater fluxes to the ocean (see Table 1 for a summary of the experiments). This results in a decrease in the simulated global annual mean surface temperature, global annual mean SST, Arctic (north of 69°N) summer temperature and summer temperatures over Europe (the region 17°W-11°E –36°-64°N), averaged between 135 and 115 kyr BP, by 0.2°C, 0.2°C, 0.2°C and 0.3°C, respectively, compared to the simulated pre-industrial values.
Broadly speaking, the simulation can be divided into an interval of transition from the previous glacial state (at the beginning of the simulation until ~131 kyr BP), a plateau, and an interval of transition towards glacial inception (at the end of the simulation, after ~121 kyr BP) (Figure 11a).
The input of additional freshwater in the North Atlantic before 131 kyr BP leads to a strong weakening of the AMOC (Figure 11b), and even to its almost complete collapse for a few centuries around 132 kyr BP. However, as soon as the additional freshwater input stops the AMOC recovers. Then, although the AMOC is less intense than under pre-industrial conditions, deep convection still takes place in the Labrador Sea, contrarily to some reconstructions (Hillaire-Marcel, 2001; Rasmussen et al., 2003a; Winsor et al., 2012) and convection is very active in the Norwegian and Barents seas. In response to the almost collapse of the ocean circulation at ~132 kyr BP, the global annual mean surface temperature (Figure 11a) experiences a rapid decrease of 0.8°C followed by a fast increase of 2.1°C, all occurring in less than 1500 years (between 132.5 and 131 kyr BP). Global annual mean surface temperature before 132 kyr BP remains lower than the pre-industrial one. Simultaneously, the simulated North Atlantic

SST and western France and Greenland surface temperatures (Figure 12abcdg) experience a decrease of several degrees. However, at the same time, the simulated tropical South Atlantic SST (Figure 12e) exhibits a slight increase. This is consistent with the so-called seesaw mechanism studied by Crowley (1992) and Stocker et al. (1992). Moreover, the simulated high latitude South Atlantic SST (Figure 12f) and the simulated surface temperature at the Dome C site (Antarctica) (Figure 12h) show almost no variations.

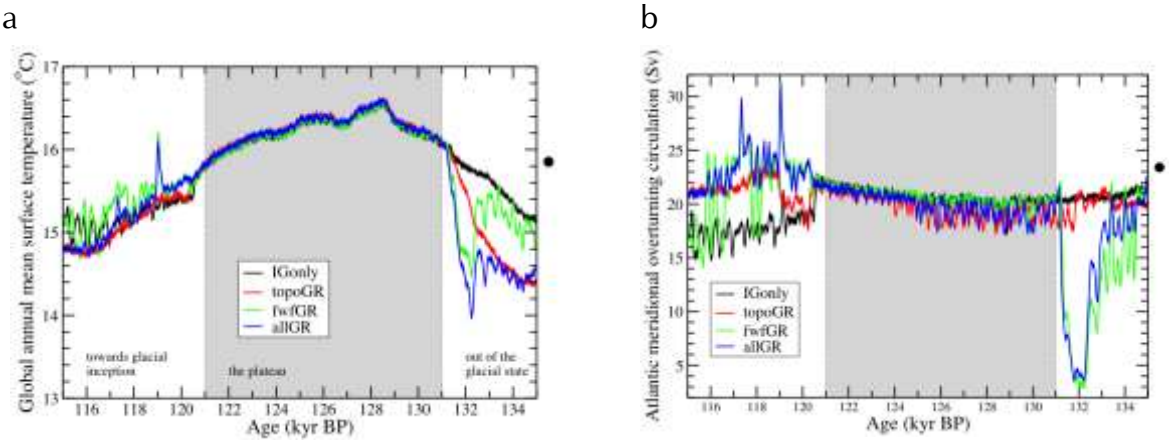

Figure 11: Time evolution of (a) (left) global annual mean surface temperature (°C); (b) (right) maximum of the meridional overturning streamfunction in the North Atlantic from model simulations using different surface boundary conditions (see text and Table 1). The series are smoothed using a moving average over 100 years.

The long-term evolution of the global annual mean surface temperature shows an increase from 131 kyr BP until the maximum of 16.6°C at 128.5 kyr BP (Figure 12a). The maximum over the LIG of the simulated global annual mean surface temperature (global annual mean SST, Arctic summer temperature, summer temperature over western France, respectively) is 0.7°C (0.4, 2.5, 4.4°C, respectively) higher than the corresponding pre-industrial value. These values are within the range of the reconstructed estimates for large-scale changes. The global annual mean cooling after the maximum at 128.6 kyr BP consists of three phases. First, there is a rapid cooling until ~126.8 kyr BP. Then, temperatures remain stable or even slightly recover until 124.8 kyr BP. Lastly, cooling proceeds at fast rate until ~121 kyr BP. However, the simulated temperature remains above the simulated PI values (15.8°C) from 131.3 kyr BP to 120.9 kyr BP. The AMOC (Figure 12b) display no significant trend during this period, although its variability is higher at the beginning than at the end of the sub-interval.

After 121 kyr BP, when the NH ice sheets start to regrow, the simulation shows a high variability of the AMOC (Figure 11b). We hypothesize that the model becomes close to a bistable regime, which makes it oscillating between two modes as previously

discussed in Jongma et al. (2007). This higher variability is mirrored in the global annual mean temperature (Figure 11a). The standard deviation is then ~0.18°C, while it was ~ 0.08°C between 125 and 122 kyr BP. This simulated high variability is also displayed in the temperature at many high northern latitude locations (Figure 12abcd).

a

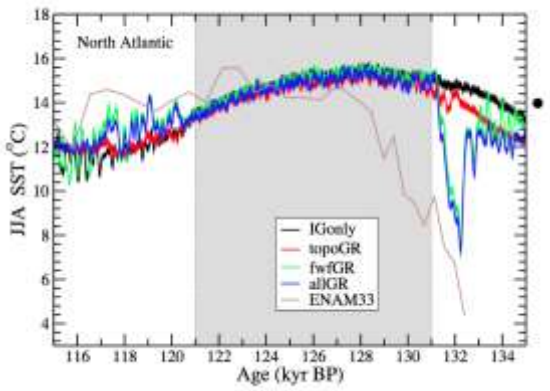

b

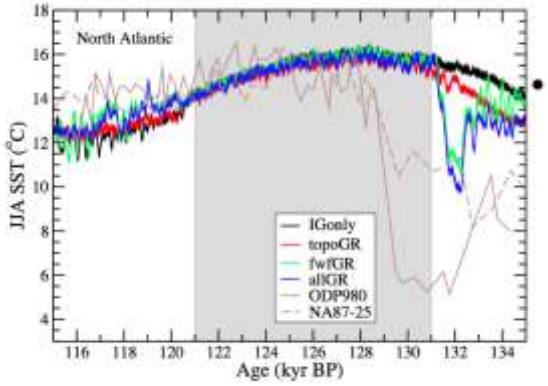

c

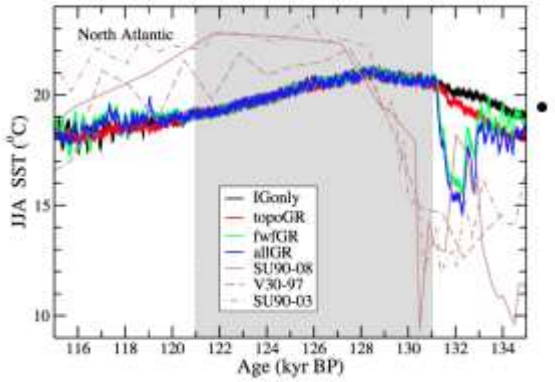

d

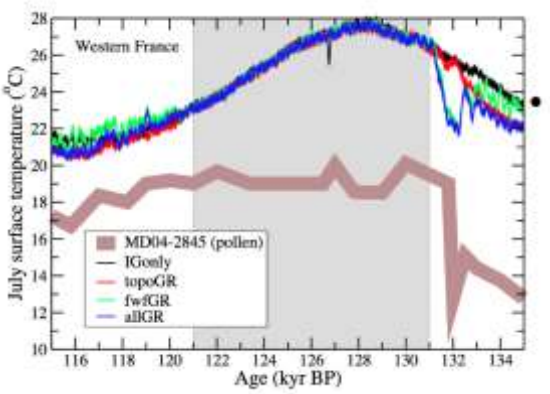

e

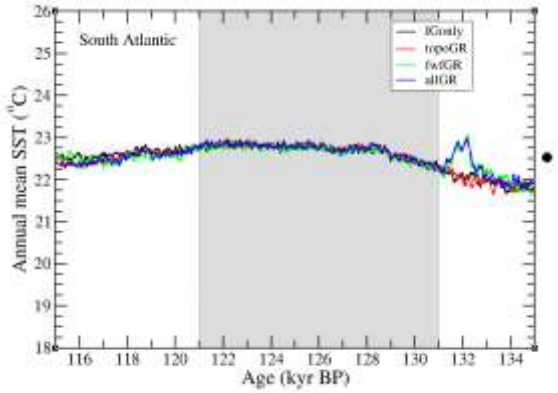

f

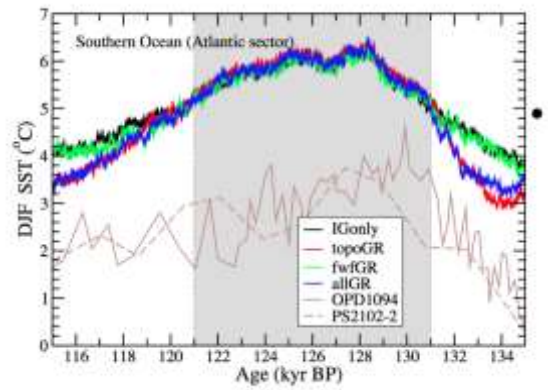

g

h

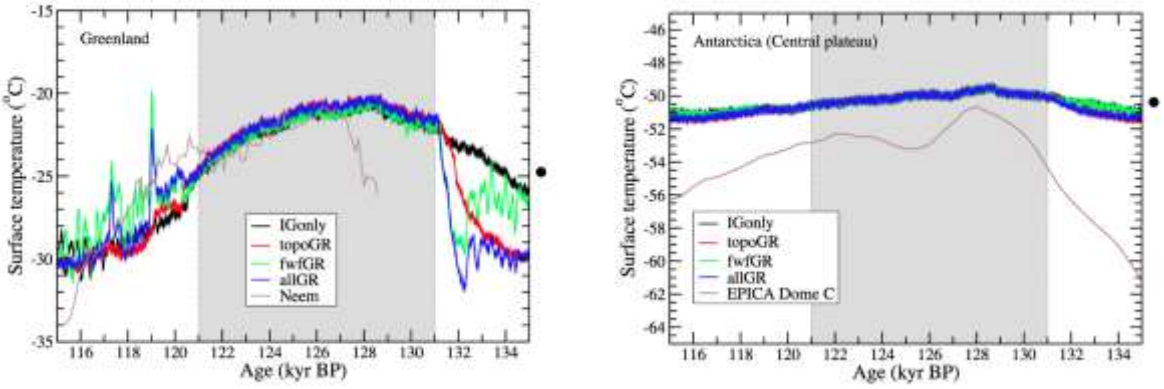

Figure 12: Comparison of reconstructed and simulated temperatures in different regions using different boundary conditions (see text and Table 1). (a) North Atlantic summer SST (°C) (ENAM33; 61.27°N, 11.16°W;; Rasmussen et al., 2003b); (b) NE Atlantic summer SST (°C) (ODP980; 55.8°N, 14.11°W, Oppo et al., 2006; NA87-25; 55.57°N, 14.75°W, Cortijo et al., 1994); (c) NE Atlantic summer SST (°C) (SU90-08, 43.35°N, 30.41W Cortijo, 1995; V30-97, 41°N, 32.93W, Mix and Fairbanks, 1985; SU90-03, 40.51°N, 32.05W, Chapman and Shackleton, 1998); (d) July surface temperature over western France(MD04-2845; 45°N, 5°W; Sánchez Goñi et al., 2012); (e) South Atlantic annual mean SST (21°S, 10°E); (f) South Atlantic summer SST (°C) (ODP1094; 53.18°S, 5.13°E, Hodell et al. 2003, Kleiven et al., 2003; PS2102-2; 53.07°S, 4.98°W, Zielinski et al., 1998) (g) Precipitation-weighted temperature reconstruction corrected for elevation change at the NEEM site, Greenland(77.45°N,51.06°W) (NEEM community members; 2013); and (h) Local surface temperature reconstruction at the EPICA Dome C site in Antarctica (75.1°S, 123.35°E, Masson-Delmotte et al., 2011). The simulated series are smoothed using a moving average over 100 years and averaged over four adjacent grid cells. The black dot on the right hand side of the figures provides the corresponding simulated pre-industrial value. The 'plateau' is shaded in grey. Note that a coherent temporal framework has been recently constructed for the ENAM33, ODP980, NA87-25, SU90-08, SU90-03, V30-97, NEEM and EDC records and they are all displayed here on the recent AICC2012 chronology (Capron et al., 2014; Bazin et al. 2013). The location of the marine and ice cores is provided in Table 2.

The NH and SH mean July surface temperatures reach a maximum at ~128 kyr BP, simultaneously with the maximum of NH/SH June insolation. The NH and SH mean January surface temperatures exhibit only a very moderate increasing trend during the LIG, with a maximum at ~119 kyr BP, in line with NH/SH October/November insolation.

The timing of maximum surface temperature (defined as MWT for timing of maximum warmth; Bakker et al., 2013) at each grid cell of the model is computed here as the time of the maximum surface temperature in the temperature time series smoothed with a Gaussian kernel regression using a bandwidth value of 100 (Loutre et al., 2014). The annual MWT occurs almost all over the globe at 128 kyr BP, i.e. simultaneously with the maximum of NH summer insolation, except over the tropical oceans, where it is observed much later. In particular, the MWT over the east tropical Pacific Ocean is

simulated at the end of the LIG. The Sahara desert and the desert regions of the Middle East show their maximum of surface temperature late during the LIG, which is in line with the maximum of grass fraction at ~122 kyr BP, quickly followed by a rapid degradation towards desert conditions (strong reduction of grass fraction) in response to a reduction in precipitation. Some locations over the tropical South Atlantic and the subtropical Pacific Oceans display a very early MWT related to an overshoot of temperature linked to the almost collapse of the AMOC (Figure 12e). The July MWT mirrors the annual MWT, except for the tropical oceans, where MWT occurs before 125 kyr BP. The January MWT is characterised by a late occurrence everywhere, except in the Southern Ocean. The January MWT occurs at the beginning of the simulation over the West Antarctic Ice Sheet and at the end of the simulation over the East Antarctic Ice Sheet.

Table 2: Location of the study sites, including marine and ice core sites. Site (12) corresponds to an unpublished marine core for which only the simulated temperature is available.

	Name	Latitude	Longitude
1	NEEM	77.45°N	51.06°W
2	ENAM33	61.27°N	11.16°W
3	ODP980	55.8°N	14.11°W
4	NA87-25	55.57°N	14.75°W
5	SU90-08	43.35°N	30.41°W
6	V30-97	41.00°N	32.93°W
7	SU90-03	40.51°N	32.05°W
8	PS2102-2	53.07°S	4.98°W
9	OPD1094	53.18°S	5.13°E
10	EDC	71.10°S	123.35°S
11	MD04-2845	45°N	5°W
12		21°S	10°E

2.4.1.5. The role of the ice sheet configuration (elevation, extent and albedo)

First, we compare the reference simulation (allGR) with a simulation that does not take into account the evolution of the NH ice sheet configuration but only includes the freshwater forcing resulting from changes in ice volume (fwfGR).

The global annual mean surface temperature (Figure 11) at the beginning of the simulation, until ~131 kyr BP, is up to 0.9°C (at 133.4 kyr BP) higher in fwfGR than in allGR and the cooling at the end of the simulation, from 119 kyr BP, is slightly smaller in fwfGR than in allGR (0.5°C at 115.8 kyr BP). Many regions in the NH, both over land and over the ocean, as well as over Greenland, also show this characteristic. The major

features of annual MWT are similar in fwfGR and allGR suggesting that the ice sheet configuration does not significantly impact MWT.
Except during the plateau, the strength of the AMOC is most of the time slightly smaller in fwfGR than in allGR, although its variability is much larger in fwfGR than in allGR. This suggests a stabilisation effect of the NH ice sheets configuration on AMOC, or rather that fwfGR is closer to a bistable regime than allGR. Indeed, when the NH ice sheets are included (as in allGR), the sea surface temperature in their vicinity decreases. This favours deep-water formation and therefore stabilizes the overall Atlantic overturning circulation (Renssen et al., 2005). During the plateau, between 131 kyr BP and 121 kyr BP, both global annual mean surface temperature and AMOC are similar in both simulations.
The conclusions drawn from the comparison of temperature between allGR and the reconstructions are not strongly modified if the changes in the configuration of the NH ice sheets during the LIG are not taken into account. The magnitude of the variations through the LIG remains too low for most of the variables. In both allGR and fwfGR, the model does not reproduce the large magnitude of the reconstructed SST variations, mostly in the NH. Moreover, the large increase in global annual mean surface temperature is simultaneous in both simulations and occurs too early compared to the reconstructions.

2.4.1.6. The role of the additional freshwater flux

The reference simulation (allGR) is compared here to a simulation that does not take into account the additional freshwater flux from the ice sheets but only includes the evolution of the NH ice sheet configuration (extent, altitude, albedo) (topoGR). Without this input in the North Atlantic, the AMOC remains more or less in its initial state until about 132 kyr BP and does not experience any collapse (Figure 11b), although there is a rapid decrease of 3Sv in 150 years at 132 kyr BP. Then, its variability becomes slightly higher (the standard deviation is 1.1Sv at the beginning of the simulation, while is rises to 1.5Sv later) and its strength becomes similar to the one simulated in allGR (~19Sv). Simultaneously, the global annual mean surface temperature (Figure 11a) smoothly increases to reach a value similar to the one simulated in allGR at 131 kyr BP. Thus the additional freshwater flux is clearly responsible for the dramatic weakening of the AMOC of almost 18 Sv at 132 kyr BP (resulting in a collapse of the AMOC) and the cooling of 1.3°C at the same time simulated in allGR. A decrease of several degrees in the simulated North Atlantic SST and western France and Greenland surface temperatures may also be attributed to the additional freshwater fluxes. During the plateau, between 131 kyr BP and 121 kyr BP, the differences between the simulations (topoGR and allGR) are only minor. After 121 kyr BP, at the end of the simulation, when

the NH ice sheets start to regrow, the AMOC variability is smaller in the simulation without freshwater flux (topoGR) than with the one that includes it (allGR).
The general pattern of annual MWT is very similar with and without additional freshwater flux due to ice sheet melting, with many regions of the globe experiencing an early MWT (~128 kyr BP). MWT occurs later than 123 kyr BP in similar regions in both allGR and topoGR. While allGR shows a rather uniform MWT for southern and eastern Asia (~119 kyr BP), topoGR displays a late MWT for southern Asia (115 kyr BP) and an early MWT for eastern Asia (122 kyr BP). July MWT is mostly characterised with a later occurrence over the southern Atlantic Ocean in topoGR compared to allGR. January MWT occurred about 1 kyr later for many places in topoGR compared to allGR. However, it is characterised with an earlier occurrence (earlier than 123 kyr BP) for topoGR than for allGR in the North Atlantic, in particular over the Greenland Sea.

2.4.1.7. The orbital and greenhouse gas forcing only

Lastly, the simulations taking into account either all (allGR) or none (IGonly) of the changes related to the growth and decay of the NH ice sheets are compared.
The global annual mean surface temperature is at maximum at ~128.4 kyr BP in IGonly as in allGR (Figure 11). Although the warming from the previous glacial maximum is fast, about 0.21°C/kyr from 135 kyr BP, there is no rapid increase as simulated in allGR at about 132 kyr BP. Even if the initial conditions of allGR and IGonly at 135 kyr BP and their general behaviour until 131 kyr BP are strongly different, the simulations converge after 131 kyr BP. The AMOC intensity reaches a minimum at ~128.7 kyr BP, almost simultaneous to the maximum of global annual mean surface temperature. However, it shows hardly any trend or variability before 121 kyr BP in IGonly. In particular, the AMOC does not experience the strong weakening simulated in allGR. During the plateau, from 131 kyr BP to 121 kyr BP, the mean values of the AMOC index and global annual mean surface temperature are similar in both allGR and IGonly. The striking feature in IGonly is the occurrence of a very rapid decrease in the meridional overturning streamfunction by almost 4 Sv in slightly more than one century at 120.5 kyr BP simultaneous to a drop in global annual mean surface temperature of 0.4°C in 500 years. After this rapid event, at the end of the simulation, both the AMOC strength and temperature display a much larger variability and smaller values than before the event.
The annual MWT is very similar in IGonly and allGR, although it occurs later in IGonly than allGR at some locations in the South Pacific and South Atlantic, which may be related to the response of the ocean in the SH to the lack of input of freshwater in the North Atlantic. In January, MWT takes place a few thousand years earlier over the North Atlantic in IGonly compared to allGR, and much earlier over the northeastern Pacific, along the coast of North America.

We can conclude from this that the evolution of the NH ice sheets greatly increases the magnitude of the temperature variations over continents as well as over the ocean at the beginning of the simulation and improves the agreement between the simulated climate and the reconstructions.

2.4.1.8. Sensitivity to the reconstructed evolution of the ice sheets

Reconstructions of sea level change during the LIG strongly suggest that ice sheets were still present over North America and Eurasia at 135 kyr BP. However, their precise extent and the exact timing of their melting are not known accurately. The impact on the simulated climate of a later NH ice sheet melting and glacial inception is analysed here through the use of two NH ice sheet reconstructions (GR and LR, Table 1) for the LIG simulation (allGR and allLR, respectively). Simulations allGR and allLR differ only from the NH ice sheet configuration and freshwater flux. Grant et al. (2012) already suggested that deep ocean temperature bias and "incorrect" orbital tuning could explain the difference in timing between both scenarios.

a

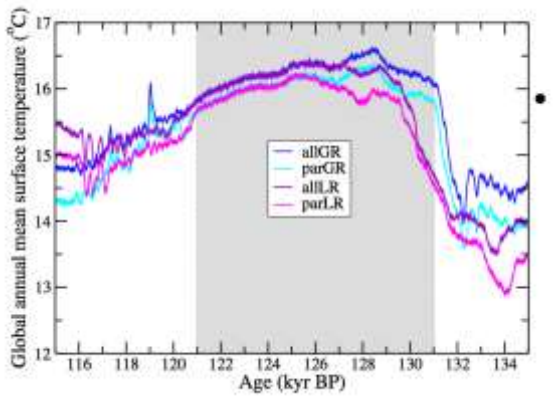

b

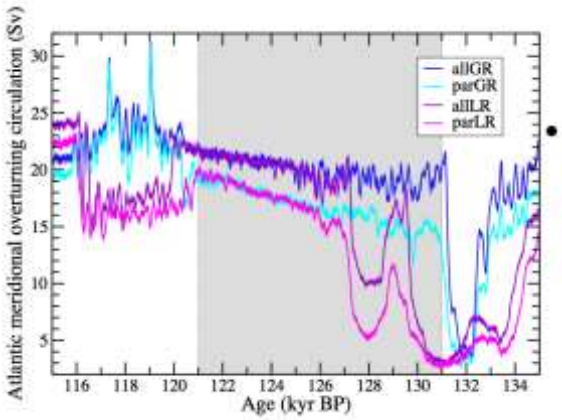

c

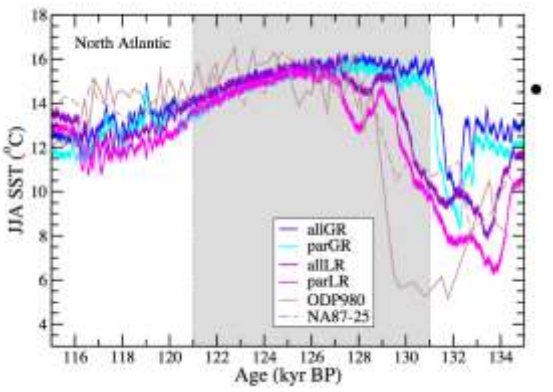

d

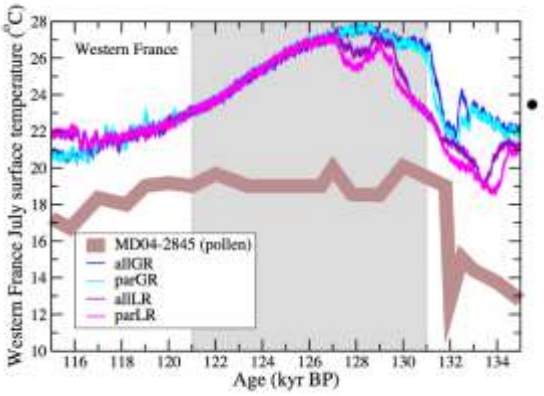

e

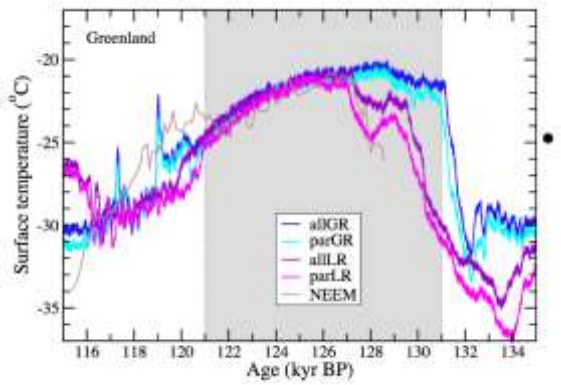

Figure 13: Comparison between the LIG climate simulated using different parameter sets (see text and Table 1) and different Northern Hemisphere ice sheet evolutions (see text and Table 1), and the reconstructed climate. Time evolution of (a) global annual mean surface temperature (°C); (b) maximum of the meridional overturning streamfunction in the North Atlantic from model simulations using different surface boundary conditions (c) NE Atlantic summer SST (°C) (ODP 980; 55.8°N, 14.11°W, Oppo et al., 2006; NA87-25; 55.57°N, 14.75°W, Cortijo et al., 1994; (d) July surface temperature over western France (MD04-2845; 45°N, 5°W; Sánchez Goñi et al., 2012); and (e) Precipitation-weighed temperature reconstruction corrected for elevation change at the NEEM site, Greenland (77.45°N, 51.06°W) (NEEM community members; 2013). The simulated series are smoothed using a moving average over 100 years and averaged over four adjacent grid cells. NA87-25, ODP980 and NEEM records are displayed here on the recent AICC2012 chronology (Capron et al., 2014; Bazin et al. 2013). The black dot on the right hand side of the figures provides the corresponding simulated pre-industrial value. The 'plateau' is shaded in grey. The location of the marine and ice cores is provided in Table 2.

The impact of this difference on the timing of the maximum of temperature (MWT) is strong. The annual MWT occurs about 5 kyr later in allLR than in allGR in southern and eastern Asia. In the southern Pacific Ocean and in the southern Indian Ocean, MWT occurs around 130 kyr BP in allLR, while it takes place between 132 and 125 kyr BP in allGR. July MWT occurs 1-2 kyr later in allLR than in allGR in the North Atlantic Ocean and southern Africa, while it is about 5 kyr earlier in allLR than in allGR in the central Pacific.

Most of the impact of the choice of the scenario for the NH sheets evolution during the LIG is concentrated on the beginning of the simulation. The moderate continuous input of freshwater in the LR scenario leads to a colder Greenland, western France and North Atlantic in allLR than in allGR (Figure 13cde); the SH is less affected (not shown). However, no strong short-lasting cooling event is simulated in allLR as is the case in allGR at about 132 kyr BP. Moreover, the freshwater flux into the North Atlantic at 128 kyr BP in allLR has a cooling effect of ~2°C over western France (0.7°C over the NH) at a time when temperature reaches its maximum in allGR. Therefore, the maximum of surface temperature over western France is delayed with allLR compared to allGR. The

warming of the North Atlantic is slower in allLR than in allGR (Figure 13c) and therefore takes longer, from 133 to 127 kyr BP. Thus, the agreement with the reconstructions is better, although the differences are still large. Over Greenland the agreement between reconstructed and simulated (allLR) surface temperature before 122 kyr BP is very good. Thereafter, the cooling proceeds differently in observations and simulations, although the general trends remain in good agreement (Figure 13e).

Compared to the GR scenario, the LR scenario induces a delayed warming, mostly over Europe and the North Atlantic, at the beginning of the simulation. This delay induces large differences in surface temperature between the simulations using either GR or LR scenario. The difference reaches almost 10°C over Greenland, 5°C locally over the North Atlantic and almost 4°C over western France. The comparison with proxy data shows that the LR scenario for the evolution of the ice sheets leads to a better agreement between modelled and reconstructed climates than the GR scenario.

2.4.1.9. The role of the parameter sets

In order to test the potential impact of the model parameter sets, we performed and compared simulations with either parameter set *std* or parameter set 22, which has a higher sensitivity to a freshwater flux in the North Atlantic than *std*. Moreover, we used both scenarios for the LIG NH ice sheet (see Table 1) configuration and freshwater flux, either based on Grant et al. (2012) or on Lisiecki and Raymo (2005) (see Table 1). In all these simulations (allGR, allLR, parGR, parLR), the model is forced with changes in insolation and atmospheric greenhouse gases.

The AMOC in parGR is weaker than in allGR throughout LIG. Moreover, the difference between the simulations decreases from 4.2Sv at 135 kyr BP to 1.4Sv at 115 kyr BP (Figure 13b). Prior to 127 kyr BP, the AMOC is strongly affected by the evolution of the ice sheets. Nevertheless, for the same ice sheet scenario, the AMOC simulated with parameter set 22 is slightly weaker than with *std*, and remains weaker until 121 kyr BP. Starting from 120 kyr BP, the role of the parameter set in the simulated AMOC is small compared to the role of the ice sheets.

The global annual mean surface temperature is cooler in parGR than in allGR during the LIG. The average difference is 0.3°C. It amounts to ~0.6°C at 135 kyr, decreasing to only ~0.2°C between 127 and 121 kyr BP, then increasing back to 0.5°C at 115 kyr BP. Between 127.0 and 120.5 kyr BP, the temperature difference related to the choice of the parameter set may vary according to the location. For most of the locations, the major driver of temperature changes is the ice sheet changes, in particular the freshwater flow from the ice sheets. Similar conclusions can be drawn from the comparison of allLR and parLR. Therefore, we can conclude that the contribution of the parameter sets is actually very modest. However, we must take care here because the sensitivity of model

configurations used are in the lower end of the full range of the tested model configurations (Goosse et al., 2007; Loutre et al., 2011; Goelzer et al., 2011).

2.4.2. Impact of Antarctic and Greenland freshwater fluxes

As a next step, ice sheet changes of the Greenland and Antarctic ice sheets are included to study their impact on the climate evolution. In this set-up the model is forced with realistic ice sheet boundary conditions from offline simulations of high-resolution models of the Antarctic and Greenland ice sheets next to reconstructions of the remaining NH ice sheets (LR as above).

2.4.2.1. Model set-up including all ice sheet components

The configuration of the Greenland and Antarctic ice sheet models and the forcing interface follows the description in Goosse et al. (2010) with the following exceptions. Forcing for the ice sheet models is derived from scaling present-day observations of temperature and precipitation with indices based on ice core records, as is standard for long-term paleo ice sheet modelling (e.g. Huybrechts, 1990; Letreguilly et al., 1991; Zweck and Huybrechts, 2005; Greve et al., 2011; Stone et al., 2013). For the GrIS the forcing record was created following Fürst et al. (2015) by combining a synthesised Greenland $\delta^{18}O$ record derived from Antarctica Dome C using a bipolar seesaw model (Barker et al., 2011) with the NEEM temperature reconstruction (NEEM community members, 2013) between 128.44 kyr BP and 120 kyr BP. The Barker δ18O record is converted to temperature with a constant factor $T = 1.5*(\delta^{18}O + 34.83)$. Positive temperature anomalies of the NEEM record are scaled by a factor 0.6 to fulfil constraints on maximal ice sheet retreat from Camp Century and Dye3 ice core locations that are assumed to have been ice covered during the LIG.

The AIS forcing is derived directly from the Antarctica Dome C record (EPICA community members, 2004). Furthermore, both ice sheet models are forced by changes in global sea-level stand based (for the GrIS) on the benthic deep-sea record of Lisiecki and Raymo (2005) and (for the AIS, where the sea-level changes are the dominant forcing) on a more recent sea-level reconstruction using Red Sea data (Grant et al., 2012). The chronology of the latter may be expected to be more accurate since, unlike for the first, ice volume is independent of deep-sea temperatures in its reconstruction. Finally, the Antarctic ice sheet model is run at a horizontal resolution of 20 x 20 km instead of 10 km x 10 km (as in the standard configuration and for the Greenland ice sheet model) due to computational constraints for the relatively long duration of the LIG simulation.

To embed the dynamic GrIS simulation in the other NH boundary conditions, the geometric evolution of the Greenland ice sheet masks out prescribed changes where ice is present. In that case, the prescribed ice sheet evolution and associated FWF are not

limited by the present-day configuration of the Greenland ice sheet as in Loutre et al. (2014) and above. With activated GrIS and AIS evolution, their dynamically calculated FWF (Figure 15b) replace the background freshwater flux from runoff over land calculated by the land model. The ice sheet evolution is illustrated in Figure 14.

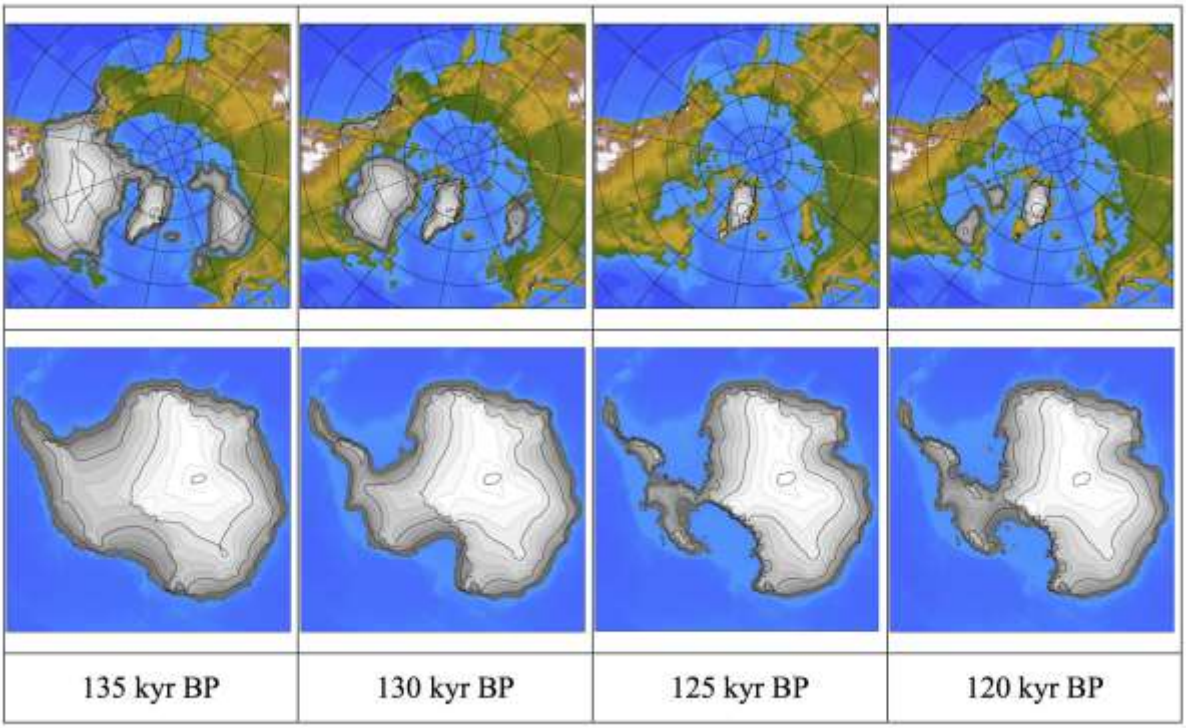

Figure 14: Evolution of reconstructed Northern Hemisphere ice sheets and embedded modelled Greenland ice sheet (top) and modelled Antarctic ice sheet (bottom) used as boundary conditions for the climate model.

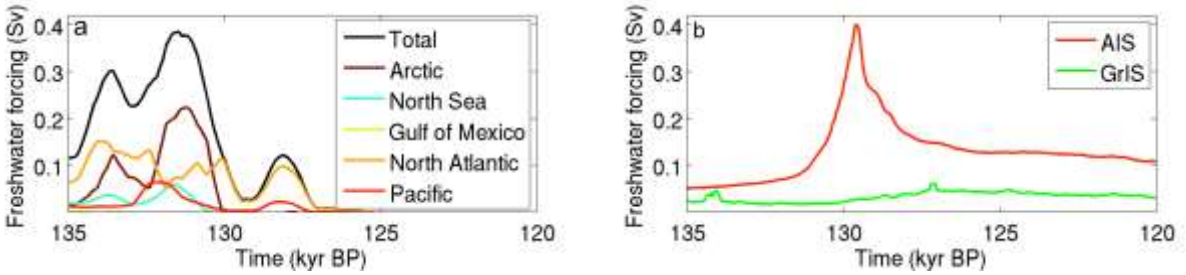

Figure 15: Reconstructed freshwater forcing from the NH ice sheets (a) and from the Greenland and Antarctic ice sheets (b). See Goelzer et al. (2012b) for definition of oceanic basins.

2.4.2.2. Initialisation of the climate model with all ice sheets included

The goal of our initialisation technique is to prepare a climate model state for the transient simulations starting at 135 kyr BP exhibiting a minimal coupling drift. Both the Greenland and Antarctic ice sheet models are integrated over the preceding glacial cycles and the entire LIG in stand-alone mode. The climate model is then initialized to a

steady state with ice sheet boundary conditions, greenhouse gas forcing and orbital parameters for the time of coupling (135 kyr BP). In this way, when LOVECLIM is integrated forward in time for transient experiments, the climate component is already relaxed to the ice sheet boundary conditions and exhibits a minimal model drift in unforced control experiments (not shown).

2.4.2.3. Experimental setup

In the following, we will compare results of the reference experiment with all ice sheet boundary conditions evolving in time (Reference) to experiments in which the ice sheet boundary conditions are partially fixed to the pre-industrial configuration (Table 3). To disentangle the effects of the individual ice sheets, the experiments noGfwf (suppressed GrIS freshwater fluxes) and noAGfwf (suppressed FWF from both AIS and GrIS) are complemented by two predecessor experiments with fixed AIS and GrIS and evolving NH boundary conditions (allLR), as well as a climate experiment forced by insolation and GHG changes only with all ice sheet boundary conditions fixed (IGonly).

Table 3: Matrix of all experiments and the respective ice sheet components that evolve in time (yes) or are fixed (no). In the latter case, freshwater fluxes (FWF, grey) are kept constant and topography and surface albedo are fixed to the preindustrial configuration.

EXP	topo NH	FWF NH	topo GrIS	FWF GrIS	topo AIS	FWF AIS
Reference	yes	yes	yes	yes	yes	yes
noGfwf	yes	yes	yes	no	yes	yes
noAGfwf	yes	yes	yes	no	yes	no
allLR	yes	yes	no	no	no	no
IGonly	no	no	no	no	no	no

2.4.2.4. Temperature evolution at the onset of the LIG

As shown by Loutre et al. (2014), including the forcing from the NH ice sheets in terms of configuration and FWF is crucial to simulate the onset of the LIG temperature increase and amplitude variations with LOVECLIM v.1.3 more in line with proxy records. This helps to partially overcome problems of EMICs (and general circulation models) to simulate the strong temperature contrasts inferred from proxy reconstructions (Bakker et al., 2013; Lunt et al., 2013). The increased amplitude of temperature changes in simulations including NH ice sheet boundary conditions is both due to albedo and elevation changes and to a larger extent due to the implied freshwater forcing from the NH ice sheets (Loutre et al., 2014). Therefore, these experiments are complemented in the present work by model runs that additionally include changes in ice sheet configuration and FWF from the Greenland and Antarctic ice sheets.

The temperature evolution (Figure 16) before 127 kyr BP is in both hemispheres strongly influenced by the ice sheet boundary conditions and in particular by the freshwater forcing from the ice sheets. The experiments including FWF from the NH ice sheets (noAG and Reference) clearly show temperature variations on the multi-millennial time scale in both hemispheres following variations in ice sheet freshwater input (cf. Figure 15). Differences in the temperature evolution between noAG and Reference are small in the NH, where the additional freshwater flux from Greenland is small compared to the other sources. In the SH, by contrast, a large perturbation arises around 130 kyr BP, when FWF from the AIS peak. Global mean and hemispheric mean temperatures are similar in all runs after ~127 kyr BP, when the ice sheets have largely reached their interglacial configuration and their FWF remain similar, except for the GrIS, which is retreating until ~120 kyr BP but accounts for only a small contribution. The location of largest freshwater induced temperature variations in the NH is the North Atlantic between 40° N and 80° N, where changes in the AMOC are the cause for a perturbation of the northward oceanic heat transport and temperature changes which are further amplified by sea ice-albedo and insulation feedbacks. Greenland experiences maximum summer warming in the Reference experiment around 125 kyr BP of less than 3°C over remaining ice covered central Greenland, but marginal warming in the north is up to 10°C and up to 14°C over southern margins over a then ice free tundra. These strong warming trends in the ice sheet periphery are due to a combination of elevation changes and local albedo changes, confined to the immediate region of ice sheet lowering and retreat. In the SH, the largest temperature perturbations linked to both NH and SH freshwater fluxes occur in the SO. The largest warming over the ice sheet itself is simulated over the WAIS and is mainly a consequence of the local elevation changes as the ice sheet retreats. However, mainly due to the marine based character of the WAIS, albedo changes are much more limited compared to Greenland as the retreating ice sheet surface is mostly replaced by sea ice.

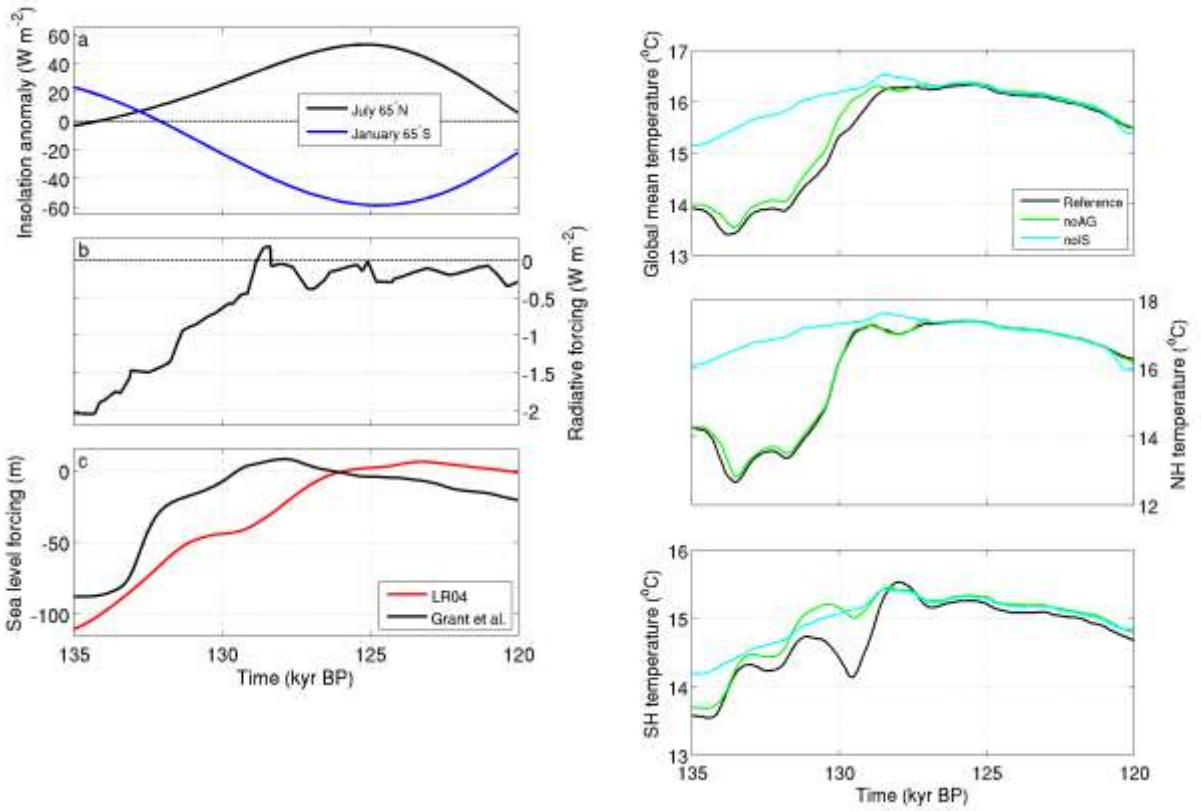

Figure 16: (Left) Prescribed model forcings. (a) Average monthly insolation anomaly relative to the pre-industrial at 65° North in July (black) and 65° South in January (blue). (b) combined radiative forcing anomaly of prescribed greenhouse gas concentrations (CO_2, CH_4, N_2O) relative to the pre-industrial. (c) sea-level forcing for the ice sheet components derived from either oceanic $\delta^{18}O$ data (Lisiecki and Raymo, 2005) scaled to a global sea-level contrast between LGM and present day of 130 m (red) or derived from a Red Sea relative sea-level record (Grant et al. 2012, black). (Right) Evolution of global mean and hemispheric mean surface temperature for experiments with different ice sheet forcing included. Curves are smoothed with a running mean of 200 years for better comparison.

2.4.2.5. Influence of ice sheet meltwater fluxes

To study the role of the different freshwater contributions from the ice sheets in more detail and evaluate their importance for the climate evolution, we compare additional simulations where FWF from the Greenland and Antarctic ice sheets are partially suppressed relative to the Reference experiment (Figure 17). The Antarctic ice sheet forcing leads to considerable changes in the Southern Hemisphere, but has very little impact on the NH temperature evolution. Conversely, variations in the NH and GrIS freshwater forcing on millennial time-scales imply temperature changes in the SH on the background of general LIG warming. Differences between the experiments in the AMOC evolution (Figure 17b) are largely explained by whether FWF from the NH ice sheets and the Greenland ice sheet are included or not. The additional effect of the FWF from the GrIS is limited compared to the large impact of the general NH ice sheet forcing and consists of an additional weakening of the AMOC. It is most pronounced

during periods of AMOC recovery and after 130 kyr BP, when melting of the GrIS beyond its present day configuration sets in. The simulated evolution of AMOC strength is in good agreement with paleo evidence based on $\delta^{13}C$ data (Bauch et al., 2012) and in particular with a recent reconstruction based on chemical water tracers (Böhm et al., 2015). The timing of Heinrich Stadial 11 and the variations in AMOC strength thereafter are well captured by our reference simulation, which gives independent credibility to our NH ice sheet reconstructions. The evolution of NH sea ice area (Figure 17c) shows maxima at times of AMOC minima and vice versa and is closely linked to NH surface temperature variations (cf. Figure 16b) by modifying the heat exchange between ocean and atmosphere. The largest sea ice area between 135 and 130 kyr BP is simulated in the Reference experiment, which also exhibits the lowest AMOC strength of all experiments.

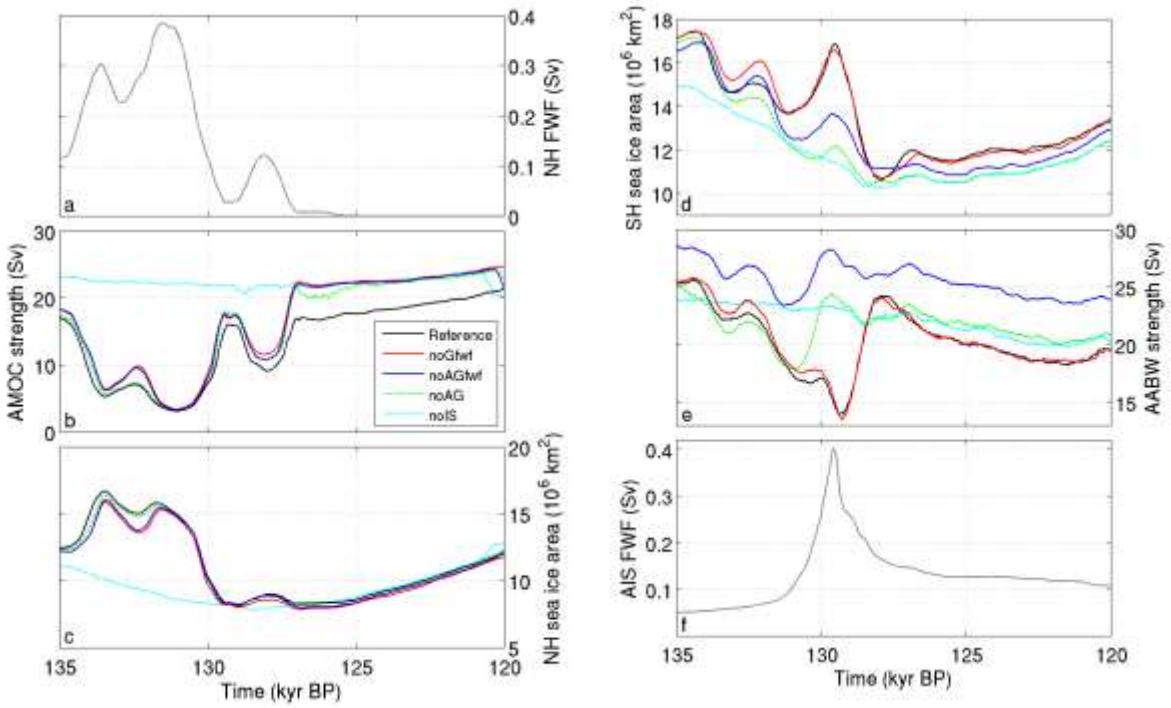

Figure 17: Freshwater forcing and oceanic response characteristics. NH (a) and Antarctic ice sheet freshwater fluxes (f), strength of the Atlantic meridional overturning circulation (b), NH sea ice area (c), SH sea ice area (d) and strength of Antarctic Bottom Water formation (e) for the different experiments with and without freshwater forcing from Greenland, Antarctic and NH ice sheet melting. Curves are smoothed with a running mean of 200 years for better comparison.

The situation in the SH is more complex as surface temperature and sea ice evolution are influenced both by freshwater forcing from the Antarctic ice sheet and also by the FWF in the NH. The AMOC variability gives rise to changes in the SH through the so-called interhemispheric see-saw effect (Stocker 1998). The SH begins to warm as the NH cools due to modified oceanic heat transport across the equator. Minima in SH temperature (cf. Figure 16c) and maxima in SH sea ice area (Figure 17d) are therefore associated with maxima in AMOC strength. The additional effect of including GrIS

freshwater forcing is consequently also felt in a warmer SH with less sea ice formation. However, the influence of GrIS freshwater fluxes and consequential AMOC variations on the SH temperature appears to be mostly limited to the beginning of the experiment between ~135 and 131 kyr BP. It could be speculated that this is related to the larger extent of the SH sea ice in a colder climate, making the system more sensitive due to an increased potential for sea ice-albedo and insulation feedbacks. We also note that modelled periods of increased NH freshwater fluxes, reduced AMOC strength and higher SH temperatures are roughly in phase with periods of steeper increase in GHG concentrations (cf. Figure 16 left), in line with evidence from marine sediment proxies that indicate that CO_2 concentration rose most rapidly when North Atlantic Deep Water shoaled (Ahn and Brook, 2008). Since GHGs and NH freshwater fluxes are (independently) prescribed in our experiments, the described in-phase relationship lends further credibility to our NH ice sheet reconstruction.

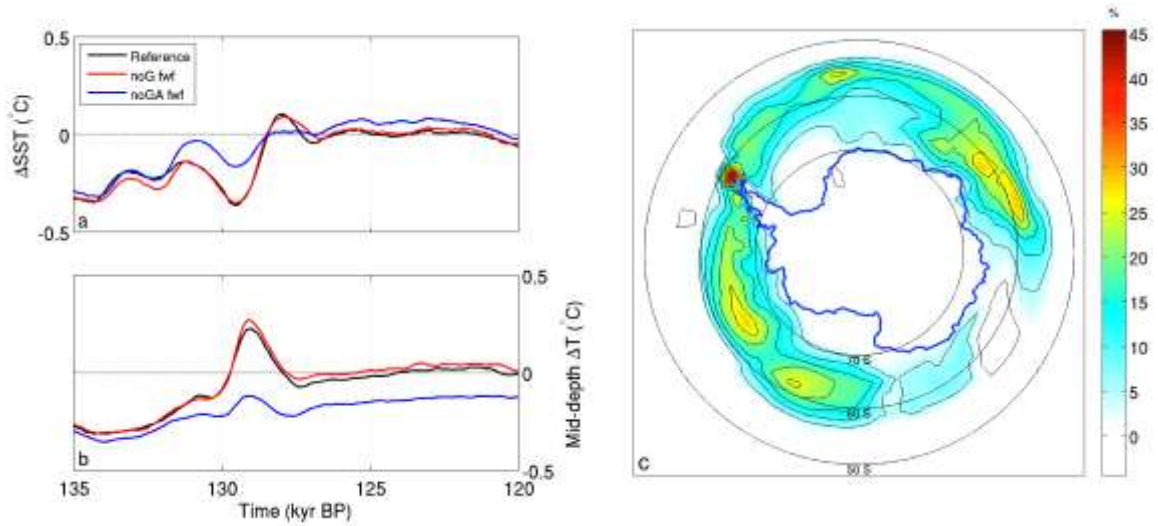

Figure 18: Evolution of annual mean sea surface temperature (a) and mid-depth (485-700 m) ocean temperature (b) anomalies relative to the pre-industrial in close proximity to the Antarctic ice sheet (south of 63°S). (c) Meltwater related changes in annual mean sea ice area at 129 kyr BP from differences between experiments Reference and noAGfwf in per cent. The blue contour outlines the observed ice-shelf edge and grounded ice margin of the present-day Antarctic ice sheet for illustration. All curves (a, b) are smoothed with a running mean of 200 years for better comparison.

The FWF from Antarctic ice sheet melting (Figure 17f) increases the SO sea ice area by freshening and stratifying the upper ocean waters, which in turn leads to lower surface temperatures. In our experiments, the increased freshwater flux from the retreating AIS between 131 and 129 kyr BP is in phase with a period of transient AMOC strengthening, which leads to a combined effect of surface cooling and sea ice expansion in the SO.

The formation of Antarctic Bottom Water (AABW) is strongly controlled by salinity and sea ice area (and therefore temperature) of the polar surface waters and hence by both

Antarctic and indirectly by NH freshwater fluxes. The AABW formation (Figure 17e) is stronger for saltier and colder surface conditions and therefore strongest in case noAGfwf, where FWF are suppressed from the AIS (saltier) and the GrIS (colder). For a similar Antarctic freshwater forcing, the AABW formation is stronger for a larger SH sea ice area. Including Antarctic FWF (in noAGfwf) leads to a generally weaker AABW formation (compared to noGfwf) as surface waters become fresher. These relationships imply also that a stronger decrease in AABW formation, associated with decreased CO_2 uptake by the ocean can be found for periods of steeper increase in prescribed radiative forcing. Again, this appears to support consistency in timing between prescribed radiative and NH ice sheet forcing in our modelling.

2.4.2.6. Temperature evolution in the Southern Ocean

The amplitude of variations in SH surface temperature at the millennial time scale induced by NH freshwater fluxes is the strongest in the SO, where anomalies can be amplified by sea ice-albedo and insulation feedbacks. This is also the region that experiences the largest temperature change due to FWF from the Antarctic ice sheet itself.

In order to study the effect of Antarctic FWF in more detail, we also analysed the oceanic temperature evolution at different levels south of 63°S (Figure 18). The effect of the AIS freshwater flux in the reference experiment becomes visible in the sea surface temperature after 132 kyr BP (Figure 18a) as a cooling due to stratification and sea ice expansion (Figure 18c). At the same time, the subsurface ocean warms (Figure 18b) as heat is trapped under the stratified surface waters and expanding sea ice area. When the FWF decline towards the end of the AIS retreat around 128 kyr BP, sea ice retreats again and the heat is released to the atmosphere, where it generates an overshoot in SST compared to the experiment with constant Antarctic freshwater fluxes (noAGfwf). The largest effect of this heat buffering is found in winter in regions of strongest warming in the Bellingshausen Sea and off the Gunnerus ridge adjacent to Dronning Maud Land. The maximum sea-ice extent in the SH (Figure 18c) occurs at the time of largest surface cooling at 129.5 kyr BP.

As a further consequence, the time of maximum annual mean surface air temperature (defined as MWT for Maximum Warmth Timing; Bakker et al., 2013) in the SO differs by several thousand years between experiments. Including Antarctic FWF leads to an earlier MWT (by up to 2 kyr) in large parts of the SO south of 60°S and in the central and eastern parts of the Atlantic sector of the SO up to 40°S. Conversely, a later MWT (by up to 3 kyr) is found in the Indian and Pacific sectors of the SO north of 60°S when Antarctic FWF is accounted for. In the Reference experiment and noGfwf, the MWT lies relatively homogeneously between -129 kyr and -128 kyr for the entire SO south of 45°S and falls together with the overshoot in SST after the peak input of Antarctic FWF

(Figure 19). The observed changes of the MWT in the SO due to the additional Antarctic freshwater input can therefore in either way be understood as a shift towards the time when heat from the mid-depth ocean buffer is released to the surface.

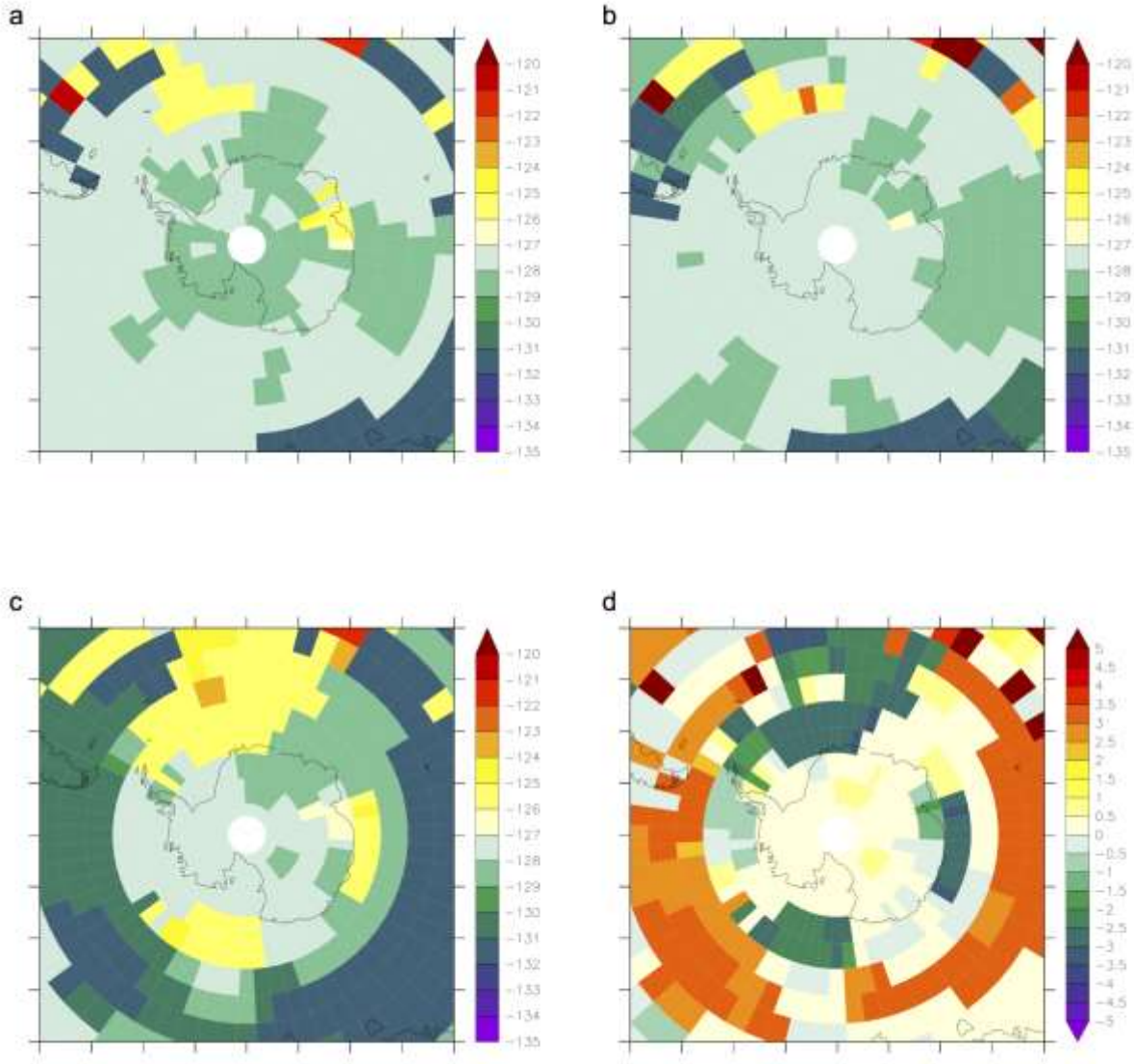

Figure 19: Time of maximum surface air temperature (MWT) in kyr BP for experiments Reference (a), noGfwf (b) and noAGfwf (c) and difference in MWT between experiments noGfwf and noAGfwf (d) in kyr, showing the shift of the MWT when Antarctic freshwater fluxes are included.

The freshwater induced surface cooling at the onset of the LIG appears to be superficial and relatively short lived and of clearly different signature compared e.g. to the Antarctic cold reversal during the last deglaciation. The cooling event is indeed not recorded in our modelled temperature evolution over central East Antarctica, in line with a lack of its signature in Antarctic ice core records for that time period (Petit et al., 1999, EPICA community members, 2004). A sea ice expansion during Termination II together with an *oceanic* cold reversal around 129.5 kyr BP is however recorded in some deep-sea

sediment cores, where the composition of planktonic diatoms suggests meltwater as the primary cause (Bianchi and Gersonde, 2002; Cortese and Abelmann, 2002).

2.4.2.7. Discussion

Despite remaining uncertainties in the timing of ice sheet retreat during Termination II, we find several lines of evidence in support of our ice sheet reconstructions and the associated climatic signatures. The NH ice sheet reconstruction shows some similarity with the IRD signal recorded in North Atlantic sediment cores (Kandiano et al., 2004; Oppo et al., 2006), while the simulated evolution of the AMOC strength (Figure 17a) is in good agreement with a recent reconstruction based on chemical water tracers (Böhm et al., 2015). The combination of NH and SH sourced freshwater forcing variations produces a stronger decrease in AABW formation, associated with decreased CO_2 uptake by the ocean for periods of steeper increase in prescribed radiative forcing, in line with evidence from marine sediment proxies that indicate that CO_2 concentration rose most rapidly when North Atlantic Deep Water shoaled (Ahn and Brook, 2008). Our modelling results furthermore suggest that the major Antarctic ice sheet retreat from its glacial configuration could be constrained by an oceanic cold event recorded in several SO sediment cores around Antarctica (Bianchi and Gersonde, 2002; Cortese and Abelmann, 2002). As a schematic sensitivity test to uncertainties in the overall glacial Antarctic ice sheet volume, we have performed one more experiment identical to Reference except for Antarctic FWF scaled to 50% of their reference value. The resulting magnitude of the SO cold event and overshoot is lower but exhibits the same timing and spatial expression as in the reference case. The described mechanisms and effects can therefore be considered robust to differences in the assumed glacial Antarctic ice sheet volume.

The Greenland ice sheet is generally assumed to have remained largely intact during the LIG (e.g. Robinson et al., 2011; Colville et al., 2011; Stone et al., 2013; NEEM community members, 2013) and indirect evidence of its freshwater contribution may be difficult to find due to the low amplitude compared to the other Northern Hemisphere ice sheets. However, recent ice core reconstructions of the temperature evolution at the NEEM ice core site (NEEM community members, 2013) point to a late retreat with a peak sea-level contribution close to 120 kyr BP. Even if the amplitude of the central estimate of the reconstructed temperature anomaly may be debated (e.g. Van de Berg et al., 2013; Merz et al., 2014; Sjolte et al., 2014; Steen-Larsen et al., 2014), the ice sheet can be assumed to lose mass approximately as long as the climatic temperature anomaly above the ice sheet remains above zero. Based on the NEEM record, which has been used as forcing time series in our stand-alone GrIS experiment, FWF from the GrIS peak at ~125 kyr BP, but remains elevated until around 120 kyr BP above the steady state background flux of an ice sheet in equilibrium with the climate. The additional FWF

from melting of the Greenland ice sheet results in relatively low temperatures over Southeast Greenland in response to a weakening of the AMOC (not shown). The interaction between GrIS meltwater fluxes and oceanic circulation hence gives rise to a negative feedback on ice sheet retreat. This aspect could play an important role for the stability of the southern dome of the ice sheet and should be examined further with fully coupled climate-ice sheet simulations.

In general, the NH freshwater forcing leads to variations in the strength of the AMOC and North Atlantic cooling and additionally through the bipolar see-saw effect, to temperature changes in the SH. The only moment mid-depth ocean temperatures close to AIS grounding lines are above pre-industrial values in our experiments is during the oceanic cold reversal around 129.5 kyr BP, induced by anomalous FWF from the retreating Antarctic ice sheet. During this period, SO mid-depth temperature anomalies relative to the pre-industrial reach up to 0.3 K, which could provide a positive but rather limited feedback on ice sheet retreat, similar to what has been suggested by Golledge et al. (2014) for meltwater pulse 1A during the last termination. However, the oceanic warming recorded in our model is not strong and the duration of the perturbation does not appear to be long enough for a sustained impact on the retreat of the ice sheet. Furthermore, the peak in freshwater flux appears when the ice sheet has already retreated considerably and WAIS grounding lines are located mostly on the continental shelves, more protected from the warm water build-up in the mid-depth ocean. A large-scale marine ice sheet retreat of the likely less vulnerable East Antarctic ice sheet sectors (Mengel and Levermann, 2014) appears particularly unlikely, given the environmental forcing at the time apparent in our modelling results. However, in depth studies of these interactions require detailed coupled simulations of the entire ocean-ice sheet system.

2.4.3. Coupled ice-sheet simulations

Where in the experiments above the ice sheet components were prescribed and used as forcing for the climate model, they are fully two-way coupled in this part with information exchanged every full year. Because of the relatively coarse resolution of the atmosphere in LOVECLIM, the ice sheet models are forced with temperature anomalies and precipitation ratios relative to the pre-industrial reference climate and using the updated interfaces as described above. The ice sheet models in turn provide the climate model with changing topography, ice sheet extent (albedo) and spatially and temporally variable freshwater fluxes, unmodified to earlier versions of the model (Goosse et al., 2010).

2.4.3.1. Modelled sea-level change

The modelled sea-level evolution takes into account contributions from the prescribed NH ice sheets, the Greenland and Antarctic ice sheets and the steric contribution due to density changes of the ocean water. The only component not explicitly modelled is the

contribution of glaciers and small ice caps, which have been estimated to give a maximum contribution of 0.42 $\pm$ 0.11 m during the LIG (Masson-Delmotte et al., 2013) and may contain as much as 5-6 m SLE during glacial times (CLIMAP, 1981; Clark et al., 2001).

The Antarctic contribution to global sea-level change is calculated taking into account corrections for ice replacing and being replaced by seawater and seawater being replaced by isostatic bedrock movement, both mainly of importance for the marine sectors of the WAIS. The additional correction for bedrock changes is responsible for a $\sim$3 m lower sea-level contribution at 135 kyr BP compared to taking only changes in volume above floatation into account. This additional sea-level depression arises from depressed bedrock under the load of the ice in the marine sectors of the ice sheet.

For the Greenland ice sheet the same corrections are applied, where the marine extent of ice grounded below sea level is parameterised. However, the corrections imply only a $\sim$30 cm lower contrast to present day sea level due to Greenland ice sheet expansion at 135 kyr BP and $\sim$15 cm higher at 130 kyr BP compared to calculations based on the entire grounded ice volume. The change in sign arises from bedrock changes in delayed response to ice loading changes.

The steric component of global sea level considers density changes due to local changes of temperature and salinity, but global salinity is restored as often done in ocean models to guarantee stability.

2.4.3.2. Model forcing

As before, the simulations are forced by time-dependent changes in greenhouse gas (GHG) concentrations and insolation. The radiative forcing associated with the reconstructed GHG levels is below preindustrial values for most of this period and hardly exceeds it at $\sim$128 kyr BP. The changes in the distribution of insolation received by the Earth are dynamically computed from the changes in the orbital configuration (Berger, 1978) and represent the governing forcing during peak LIG conditions.

In order to account for coastline changes and induced grounding line changes, both ice sheet models are forced by changes in global sea-level stand using a recent sea-level reconstruction based on Red Sea data (Grant et al., 2012). The chronology of the latter assumes ice volume to be independent of deep-sea temperatures, in contrast to directly using the scaled benthic $\delta^{18}O$ record as sea-level proxy (Shakun et al., 2015). In this sea-level forcing approach, local changes due to geoidal eustasy are not taken into account, which would result in lower amplitude sea-level changes close to the ice sheets, but would not be inconsistent with the spin-up of the models.

As a measure to ensure a realistic simulation of the Greenland ice sheet evolution, the temperature forcing from the climate model over the ice sheet needs to be rescaled. In absence of such scaling, the ice sheet almost completely melts away over the course of

the LIG in disagreement with the ice core data, which suggests a large remaining ice sheet during the LIG (Dansgaard et al., 1982; NEEM community members, 2013). In the absence of firm constraints on climate evolution over the ice sheet, the temperature scaling in the present study represents a pragmatic solution to produce an ice sheet evolution reasonably in line with ice core constraints on minimum ice sheet extent during the LIG. A uniform scaling factor relative to the unmodified atmospheric temperature of R = 0.4 was adopted in the reference experiment and is later compared to two sensitivity experiments with modified scaling (R = 0.5, 0.3).

The fully coupled experiments are accompanied by additional sensitivity experiments, in which the ice sheet models are forced in stand-alone mode with (modified) climate forcing produced by the fully coupled runs. These experiments serve to study ice sheet sensitivity in response to changes in the climate forcing and are also used to evaluate ice sheet-climate feedbacks in comparison between the coupled and un-coupled system. The ice sheet response in the reference stand-alone experiment (forced offline with the recorded climate forcing of the coupled reference run) is by construction identical to the response in the fully coupled run. Additional experiments have been run with modified temperature scaling for the Greenland ice sheet (R = 0.5, 0.3), which can be compared to the respective fully coupled experiment. For the AIS, experiments with suppressed shelf melting have been performed to isolate the effect of ocean temperature changes on the ice volume evolution and sea-level contribution.

2.4.3.3. Climate evolution of the coupled model

The modelled LIG climate evolution and comparison with reconstructions were presented in detail above. Differences arise from a different ice sheet evolution and feedbacks between climate and ice sheets that are taken into account in the fully coupled approach.

Global annual mean near-surface air temperature in the Reference experiment shows a distinct increase until 129 kyr BP in response to orbital and greenhouse gas forcing and to an even larger extent in response to changes in ice sheet boundary conditions (Figure 20). The peak warming reaches 0.3 °C above the pre-industrial at 125.5 kyr BP. Thereafter, cooling sets in and continues at a much lower rate compared to the rate of warming before 129 kyr BP. The importance of ice sheet changes is illustrated by comparing the Reference experiment with a climate simulation forced by insolation and GHG changes only (noIS) and with a one-way coupled climate model run forced with prescribed NH, Antarctic and Greenland ice sheet changes (one-way). The much larger temperature contrast at the onset of the LIG compared to noIS arises from changes in surface albedo and melt water fluxes of the Northern Hemisphere ice sheets. The episode of relative cooling in Reference with a local temperature minimum at 128 kyr BP is due to cooling of the Southern ocean and sea-ice expansion in response to large

Antarctic freshwater fluxes, which occur 2 kyr later compared to the one-way experiment.

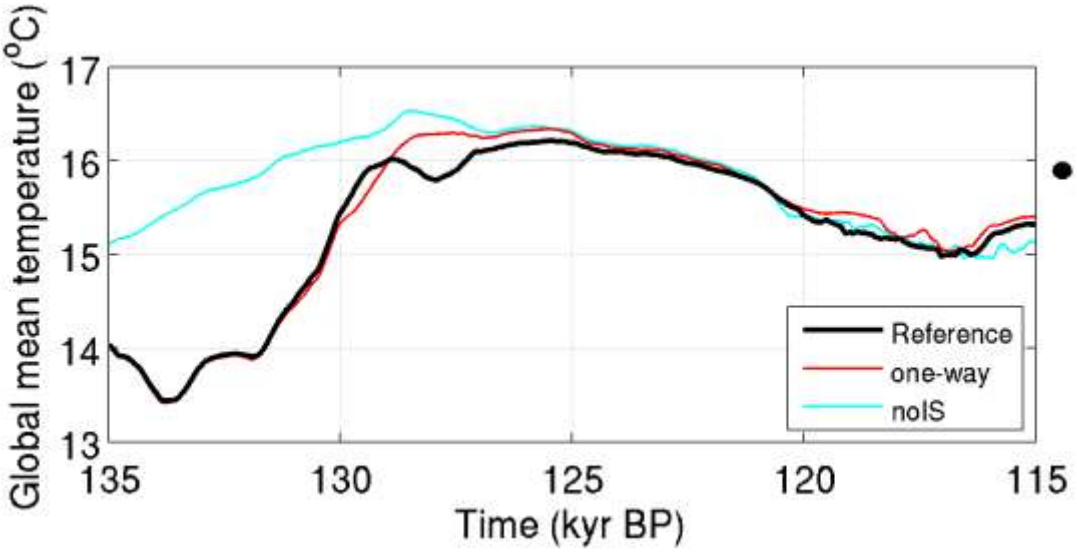

Figure 20: Global annual mean near-surface air temperature evolution of the Reference run (black) compared to experiments with prescribed Greenland and Antarctic ice sheets (one-way, red) and no ice sheet changes at all (noIS, light blue). The filled circle on the right axis indicates the temperature for a pre-industrial control experiment of the Reference model with present day ice sheet configuration.

2.4.3.4. Greenland ice sheet

The Greenland ice sheet evolution over the LIG period is largely controlled by changes in the surface mass balance with predominant importance of the ablation (Figure 21). Marginal summer surface melt water runoff is the dominant mass loss of the ice sheet after 130 kyr BP, when the ice sheet has retreated largely on land. Due to increased temperatures over Greenland, the mean accumulation rate (averaged over the ice covered area) is consistently above the present-day reference level after 128 kyr BP, but increases to at most 18% higher. Conversely, the mean ablation rate over Greenland shows an up to threefold increase compared to the present day with consistently higher-than present rates between 130.5 kyr to 120.5 kyr BP. Temperature anomalies responsible for the increased ablation are on average above zero between 129.5 kyr to 120.5 kyr BP and peak at 1.3 °C (after scaling) around 125 kyr BP. The calving flux decreases as the ice sheet retreats from the coast (in line with decreasing area and volume, Figure 21) and as surface melting and runoff increase, removing some of the ice before it can reach the coast. In the second half of the experiment, runoff decreases with decreasing temperature anomalies and the calving flux increases again with increasing ice area and volume.

Entering the warm period, the furthest retreat of the ice sheet occurs in the southwest and northwest (Figure 22), accompanied by an overall retreat from the coast. Conversely, the ice sheet gains in surface elevation over the central dome due to increased accumulation. By 115 kyr BP, the ice sheet has regrown beyond its present day area almost everywhere and contact with the ocean is increasing. The GrIS volume change translates into a sea-level contribution peak of 1.4 m at 123 kyr BP (Figure 26, left). For the two sensitivity experiments (high, low) with modified scaling (R = 0.5, 0.3), the contribution changes to 2.8 m and 0.6 m, respectively.

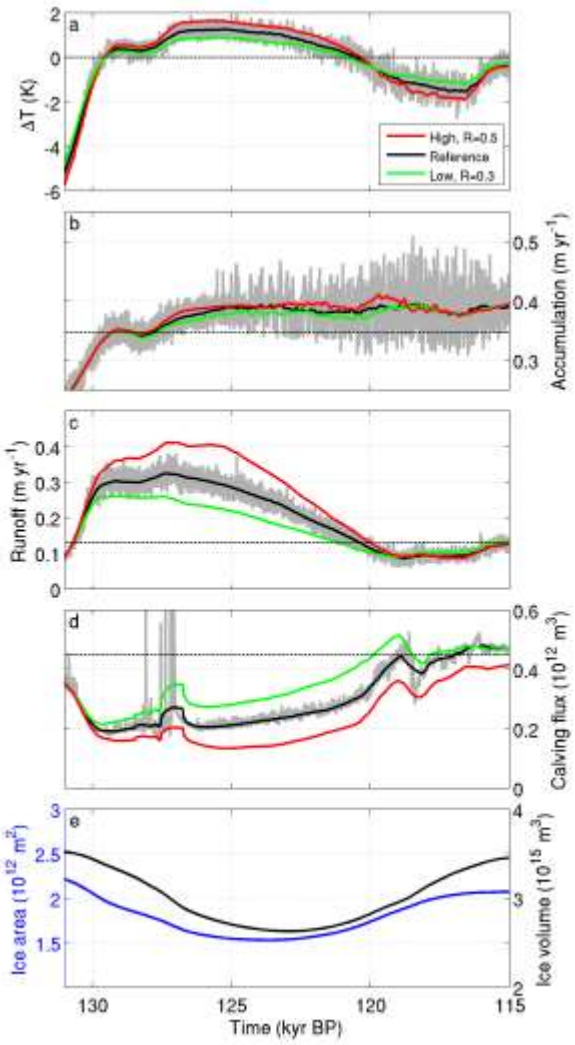

Figure 21: Greenland ice sheet forcing characteristics for the reference run (black) and with higher (red) and lower (green) temperature scaling. Climatic temperature anomaly (a), accumulation rate (b) and runoff rate (c) are given as ice sheet wide spatial averages over grounded ice. Calving flux (d) and other mass balance terms (b, c) are given in water equivalent. (e) Ice area (blue) and ice volume (black) for the Reference run. All lines are smoothed with a 400 years running mean except for the grey lines giving the full annual time resolution for the reference run.

NEEM ice core data (NEEM community members, 2013) and radiostratigraphy of the entire ice sheet (MacGregor et al., 2015) indicate that the NEEM ice core site was ice covered through the entire Eemian as is the case for our Reference experiment. Elevation changes from that ice core are however not well constrained and leaves room for a wide range of possible retreat patterns of the northern GrIS (e.g. Born et al., 2012). The Camp Century ice core record contains some ice in the lowest part with a colder signature then ice dated as belonging to the Eemian period (Dansgaard et al., 1982). It is likely that this ice is from before the Eemian even in view of possible disturbance of the lower levels, which was shown to exist for the NEEM core site (NEEM community members, 2013). Reconstruction of the age structure from radiostratigraphy (MacGregor et al., 2015) shows no ice at the Camp Century location before 115 kyr BP. However, it is possible that isochrones were disturbed or not possible to interpret. In view of this evidence, the north-western retreat of the ice sheet in our Reference simulation may be too far, a direct result of the climatic forcing, which is largely unconstrained. However, a different climate forcing could equally produce e.g. a larger northern retreat still in line with the paleo evidence (Born et al., 2012). Some more thinning and retreat in the south is also possible without violating constraints on minimal ice sheet extent from Dye-3 (Dansgaard et al., 1982). LIG ice cover of the Dye-3 site is not a necessity when taking into consideration that older ice found at the base of the core could have flowed in from a higher elevation.

The climatic temperature anomaly over central Greenland in the coupled model shows a flat maximum around 127 kyr BP, similar to the global temperature evolution, but 2 kyr earlier compared to the NEEM reconstructions (NEEM community members, 2013). If assuming present-day configuration and spatially constant warming, ice mass loss from the GrIS could be expected to occur approximately as long as the temperature anomaly remains above zero, which is the case until ~ 122 kyr BP in the model and until ~ 119 kyr BP in the NEEM reconstruction. With a lower surface elevation, the time the ice sheet starts to gain mass again would be further delayed. Even with considerable uncertainty due to uncertain spatial pattern of the warming, which modify this simply reasoning, we argue that the peak sea-level contribution from the GrIS has to occur late during the LIG. Based on the same argument, there is no evidence in the reconstructed NEEM temperature evolution suggesting a regrowth or substantial pause of melting of the Greenland ice sheet any time during the LIG.

The need for scaling the temperature forcing to produce a realistic Greenland ice sheet evolution equally applies when forcing our stand-alone ice sheet model with the temperature reconstructed from the NEEM ice core record (NEEM community members, 2013). It appears that practically any ice sheet model with (melt parameters tuned for the present day) would project a near-complete GrIS meltdown, if the amplitude and duration of warming suggested by the NEEM reconstructions would apply for the entire

ice sheet. This problem would be further amplified if insolation changes were explicitly taken into account in the melt model (Robinson and Goelzer, 2014). We refer to this mismatch between reconstructed temperatures and assumed minimum ice sheet extent as the "NEEM paradox". Several attempts to solve this paradox have been made by suggesting possible biases in the interpretation of the relationship between isotope ratio and temperature, which may not be assumed temporally and spatially constant (e.g. Merz et al., 2014; Sjolte et al., 2014; Steen-Larsen et al., 2014, Masson-Delmotte et al., 2015) and may be affected by changes in the precipitation regime (van De Berg et al., 2013). From the modelling point of view, the decisive question is over what spatial extent and when during the year the temperature reconstruction (and possible future reinterpretations) for the NEEM site should be assumed. A central Greenland warming of large magnitude could only be reconciled with the given geometric constraints if a (much) lower warming was present over the margins and during the summer, which is where and when the majority of the mass loss due to surface melting is taking place.

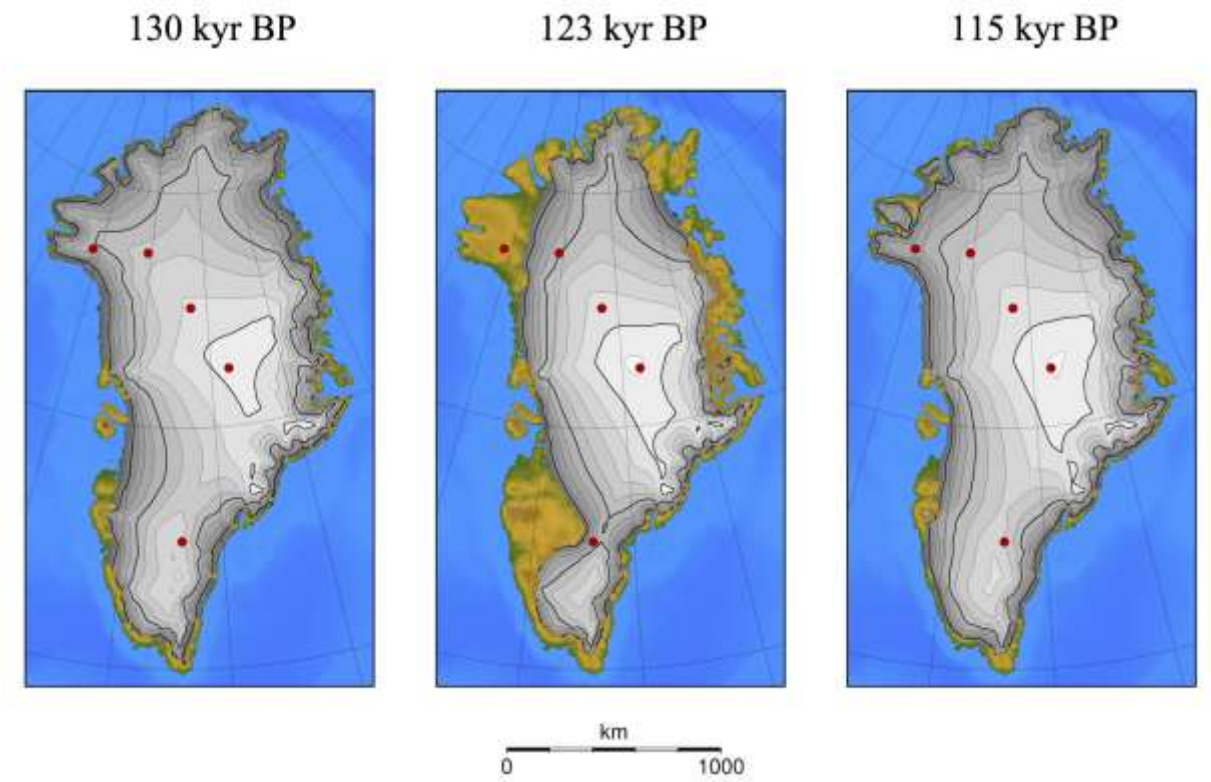

Figure 22: Greenland ice sheet geometry at 130 kyr BP (left), for the minimum ice sheet volume at 123 kyr BP with a SL contribution of 1.4 m (middle) and at the end of the reference experiment at 115 kyr BP (right).

The strength of the ice-climate feedback on Greenland was examined by comparing additional experiments in which the coupling between ice sheet and climate is modified. Results from the fully coupled model (FC) are compared to those from forced ice sheet runs (SA), which are driven with the climate forcing from the coupled

reference model run. In both cases the scaling of Greenland forcing temperature is set to a magnitude of 0.3 (low), 0.4 (ref) and 0.5 (high), respectively. When the feedback between ice sheet changes and climate is included in the coupled experiments, the warming over the margins is considerably increased (reduced) for experiment high (low) compared to the stand-alone experiments. Consequently, sea-level contributions show a non-linear dependence on the temperature scaling for the fully coupled run, while they are near linear for the forced runs (Figure 23, left). The dominant feedback mechanism arises from how changing albedo characteristics are taken into account for a melting ice sheet surface. The albedo can change due to changes in snow depth and also due to changes of the snow cover fraction, which indicates how much surface area of a grid cell is covered with snow (Figure 23, right). Both lead to lower albedo and increased temperatures in places where the ice sheet starts melting at the surface. The difference in warming between stand-alone and fully-coupled experiments is therefore located over the ice sheet margins and does not have a considerable influence on the NH or global temperature response. The albedo effects are near-instantaneous and their importance for the ice sheet response underline earlier findings that a basic albedo treatment is an essential aspect of a coupled ice–climate modelling system (e.g. Robinson and Goelzer, 2014). A third, but comparatively smaller effect arises from the retreating ice sheet margin being replaced by lower albedo tundra (Figure 23, right), which operates on much longer time scales.

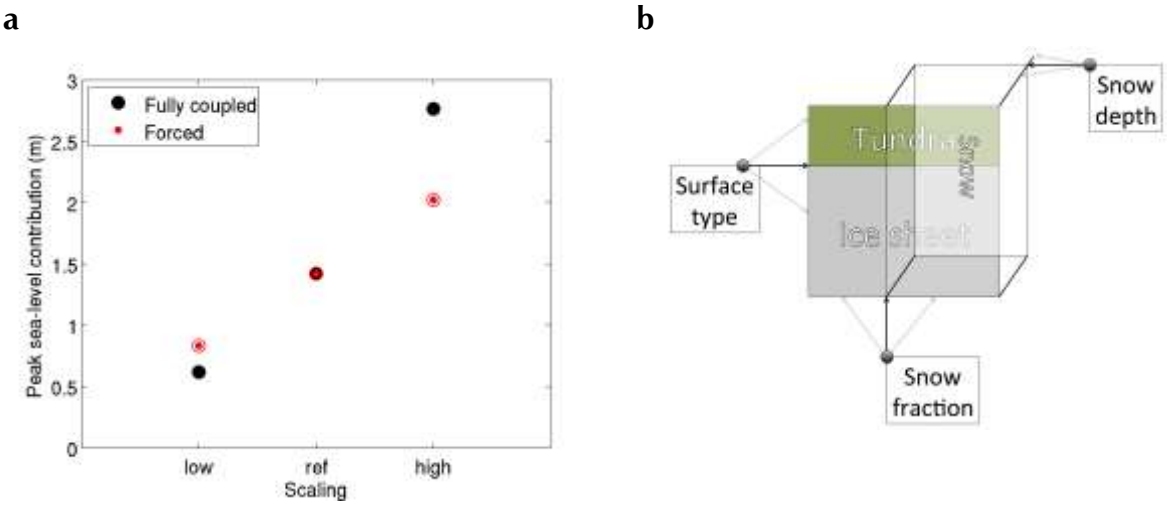

Figure 23: (a) Scaling of sea-level contribution from the Greenland ice sheet as a function of temperature changes for the full model (black) and forced model (red) in comparison. (b) Schematic of the albedo parameterisation in the land model for (partially) ice-covered areas.

2.4.3.5. Antarctic ice sheet

The annual mean air temperature anomaly over Antarctica (averaged over grounded ice) increases in the beginning of the experiment to a flat peak at 125 kyr BP (Figure 24),

before cooling sets in and continues until 115 kyr BP. The warming necessary to reach temperatures anomalies of up to two degrees is around a factor two faster than the cooling trend afterwards, with both transitions being near linear on the millennial time scale. The Antarctic ice sheet surface climate appears to be largely isolated from millennial time scale perturbations occurring in the Southern Ocean in response to changing freshwater fluxes and due to the interhemispheric see-saw effect (Goelzer et al., 2015). Pre-industrial surface temperatures levels are first reached 128 kyr BP and after cooling again at 118 kyr BP. The accumulation rate (averaged over grounded ice) shows an initial increase in line with the warmer temperatures until 130 kyr BP but records a changing grounded ice sheet area further on, which mostly indicates retreat of the ice sheet from regions of higher accumulation. Relative to the pre-industrial, accumulation increases at most 20 % in annual values and up to 12 % for the long-term mean (grey and black lines in Figure 24, respectively). As a consequence of the surface forcing, the AIS shows a small volume gain until 130.5 kyr BP due to increase in precipitation before a large-scale retreat of the grounding line sets in. The average ablation rate over grounded ice equally increases with increasing temperature but remains of negligible importance for the mass balance of the ice sheet (note difference of vertical scales between panel b and c in Figure 24).

Changes in the sub-shelf melt rate play an important role for the present mass balance of the AIS and are often discussed as a potential forcing for a WAIS retreat during the LIG (e.g. Duplessy et al., 2007; Holden et al., 2010) and during the last deglaciation (Golledge et al., 2014). The average sub-shelf melt rate diagnosed for the area of the present-day observed ice shelves in our Reference simulation increases to at most 20 % above the pre-industrial with a peak in line with the air temperature maximum. However, ocean warming to above pre-industrial temperatures occurs already before 130 kyr BP, more than 2 kyr earlier compared to the air temperature signal, a consequence of the interhemispheric see-saw effect.

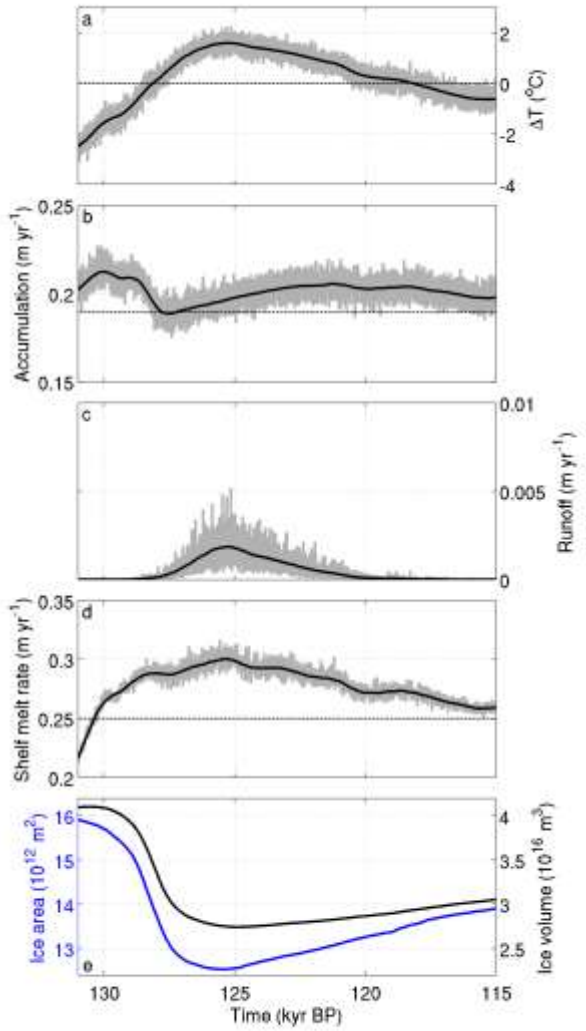

Figure 24: Antarctic ice sheet forcing and characteristics. Temperature anomaly (a), average ice sheet wide accumulation rate (b), average ice sheet wide runoff rate (c), average shelf melt rate diagnosed for the area of the present-day observed ice shelves (d). (e) Grounded ice sheet area (blue) and volume (black). Grey lines give full annual time resolution, while black lines (and blue in e) are smoothed with a 400 years running mean.

Ice sheet area and volume decrease rapidly between 129 and 127 kyr BP and indicate a gradual regrowth after 125 kyr BP. Those changes arise mainly from a retreat and re-advance of the WAIS (Figure 25). In our model the retreat exhibits characteristics of an overshoot behaviour due to the interplay between ice sheet retreat and bedrock adjustment. The rebound of the bedrock, which is initially depressed under the glacial ice load, is delayed compared to the relatively rapid ice sheet retreat, giving rise to a grounding-line retreat well beyond the pre-industrial steady-state situation. These results are in line with earlier work with a stand-alone ice sheet model (Huybrechts, 2002), but also rely on a relatively large glacial-interglacial loading contrast in these particular

models. The sea-level contribution above the present-day level from the Antarctic ice sheet peaks at 125 kyr BP at 4.4 m.

Stand-alone sensitivity experiments, in which specific forcing processes are suppressed show that surface melting and sub-shelf melting play a limited role for the AIS retreat in our experiments. The sea-level contribution peak in an experiment with supressed sub-shelf melting is about 40 cm lower compared to the reference experiment and remains around one meter lower between 123 kyr BP until the end of the experiment. The difference between the experiments at a given point in time arises from a lower overall sea-level contribution when sub-shelf melting is suppressed, but also from a difference in timing between both cases. The dominant forcing for the Antarctic ice sheet retreat in our model is a combination of rising global sea level and increasing surface temperature, which leads to increasing buoyancy and reduced ice shelf viscosity, respectively. The relative timing between sea level forcing and temperature forcing is therefore of critical importance for the evolution of the ice sheet at the onset of the LIG.
The limited effect of surface melting and sub-shelf melting on the sea-level contribution is ultimately due to a limited magnitude of surface temperature and ocean temperature changes. The limited Antarctic and SO temperature response has already been highlighted in earlier studies with the same climate component (Loutre et al., 2014; Goelzer et al., 2015) and is confirmed here with a fully coupled model. The feedback mechanism suggested by Golledge et al. (2014) for Termination I, which draws additional heat for sub-shelf melting from freshwater-induced SO stratification and sea-ice expansion is active in our experiment, but too short-lived and of too little amplitude to lead to substantially increased melt rates. Our limited AIS response to environmental forcing is also in line with other modelling results for the LIG period (Pollard and DeConto, 2015) albeit with a different forcing strategy, where substantial retreat of marine based sectors of the EAIS can only be achieved by including special treatment of calving fronts and shelf melting, which was not attempted here.
As mentioned earlier, direct constraints of the Antarctic ice sheet configuration during the LIG are still lacking. Goelzer et al. (2015) suggested that the timing of the main glacial-interglacial retreat of the AIS could be constrained by a freshwater induced oceanic cold event recorded in ocean sediment cores (Bianchi and Gersonde et al. 2002). The main retreat in their model happened $\sim$129.5 kyr BP, a timing predating the time of retreat in the coupled model by $\sim$2 kyr due to the difference in atmospheric and oceanic forcing. It is noteworthy in this context that the prescribed sea level forcing imposes an important control for the timing of the Antarctic retreat. Sensitivity experiments indicate that the main retreat appears another 2 kyr later when LR sea level forcing is used instead of Grant et al. (2012).

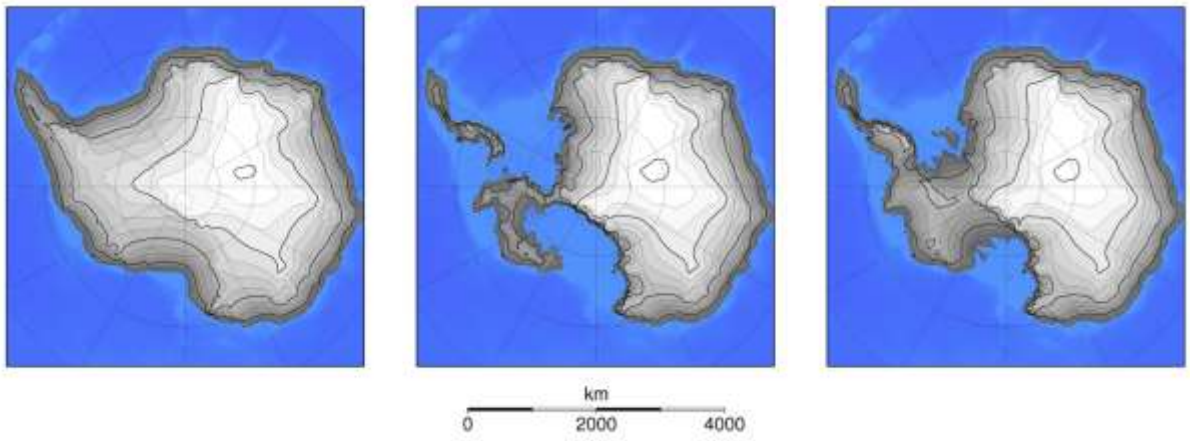

Figure 25: Antarctic grounded ice sheet geometry at 130 kyr BP (a), for the minimum ice sheet volume at 125 kyr BP with a SL contribution of 4.4 m (b) and at the end of the reference experiment at 115 kyr BP (c).

2.4.3.6. Thermal expansion of the ocean

The steric sea-level component due to ocean thermal expansion (Figure 26c) is largely following the global temperature evolution, but is also strongly modified by changes in ice sheet freshwater input. Ocean expansion is steep during peak input of freshwater and stagnant during episodes of decreasing freshwater input. This is because the net ocean heat uptake is large when freshwater input peaks, which happens in three main episodes in our experiment. Two episodes of freshwater input from the NH centred at 133.6 and 131.4 kyr BP are followed by an episode of combined input from the NH and the AIS centred at 128.2 kyr BP (not shown). The anomalous freshwater input leads to stratification of the surface ocean, sea-ice expansion and reduction of the air-sea heat exchange, effectively limiting the ocean heat loss to the atmosphere. This implies that global sea-level rise due to ice sheet melting is (weakly and temporarily) amplified by the freshwater impact on ocean thermal expansion. We simulate a peak sea-level contribution from thermal expansion of 0.35 m at 125.4 kyr BP, which forms part of a plateau of high contribution between 127.3 and 124.9 kyr BP (Figure 26c). The amplitude is at the lower end, but well within the range of IPCC AR5 estimates of 0.42 ± 0.11 m (Masson-Delmotte et al., 2013).

2.4.3.7. Global sea-level change during the LIG

Combining contributions from GrIS, AIS, thermal expansion, global sea level peaks at $\sim$5.3 m at 124.5 kyr BP with a slow decrease thereafter as first the Antarctic ice sheet and 2 kyr later the Greenland ice sheet start to regrow. For the Antarctic ice sheet the model indicates a clear asymmetry between relatively fast retreat and much slower regrowth.

Modelled GrIS and AIS sea-level contributions together with prescribed NH sea level are within the 67% confidence interval of probabilistic sea-level reconstructions (Kopp et al., 2009) for the period ~125-115 kyr BP (Figure 26, right). The last 20 m rise in sea-level contributions from the NH (including Greenland) is steeper and occurs 1~2 kyr earlier in our model compared to what the reconstructions suggest, which is consequently also the case for the rise in global sea level at the onset of the LIG. The Antarctic retreat in our model is more rapid compared to the reconstruction and does not show the hiatus ~131-129 kyr BP suggested by the data. The modelled ice sheet evolution in our reference run reproduces well the global average sea-level contribution 125-115 kyr BP based on the best estimate of Kopp et al. (2009) when taking into account the modelled steric contribution (0.35 m) and assuming an additional contribution (0.42+-0.11 m) of glaciers and small ice caps (Masson-Delmotte et al., 2013). The multi-peak structure of global sea-level contributions during the LIG suggested by the reconstructions (Kopp et al., 2009; 2013) is not reproduced with our model, mainly owing to the long response times of the ice sheets during regrowth to changing climatic boundary conditions.

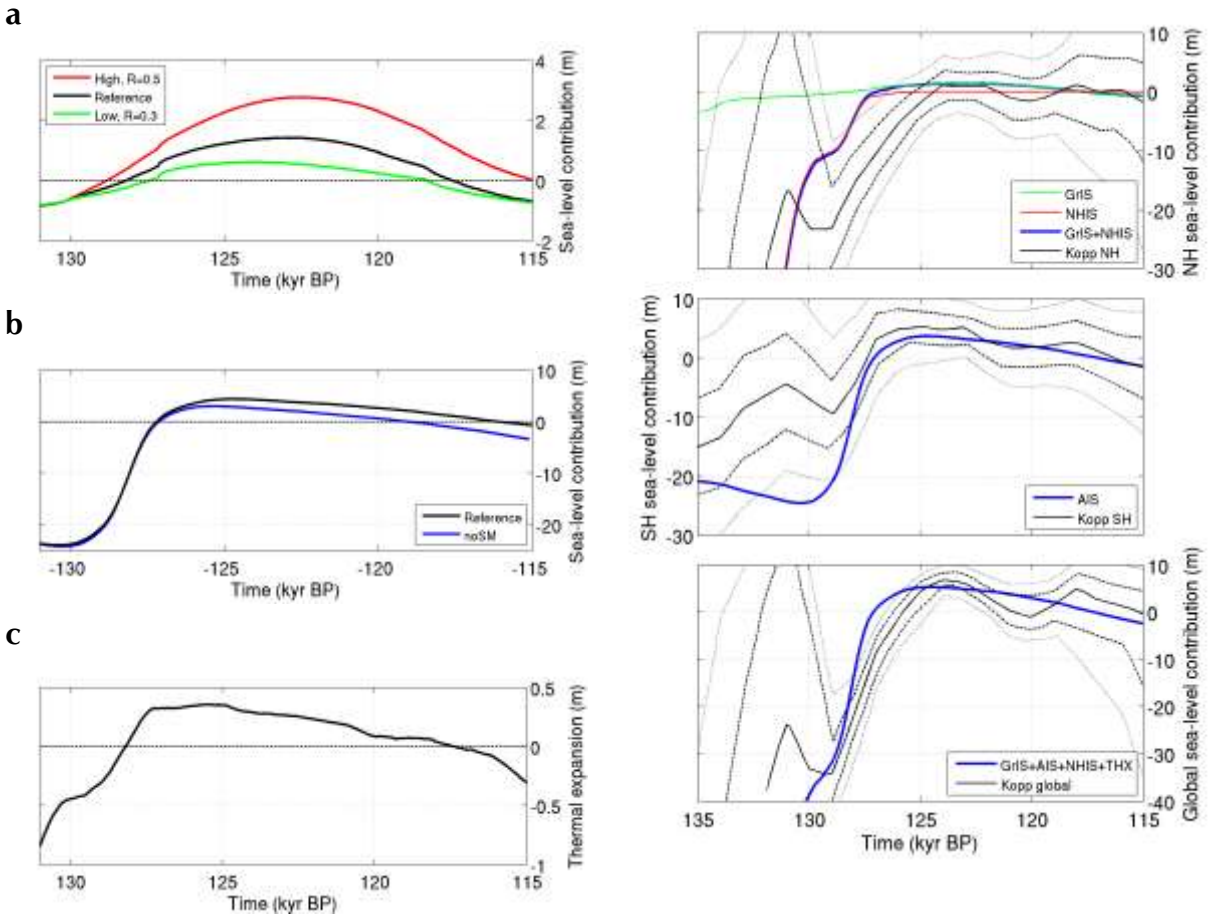

Figure 26: Left: Sea-level contribution from the Greenland ice sheet for the Reference run (black) and two sensitivity experiments with higher (red) and lower (green) temperature scaling. (b) Sea-level contribution from the Antarctic ice sheet from the Reference run (black) and from a sensitivity experiment without shelf melting (blue). (c) Sea-level contribution from oceanic

thermal expansion from the Reference run. Right: Modelled sea-level contributions from this study (colour lines) compared to probabilistic sea-level reconstructions (black lines) from Kopp et al. (2009).

2.4.4. Concluding remarks

Transient simulation with realistic ice sheet boundary conditions from reconstructed Northern Hemisphere ice sheets and detailed stand-alone simulations of the Greenland and Antarctic ice sheets show that the temperature evolution at the onset of the Last Interglacial was in both hemispheres considerably influenced by meltwater fluxes from the decaying ice sheets. While Antarctic freshwater fluxes lead to strong perturbations of the Southern Ocean, Northern Hemisphere freshwater fluxes have an influence both on the Northern and Southern Hemisphere temperature evolution through the oceanic see-saw effect. The importance of additional freshwater input from the Greenland ice sheet during Termination II is small compared to the much larger fluxes from the other NH ice sheets and becomes more important only later during the Interglacial when it is the only remaining ice sheet contributing freshwater fluxes to the North Atlantic. In the Southern Hemisphere, anomalous freshwater input from the Antarctic ice sheet leads to an episode of surface freshening, increased stratification and sea ice cover and consequently reduced ocean heat loss to the atmosphere, with temporary heat build-up in the mid-depth ocean. We argue that the surface ocean cooling associated with this event may be used to constrain an early Antarctic retreat when matched with similar signatures evident in some deep-sea sediment cores from the Southern Ocean.

Our transient simulations confirm results from earlier studies that stress the importance of ice sheet boundary for the climate evolution at the onset of the LIG. However, most of the freshwater induced changes remain visible for at most 1-2 kyr after cessation of the perturbations, indicative of a relative short memory of the (surface) climate system.

In our results of the fully coupled experiments, both ice sheets contribute to the sea-level high stand during the Last Interglacial, but are subject to different forcing and response mechanisms. While the GrIS is mainly controlled by changes in surface melt water runoff, the Antarctic ice sheet is only weakly affected by surface and sub-shelf melting. Instead, grounding line retreat of the AIS is forced by changes in sea level stand and surface warming, which lowers the shelf viscosity. Limited by the existing ice core constraints on minimal ice sheet extent, the peak Greenland ice sheet contribution in our Reference experiment is 1.4 m, while the Antarctic contribution is 4.4 m predominantly sourced from WAIS retreat. The modelled steric contribution is 0.35 m, in line with other modelling studies. Taken together, the modelled global sea-level evolution is consistent with reconstructions of the sea-level high stand during the LIG, but no evidence is found for sea-level variations apparent in some reconstructions. Ice-climate feedbacks and in particular the treatment of albedo changes at the atmosphere-

ice sheet interface play an important role for the Greenland ice sheet. Large uncertainties in the projected sea-level changes remain due to a lack of comprehensive knowledge about the climate forcing at the time and a lack of constraints on LIG ice sheet extent, which are limited for Greenland and virtually absent for Antarctica.

2.5. THE NEXT MILLENNIUM

Global mean sea level rose at an average rate of ~ 3.1 mm $yr-1$ since the early 1990s and is projected to rise 0.28 to 0.98 m until the year 2100, strongly depending on the assumed anthropogenic forcing scenario (Church et al., 2013). This global rise in sea level is a combination of contributions from ocean thermal expansion, glaciers and small ice caps, from the Greenland and Antarctic ice sheets and changes in land water storage. Except for the latter, all components are expected to contribute to further sea-level rise well beyond the end of this century due to the long residence time of CO_2 in the atmosphere.

The new version of LOVECLIM, improved in the context of the Last Interglacial simulations has also been applied for projections of future sea-level rise. We have performed long-term future sea-level change experiments over 1000 years with LOVECLIM forced by four extended RCP scenarios. Aside from including fully coupled three-dimensional thermomechanical models of the Greenland and Antarctic ice sheets, LOVECLIM is extended with a global glacier melt algorithm to account for the response of mountain glaciers and small ice caps (Raper and Braithwaite, 2006), and a diagnostic for oceanic thermal expansion to fill the total sea-level budget. A range of the model's sensitivity to greenhouse warming was sampled by systematic parameter variations leading to an ensemble of model versions that simulate the present-day climate consistent with observations, while producing contrasted results for the future period (Loutre et al., 2011, Goelzer et al., 2012a).

The reference parameter set (P71) and parameter set P22 (defined and used in Loutre et al. (2011), Goelzer et al. (2011), Goosse et al. (2007) and in Loutre et al. (2014) for the last interglacial are used to simulate future climate. Two additional parameter sets (P11 and P34) are also used here. The climate sensitivity (defined here as the temperature response 1000 years after a doubling of CO_2) of LOVECLIM using parameter sets P11, P71, P22 and P34 is respectively 1.5, 2.0, 2.0 and 2.4°C, at the lower end of the IPCC range (1.5-4.5°C).

2.5.1. Preparation of forcing scenarios

CMIP5 promotes a standard set of model simulations in order to provide projections of future climate change on the long term (up to 2100 and beyond). Several emission scenarios for future climate, called "Representative Concentration Pathways" (RCPs) were designed (Moss et al., 2010) and subsequently adopted by the IPCC for its fifth

Assessment Report (AR5). These scenarios (RCP2.6, RCP4.5, RCP6.0 and RCP8.5) are named after their radiative forcing increase in the year 2100 AD relative to pre-industrial. Extended Concentration Pathways (ECPs) are defined until 2300 AD (Meinshausen et al., 2011). In our simulations greenhouse gas concentration are held at their 2300 AD values until 3000 AD. The evolution of the prescribed CO_2 concentration is illustrated in (Figure 27). These scenarios reach a maximum of atmospheric concentration of 442ppmv (at 2052 AD), 543ppmv (at 2130 AD), 752ppmv (at 2150 AD), 1962ppmv (at 2250 AD) for RCP2.6, RCP4.5, RCP6.0 and RCP8.5, respectively.

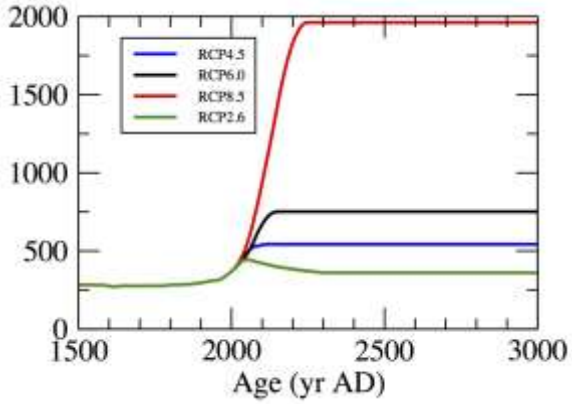

Figure 27: Evolution of the atmospheric greenhouse gas concentration from 1500 AD to 3000 AD for the four RCPs scenarios RCP2.6 (green), RCP4.5 (blue), RCP6.0 (black) and RCP8.5 (red).

The insolation at the top of the atmosphere is computed based on the astronomical solution of Berger (1978) with parameters given in Table 4. Insolation does not experience large variation over the next millennium. Consequently, future GHG forcing will play a major role.

Table 4: orbital parameter at present and at the end of the third millennium

	1950 AD	**3000 AD**
Eccentricity	0.016724	0.017483
Longitude of the perihelion (°)	102.04	67.97
Obliquity (°)	23.466	23.701

The total solar irradiance (TSI) is known to have a cycle of 11 years, and possibly longer not well-known periodicities. However, there is no TSI model yet for the future. Therefore, the 11-yr cycle for the period 2001-2013 is repeated until 3000 AD.
Volcanic activity is highly unpredictable although volcanic eruption may have significant climatic impact over a few years. No volcanic aerosol is included in these simulations. The sulphate concentration is assumed to decrease to zero after the year 2100 AD and does not change anymore until the end of the simulations in year 3000

AD. Vegetation changes according to a vegetation scenario until 2100 AD and then remains fixed to its 2100 AD value until the end of the simulation in year 3000 AD

2.5.2. Model spin-up

The long-term future climate and sea-level projections are started at 2005 AD from a well-defined initial state of the coupled climate-ice sheet system. In order to prepare this configuration, a spin-up procedure is used that consists of a series of uncoupled and coupled climate and ice sheet simulations.

The climate component of LOVECLIM (ECBILT, CLIO and VECODE) is run with constant historical forcing representative of the year 1505 AD as equilibrium simulation over several thousand years. The initial (1505 AD) conditions for AGISM (GrIS and AIS) are obtained from standalone ice sheet experiments forced with temperature reconstructions over the ice sheets derived from ice core data. The GrIS model is run through two glacial-interglacial cycles while the AIS model is assumed in a steady state.

A one-way coupled quasi-equilibrium simulation at 1505 AD is then performed combining the previously generated initial conditions. In this simulation, the ice sheets are fixed, while the climate components adjusts to the ice sheet boundary conditions, such as background freshwater fluxes, albedo and elevation, which generally differ from the prescribed boundary conditions of the uncoupled climate model. The purpose of this simulation is to get a climate state at 1505 AD in equilibrium with the ice sheet conditions at that time.

The fully coupled simulation is started at 1505 AD using the quasi-equilibrium climate information of the simulation before and the ice sheet information from the standalone simulation as initial conditions. LOVECLIM is run until 2005 AD with known greenhouse gas concentrations, total solar irradiance and volcanic forcing in accordance with the Paleoclimate Modelling Intercomparison Project Phase 3 (PMIP3).

Several iterations of the simulation 1505 to 2005 AD, are performed with five ensemble members to reach convergence of the reference climate information (1975-2005 AD) used to construct the climatic forcing anomaly for the ice sheet components.

2.5.3. Temperature and climate change over the third millennium

In this section we will give an overview of the climate evolution simulated with the different parameter sets and the different greenhouse gases scenario. The focus will be on the major global climate changes, with a specific interest in the polar/zonal amplification.

2.5.3.1. Global overview

The global average temperature anomaly (Figure 28a) at the end of simulation varies between 0.5 and 5.2 ° C. It is 0.5 ° C, respectively, 1.7 ° C, 2.3 ° C and 4.4 ° C for scenarios RCP2.6, RCP4.5, RCP6.0 and, RCP8.5 on average for the four parameter sets.

Anomaly is defined here as the deviation from the average value over 1986-2005 AD. Almost half of this warming is already reached in 2100 AD for scenarios RCP4.5 and RCP6.0, but it is less than 40% for RCP8.5. Temperature is almost stabilised at the end of the simulation with RCP2.6 while it is still increasing under the other RCP scenarios. All the simulations show an initial reduction in the intensity of the thermohaline circulation (Figure 28b). Then, the thermohaline circulation completely recovers for the scenarios RCP2.6 as soon as about 2200 AD. At 3000 AD, it remained slightly below its 1986-2005 value for the scenarios RCP4.5 and RCP6.0. For scenario RCP8.5, different evolutions of the thermohaline circulation are identified according to the parameters sets. It ranges from an almost complete collapse (P34) to an almost total recovery (P 11). All the simulations experience a reduction of the summer arctic sea ice (Figure 28c) at the beginning of the simulations. It melts almost completely in the summer before 2200 AD under the RCP8.5 scenario. On the contrary, the summer arctic sea ice area is only slightly smaller than the reference value for the RCP2.6 scenario. Its evolution varies between these two extremes for RCP4.5 scenarios RCP6.0, depending on parameter sets. For example, P34 leads to an almost complete melting of summer arctic sea ice after 2200 AD while one third (RCP6.0) to more than half (RCP4.5) of the summer arctic sea ice area maintains after 2200 AD with P11. Note that, even in winter, arctic sea ice area (Figure 28d) suffers a strong reduction of over 50% in the case of scenario RCP8.5 with the parameter sets 34 and 71. While, at present, the simulated summer sea ice area in the Southern Hemisphere (Figure 28e) is significantly lower than in the northern hemisphere, it manages to maintain a minimum coverage in most of the simulations. In winter, the reduction in the area of southern hemisphere sea ice (Figure 28f) is very much depending on the simulation; it varies between -10% and -80%.

As expected, the increase in the annual mean surface temperature due to the increase in atmospheric CO_2 concentration is greater in the high latitudes than in lower latitudes (polar amplification phenomenon). It is also generally greater over land than over the ocean. Nevertheless, in the southern hemisphere latitudes off the Antarctic continent are warming more than the continent itself. Despite the general warming, some simulations indicate local cooling. This is essentially the case in the Denmark Strait, where this cooling can reach several degrees depending on simulation. Other model than LOVECLIM also show a weaker warming or slight cooling in the North Atlantic as a result of the reduction in deep-water formation and shifts in ocean currents (IPCC AR5).

In the case of scenario RCP2.6, the initial warming at high latitudes of the Northern Hemisphere is followed by a slight cooling. In other words, the warming of these regions peaks in 2100 and is thus larger than at the end of simulation. It should be recalled that the RCP2.6 scenario is a scenario in which the CO_2 concentration reached a maximum in 2050 AD (442ppmv) then decreases until 2300 AD (361ppmv) and then remains at that level, slightly lower than the reference level.

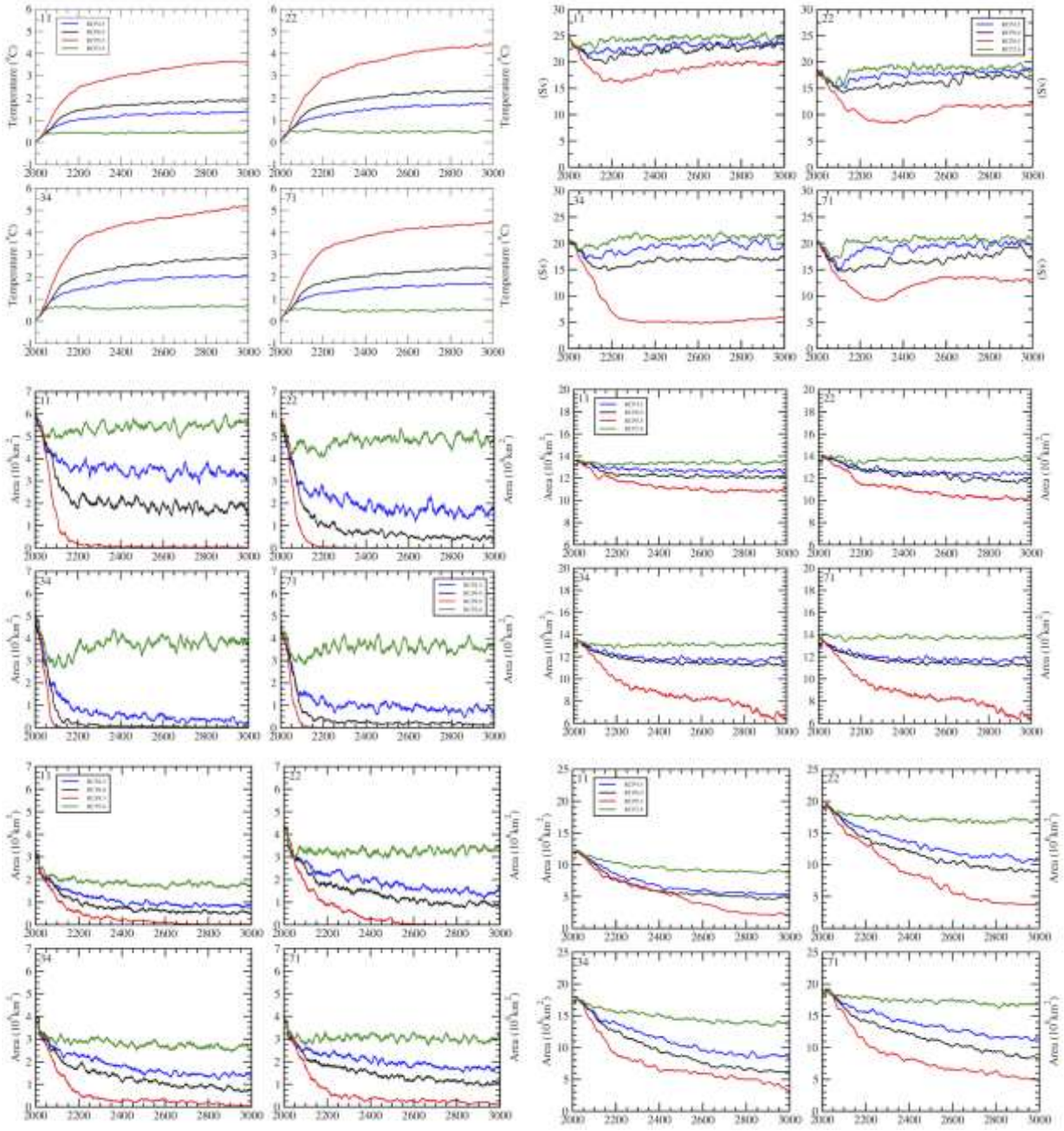

Figure 28: (a) global mean surface temperature anomalies (°C), (b) maximum of the annual mean meridional overturning circulation in the North Atlantic below 500 m (Sv), arctic sea ice area in summer (c) and winter (d), southern hemisphere sea ice area in summer (e) and winter (f). Values a provided for four RCPs and four parameter sets. Curves are smoothed with a 20-year running mean.

2.5.3.2. Polar temperature response

The change of mean surface temperature at the end of the simulations rises up to 16°C over the northern latitudes (north of 70°N) and up to 12°C over the southern latitudes (south of 65°S). Moreover, the warming is always larger over the Northern Hemisphere than over the Southern Hemisphere. Therefore, at the end of the simulations, the warming is between a factor of 1.7 and 3.8 in both polar regions compared to the global

average because of the polar amplification although previous studies suggested that polar amplification is not found in Antarctic regions (IPCC-AR5). The value of this polar amplification is depending on the time in the simulation, on the RCP scenario and on the parameter set. It has already been pointed out that the polar amplification is not constant over time (Köhler et al., 2015) and may vary among different models (IPCC-AR5).

In order to get a better insight into the surface temperature amplification we analysed the zonal amplification. The zonal amplification is defined as the ratio of the zonal to the global annual average surface temperature increase from the reference period (1986-2005). The zonal amplification is larger in the high northern latitudes than in the southern ones for all the simulations except for the parameter set P11 with the scenario RCP2.6. The tropical region is characterised by a zonal amplification smaller than one, meaning that there is actually a dimming in this region. Zonal amplification is smaller at the end of the 21st century (2100) than later in the Southern Hemisphere, while it is the reverse in the Northern Hemisphere. According to Goosse and Renssen (2001) who studied the response of the southern ocean to an increase in greenhouse gas concentration in LOVECLIM, this response of the Southern Hemisphere can be decomposed into two consecutive steps. First the ocean damps the surface warming because of its large heat capacity. In a second step, the warming is amplified because of a positive feedback associated with a stronger oceanic meridional heat transport toward the Southern Ocean and induces large decrease in sea ice area in the Southern Hemisphere. Therefore, the warming of the Southern Hemisphere, in particular in the high latitudes, is delayed compared to the increase in greenhouse gas forcing. Consequently, the zonal amplification in these latitudes is larger at the end of the simulation than during its first century. The situation is different in the Northern Hemisphere. Indeed the ocean surface is much smaller in the North than in the South. For most of the simulations, in particular those forced with RCP4.5, RCP6.0 and RCP8.5, temperature increases in the high latitude at the same pace as over the hemisphere. In other words the zonal amplification relative to the Northern hemisphere is the same at the end of the 21st, 23rd and 30th century for most of the simulations. The ratio of the local (grid cell) temperature anomaly to the Northern Hemisphere temperature anomaly shows mostly a zonal behaviour although some divergence from it can be identified. In particular, in the mid-latitudes, this ratio is slightly larger over North America and Eurasia than over the oceans at the same latitude. However, Greenland and the North Atlantic region along the Greenland coast have a generally smaller ratio than regions at the same latitudes. This could most probably be related to the melting of the ice sheet and the subsequent freshwater supplied to the ocean.

2.5.3.3. Climate changes over the ice sheets

Temperature increase over GIS (Figure 29a) is depending both on the parameter set and the RCP scenarios. However, general features can be identified. With RCP2.6, temperature is stabilised at the end of the simulation to a value lower than 2°C compared to the present. In contrast, the temperature is still rising under the three other RCPs scenario by 3000 AD. In this case, about half of the temperature increase is reached before 2200 AD. As expected the largest warming is obtained under scenario RCP8.5 although the magnitude of the warming is depending on the parameter set, the smallest values are with P71 (2.7, 6.5 and 9.0 respectively at 2100 AD, 2300 AD and 3000 AD) and the largest values are with P34 (3.9, 8.6 and 12.1 respectively at 2100 AD, 2300 AD and 3000 AD). The ranges in temperature response for a given scenario, representative of the parametric uncertainty, increase with increasing scenario strength from ~1°C (RCP2.6) to more than 4°C (RCP8.5). For most of the simulations, the surface temperature forcing is larger over Antarctica (Figure 29b) than over Greenland, but follows a similar time dependence and parameter range. Precipitation increases over both ice sheets in all experiments by 5-30% depending on the warming (not shown).

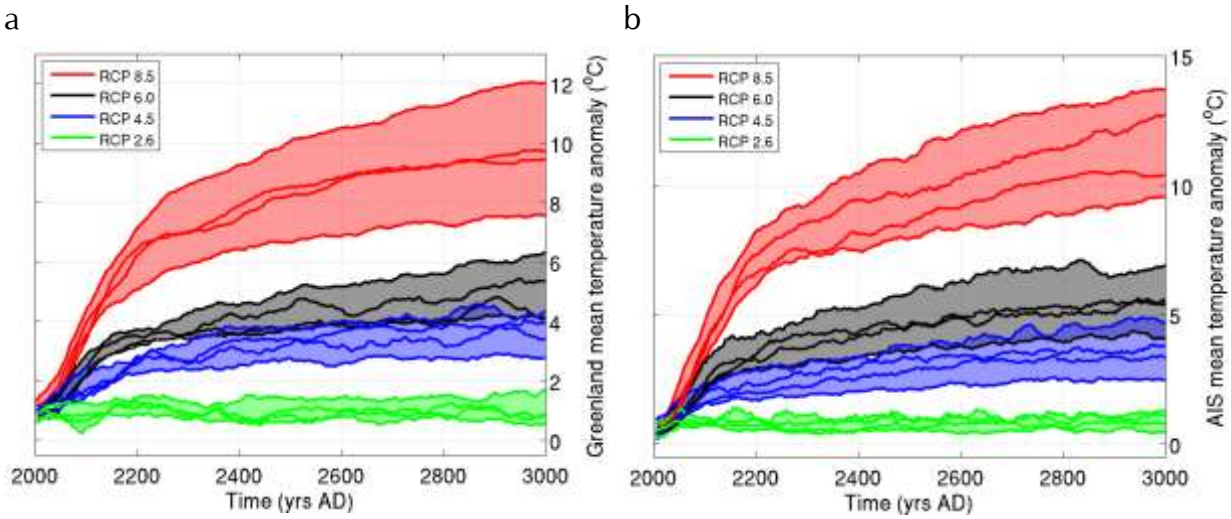

Figure 29: Range of the temperature anomaly for the four climatic parameter sets over the Greenland ice sheet (a) and over the Antarctic ice sheet (b) for the four prolonged RCP scenarios.

2.5.4. Dynamic response of the ice sheets over the third millennium

The ice sheet response over the third millennium is mainly determined by the strength of the atmospheric (and oceanic) temperature forcing arising from a combination of scenario strength and climatic parameter set. In the following we present results for the Greenland and Antarctic ice sheets separately before discussing their contributions to the global sea level budget.

2.5.4.1. Greenland ice sheet

The temperature increase over Greenland leads to an increase in surface meltwater runoff in all experiments resulting in an up to tenfold increase of the ablation ratio (mean ablation to mean accumulation) for the most sensitive model version (P34) under forcing scenario RCP8.5 (Figure 30). As the ice sheet retreats from the coast, the calving flux decreases and practically vanishes for the experiments with the largest warming. This retreat of the ice sheet is accompanied by an increase of the runoff of precipitation over ice-free land (Figure 30f). After an initial steep increase, the total freshwater flux from the Greenland ice sheet is close to constant for the low scenarios, steadily increasing for the medium scenario and shows more variations for the three most sensitive experiments. A final decrease of the total freshwater flux sets in when the ice sheet loses enough volume so that the ablation zone is considerably reduced.

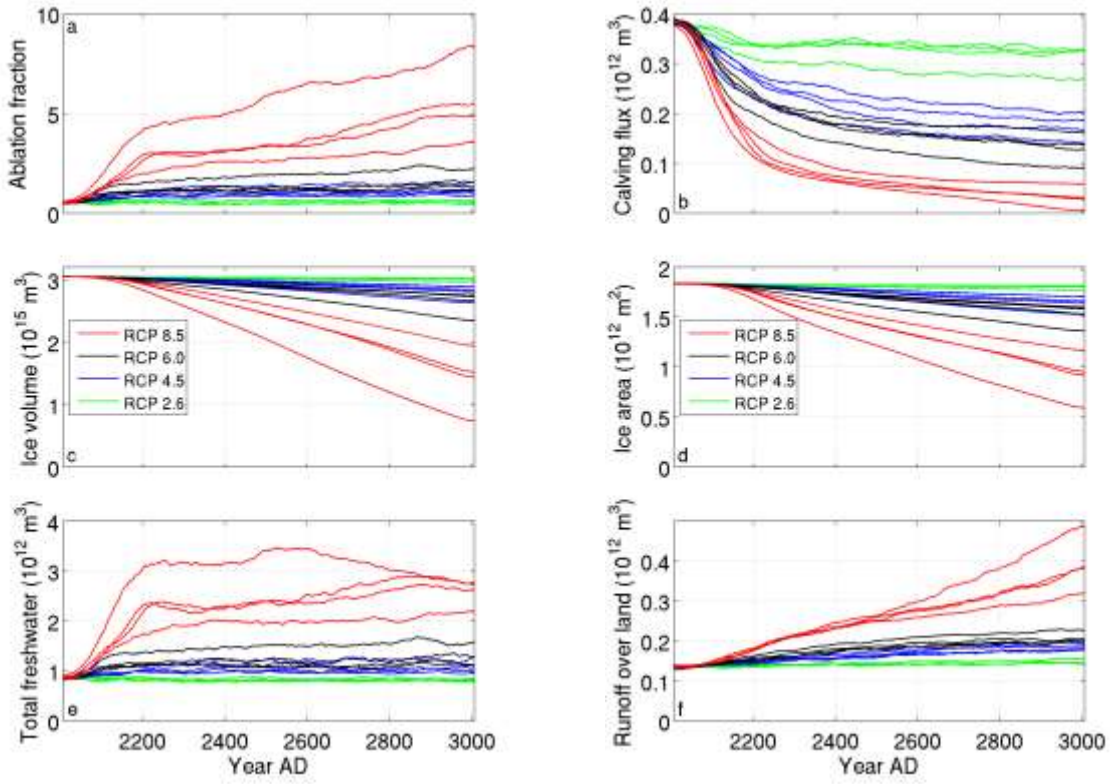

Figure 30: Time evolution of major characteristics of the Greenland ice sheet for four different parameter sets for each of four different RCP scenarios. Ratio of mean ablation to mean volume (a), calving flux (b), ice volume (c), ice area (d), total freshwater flux (e) and runoff over land (f). All lines are smoothed with a 30 years running mean.

The GrIS is responsible for a sea level contribution of up to 5.8 m (with P34 under RCP8.5) at 3000 AD (Figure 31a). From less than 0.1 m at 2100 AD and already more than 1.1 m at 2300 AD the contribution steadily increases. A complete melting of the Greenland ice sheet on the millennial time scale of interest here is not projected in any

of the experiments. The lowest sea-level rise is simulated for each RCP scenario with P71 compared to the other parameter sets. The highest simulated sea-level rise with P71 under RCP8.5 is almost 4 m at 3000 AD and much smaller with the scenarios other than RCP8.5. At the end of the simulation (3000 AD), it is less than 0.2 m with RCP2.6, and it is between 0.4 and 1.1 m with RCP4.5 and between 0.8 and 1.8 m with RCP6.0.

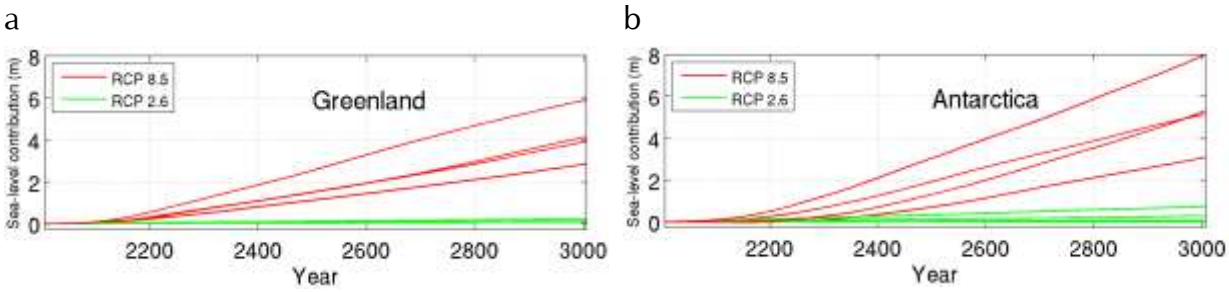

Figure 31: Sea-level contribution from the Greenland ice sheet (a) and the Antarctic ice sheet (b) for the highest (RCP8.5) and lowest (RCP2.6) scenario.

The resulting ice sheet geometries at year 3000 AD for the four parameter sets under forcing scenario RCP8.5 are given in Figure 32, which indicate a similar retreat pattern for the different parameter sets. The first and furthest retreat occurs in the southwest, followed by an overall retreat from the coast. Ice remains present at the central and southern domes, while melting of the northern part reveals bedrock below sea level that is still isostatically rebounding at 3000 AD.

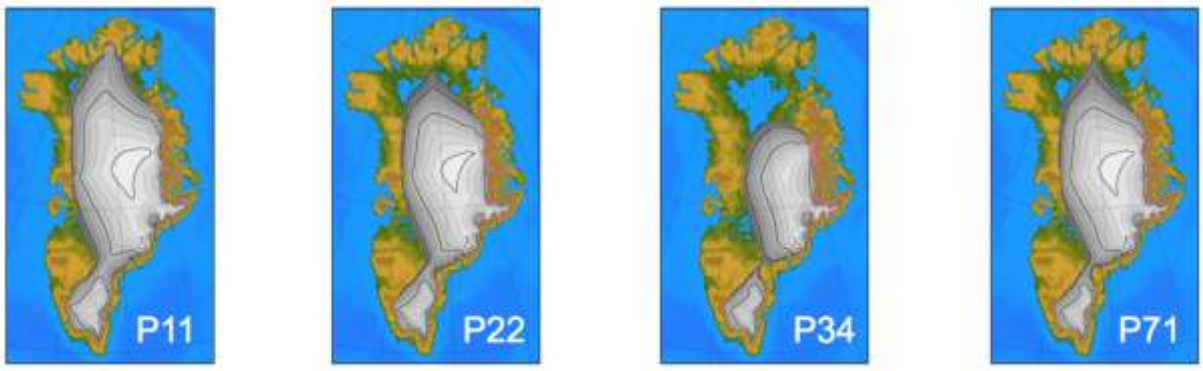

Figure 32: Greenland ice sheet geometries for the year 3000 AD for scenario RCP8.5 and four different parameter sets.

2.5.4.2. Antarctic ice sheet

Mass balance characteristics and evolution of grounded ice volume and area of the Antarctic ice sheet are given in Figure 33. Accumulation volume over grounded ice increases by 5-30% depending on the warming. Surface runoff, which is negligible at present, remains negligible for scenario RCP2.6, exhibits an increase of similar magnitude to the accumulation increase in scenarios RCP4.5 and RCP6.0 and widely exceeds it by up to a factor eight for the highest scenario RCP8.5. The surface melting is

accompanied by an up to threefold increase in sub-shelf melt rates, which exhibits a delayed response compared to the surface owing to the adjustment time scale of the ocean. The increasing ice flux across the grounding line (Figure 33c), which initially balances the grounded ice accumulation, is indicative of accelerated marginal ice flow and an overall retreating grounding line. The final ice volume at year 3000 AD is in all experiments lower compared to the initial state, but four of the mid-range scenario experiments show a small and temporary increase in ice volume with peak volume between 2200 and 2500 years AD. For those experiments the accumulation increase is overcompensating the volume loss due to grounding line retreat and surface melting. Aside from short-term variations, the grounded ice sheet area is monotonically decreasing in all experiments, confirming that temporary volume increases are mainly due to the relative importance of surface mass balance components.

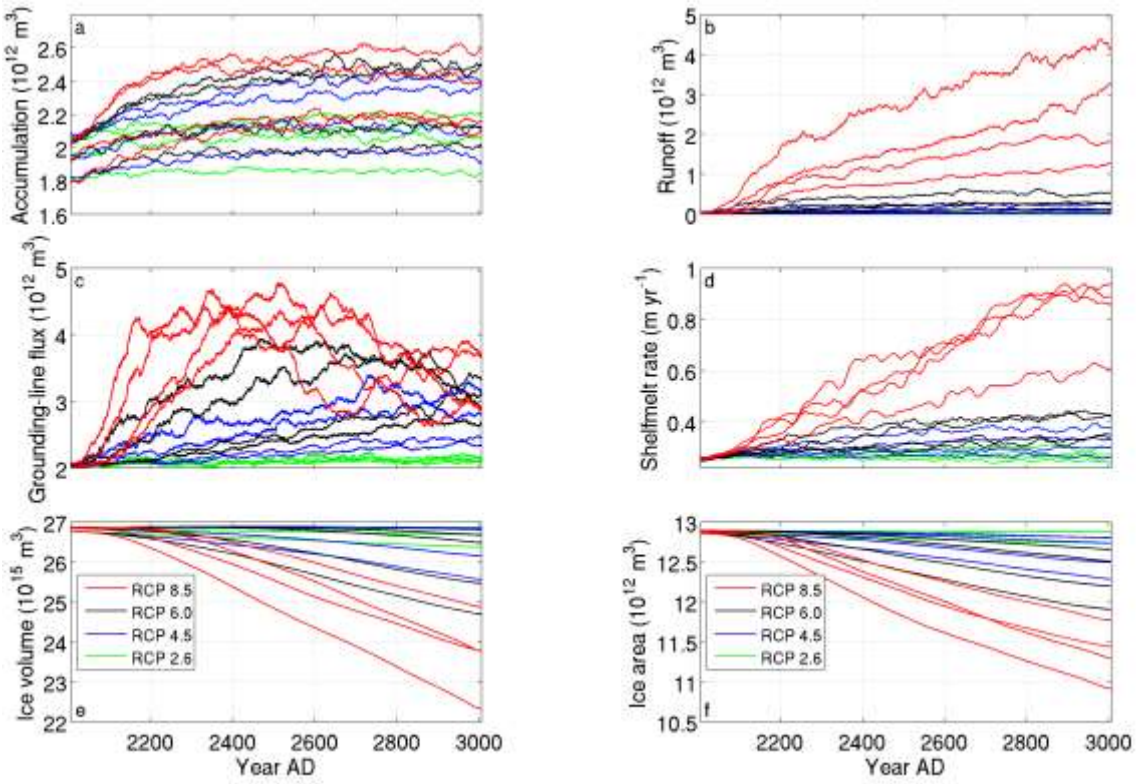

Figure 33: Time evolution of major characteristics of the Antarctic ice sheet for four different parameter sets for each of four different RCP scenarios. Accumulation volume (a) and runoff (b) on grounded ice, flux across the grounding line (c), average shelf melt rate (d), grounded ice volume (e) and area (f).

The largest Antarctic sea-level contribution at year 3000 AD is simulated for parameter set P22 (RCP8.5) as a consequence of the strong and combined increase in surface runoff and sub-shelf melting (Figure 31b). For this highest scenario, the results show a wide range of contributions from 3 to 8 m. Simulations for the low-end scenario RCP2.6

in comparison give sea-level contributions from close to zero to up to only 75 cm. The sea-level contribution due to the melting of the Antarctic ice sheet is larger compared to the Greenland ice sheet with parameter sets P11 and P22, while it is the opposite with P34 and P71. The latter two parameter sets notably produce a small negative Antarctic sea-level contribution at year 3000 AD under forcing scenario RCP4.5 as a consequence of a dominant precipitation increase. Larger negative sea-level contributions under forcing scenario RCP6.0 for the same parameter sets earlier in the experiments are already over-compensated by increasing runoff and grounding line retreat to yield positive sea-level contributions by 3000 AD.

The resulting grounded ice sheet geometries at year 3000 AD for the four different scenarios and parameter set P22 are given in Figure 34. Differences in final geometry between scenarios are foremost visible for the West Antarctic ice sheet configuration, which is close to the present for RCP2.6 and shows increasing grounding line retreat for scenarios RCP4.5, RCP6.0 and RCP8.5. Substantial changes of the EAIS are only found for RCP8.5 with marked retreat in the Amery basin and marginal thinning and grounding line retreat all around.

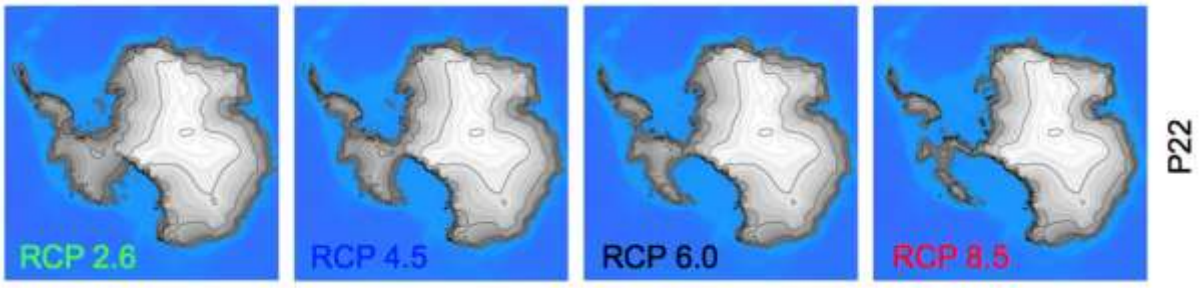

Figure 34: Antarctic ice sheet geometries at 3000 AD for parameter set P22 and four different RCP scenarios.

2.5.4.3. Rates of sea level change

Sea-level rates from the Greenland ice sheet for RCP 8.5 increase at the beginning with increasing radiative forcing (Figure 35). Thereafter, rates remain elevated and finally increase again as ice-albedo feedback becomes important. For the shown parameter set P22 the rates start to decrease again at 3000 AD when the size of the ablation starts to decreases, while for the most sensitive parameter set P34 this happens already after year 2600 AD (not shown). The rate of sea-level change of the Antarctic ice sheet shows the largest range of all components and increasing rates at year 3000 for the highest scenario RCP8.5. The results indicate a strongly non-linear dependence on scenario strength for the parameter sets P34 and P71 (not shown). Sea-level rates of oceanic thermal expansion are already high at 2000 AD, before they further increase for some time depending on the scenario. After that peak (at the latest ~ 2200 AD) rates decrease steadily but remain larger than zero for all but the lowest scenario. This behaviour is

similar for the four different parameter sets. For glaciers and ice caps, the rates reach a peak before the end of the 21st century and then rapidly decrease for all scenarios and parameter sets with decreasing glacier and ice cap area.

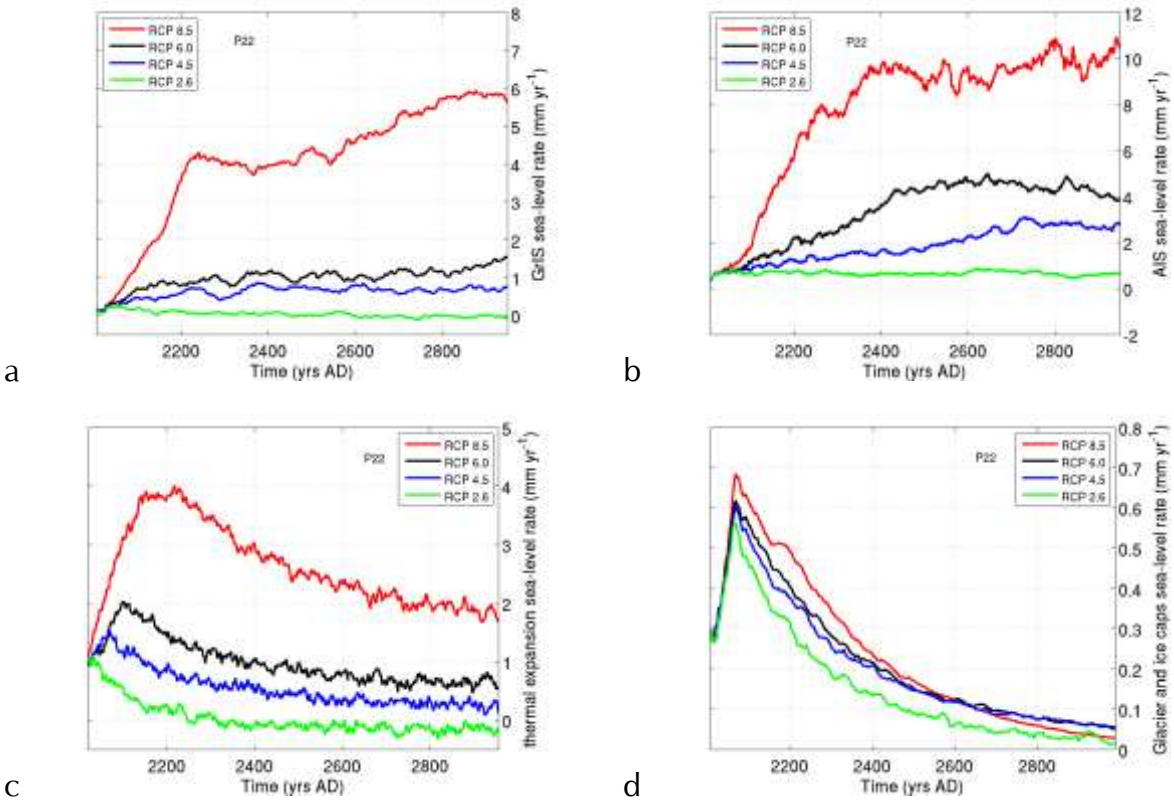

Figure 35 Rates of sea-level change from the Greenland ice sheet (a), the Antarctic ice sheet (b), thermal expansion (c) and glaciers and small ice caps combined (d) for parameter set P22.

2.5.4.4. Total sea level change

The resulting sea-level contributions and total sea-level rise is given in Figure 36. Relative contributions from the different components to total sea level change at 3000 AD vary with scenario and parameter set, but show some dominant patterns. The largest contributions and largest range in contributions is simulated for the Antarctic ice sheet, which may contribute anywhere between close to zero and 8 m to global sea-level change by year 3000. Greenland ice sheet sea-level contributions span a smaller range (0-6 m), but exceed the Antarctic contributions for individual experiments. The contribution from both ice sheets combined is always the largest and the contribution from glaciers and ice caps is small compared to the other components. The latter is similar for the three highest scenarios that yield close to the maximum attainable value of ~ 25 cm SLE as mostly all glaciers have disappeared. For the highest scenario the Greenland ice sheet contribution is consistently larger than thermal expansion, while for the other scenarios there is at least one parameter set for which the opposite is the case. The Antarctic contribution is always the largest for the parameter sets P11 and P22 and

lower than the GrIS contribution for P71 and P34. Projected global sea-level rise by the end of the third millennium ranges from a few centimetres for the lowest scenario to 15 m for the highest scenario and most sensitive parameter set.

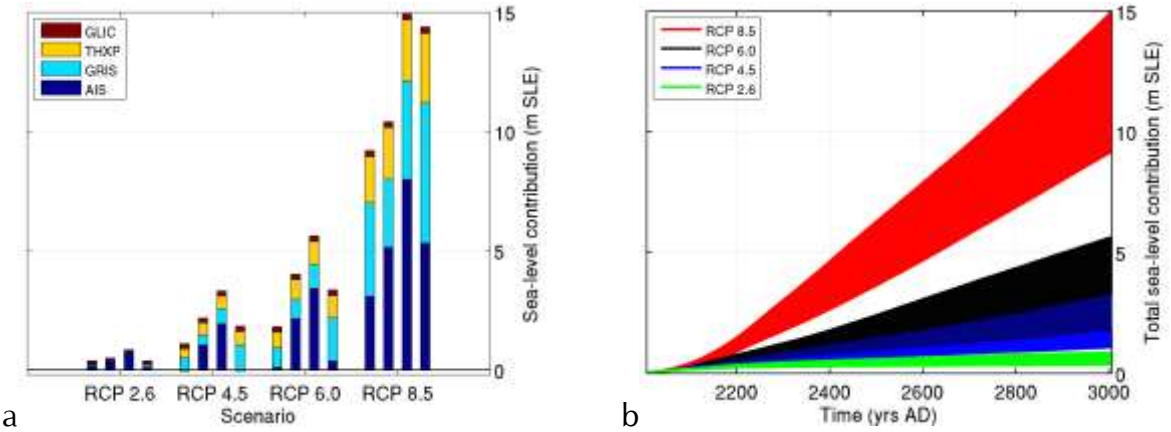

Figure 36 Sea-level contributions at year 3000 AD (a) and range of total sea-level rise projections (b) for the four scenarios and four different parameter sets (P71, P11, P22, P34).

2.5.5. Concluding remarks

The uncertainty on global annual mean surface temperature due to the parametric uncertainty may be as large as 1.5°C. However, the uncertainty related to the scenario of future greenhouse gas forcing is much larger. Along the same line, the uncertainty on the Atlantic meridional overturning circulation (AMOC), in particular for RCP8, is strongly dependent on the parameter set, leading to a behaviour ranging from almost collapse at 3000AD to an almost recovered state at 3000AD. The Northern Hemisphere polar amplification is very strong (a factor 1.7 to 3.8 to the global annual mean surface temperature) in agreement with previous studies. Moreover, a Southern Hemisphere polar amplification is also identified at odds with several previous studies. The polar amplification in the Southern Hemisphere is delayed compared to the Northern Hemisphere because of ocean damping of surface warming and feedback associated with oceanic meridional heat transport to the southern ocean.

The feedbacks are playing an important role in the polar/zonal/local amplification of temperature changes. For example, the freshwater flux from melting Greenland ice sheet in the Northern Hemisphere locally reduces the amplification in the northern North Atlantic, in particular along the Greenland coast, compared to the zonal mean. This illustrates the importance of the coupling between the ice sheets and the climate components of the Earth system.

The results indicate a very large spread in the projected global sea-level changes arising from parametric uncertainty, but also and foremost from uncertainties due to the scenario of future greenhouse gas forcing

3. POLICY SUPPORT

The work made within iCLIPS is a contribution to the on-going international scientific effort to better understand climate change and to assess more accurately the uncertainties associated with climate and sea level projections. This is needed in order to provide a sound basis for policies designed to address the challenge of climate change. The problem is most likely to become more and more important. This is why each Party to the United Nations Framework Convention on Climate Change (UNFCC) has committed itself to "promote and cooperate in scientific (...) research (...) related to the climate system and intended to further understand and reduce the remaining uncertainties (...)" (UNFCC Article 4.1 (g)).

The specific objective of iCLIPS, i.e. assessing model uncertainties in long-term climate and sea level change projections, fully meets one of the major goals of the IPCC for its assessment reports. The iCLIPS outcomes have been part of the IPCC Fifth Assessment Report (AR5), an invaluable tool for policymakers. The two iCLIPS promotors (Thierry Fichefet and Philippe Huybrechts) have been involved as key contributors of the IPCC AR5, and therefore have contributed directly in the underpinning of the scientific basis of climate change. Finally, the iCLIPS project has allowed Belgian teams to keep a global climate modelling potential operational. The expertise build up in these teams has been solicited by policy makers at both the national and international level, for instance for risk analysis assessments on future sea level rise.

Within Belgium the iCLIPS team was solicited by the Belgian National Agency for Radioactive Waste and enriched Fissile Material (ONDRAF/ NIRAS) to produce a report on the vulnerability of a potential underground radioactive waste repository to future glaciotectonic and glaciofluvial processs below and adjacent to an advancing ice sheet-margin. A second report for ONDRAF/ NIRAS assessed the risk that the Mol location would be submerged by a rising sea level within the next 10000 years. Another policy relevant activity is the role played by Philippe Huybrechts in the Denktank Klimaatadaptatie Vlaanderen (DKA).

Furthermore Philippe Huybrechts and Thierry Fichefet represent Belgium in various international bodies such as the International Association of Cryospheric Sciences (IASC), the Scientific Committee on Antarctic Research (SCAR), and the International Union of Geodesy and Geophysics (IUGG).

4. DISSEMINATION AND VALORISATION

Scientists involved in iCLIPS disseminated the results of this project through international research programmes on and assessments of climate change such as the European Union's Seventh Framework Programme and Horizon2020, WCRP (CliC, CLIVAR, COPES), IGBP (SOLAS), SCAR (ACE) and IPCC.
Dissemination took place via the training of Master students, PhD students and postdoctoral researchers, participation in working groups, presentations at national and international scientific workshops and meetings (see list below), and publication of results in international, peer-reviewed scientific journals (see further in section 5).
iCLIPS results were also transferred to the Belgian Science Policy through annual reports and a meeting with the follow-up committee. These meeting allowed constructive discussion between scientists of slightly different horizons: those who model the global and regional climate, and those who have expertise in impact studies. The discussion between these two groups led to a better tuning between offer and demand of model outputs.
In addition, a web site devoted to iCLIPS was created (http://www. http://homepages.vub.ac.be/~hgoelzer/iclips/). This web site provides full information about the objectives, the model, the progress of the project and some important findings. The numerical results themselves, because of their size, are stored on a mass storage repository. This database (atlases and numerical values) is accessible to the whole scientific community upon request.
Members of iCLIPS also took part in dissemination activities intended for the general public. In particular, the iCLIPS results were presented to students in primary and secondary schools during the "Atelier Science infuse", "Festival Science Infuse – Printemps des Sciences" and "Journée des Rhétos". Some results were also forwarded to the PolarFoundation for a climate exhibition. The researchers also gave numerous interviews on the issue of global change to the international and local press (TV, radio and newspapers), presentations for several organisations as part of university outreach programmes and lectures for different societies as well as intended for the general public.

4.1. Networking

The iCLIPS project has fostered and strengthened collaborations with other research groups using the same modelling tool. The improvements made within the project and the results obtained have helped to launch new collaboration with foreign researchers, e.g. the University of Hawaii. Furthermore, we could count on help from colleagues abroad to address some weaknesses of the model and thus to produce an improved

version (e.g. MIT). These improvements allowed us making available to the scientific community a new version of LOVECLIM. The ongoing close collaboration with the Vrije Universiteit Amsterdam (The Netherlands) was also made possible through the work done within iCLIPS. More than ten research groups in the world are now using LOVECLIM, e.g., ETH (Switzerland), Universidade de Vigo (Spain), University of Hawaii (USA), Rutgers University (USA), Yokohama Institute for Earth Sciences (Japan), Vrije Universiteit Amsterdam (The Netherlands), University of Tulan (USA), Deferal Univseriyr if Viçosa (Brazil), University of Kiel (Germany), Penn State University (USA) and University of Bremen (Germany). The iCLIPS project has allowed to establish or reinforce such collaborations. Collaboration was also strengthened with Oregon State University and the Bristish Antarctic Survey in order to continue the data-model intercomparison for the Last Interglacial, taking advantage of recently updated chronologies for marine data.

The expertise gained through this project allowed us taking part in several research programmes. PMIP3 studies the role of climate feedbacks arising for the different climate subsystems (atmosphere, ocean, land surface, sea ice and land ice) and evaluate the capability of the climate models to reproduce climate states that are radically different from those of today. Past4Future was a Collaborative Project under the 7th Framework Programme (FP7) of the European Commission. It investigates the climate and environment of past warm periods (interglacials) to inform on future climate and possible abrupt changes. Ice2sea, funded by FP7 aimed at improving projections of the contribution of ice to future sea-level rise. More recently, the team participated in various CMIP6 model intercomparison exercises intended for the next Sixth Assessment Report of IPCC and took a leading role in ISMIP6 (Ice Sheet Model Intercomparison Project).

4.2. Scientific missions with communication involving iCLIPS members

2011

International Workshop on Earth System Models of Intermediate Complexity, Potsdam (Germany), 18-19 January 2011

1. Goelzer, H., P. Huybrechts, M.-F. Loutre, H. Goosse, T. Fichefet and A. Mouchet: Assessment of modelling uncertainties in long-term climate and sea level change projections.
2. Goelzer, H., I. Janssens, J. Nemec and P. Huybrechts: A dynamic continental runoff routing model applied to the last Northern Hemisphere deglaciation.

ICE seminar series, Norsk Polarinstitutt, Tromsø (Norway), 16 February 2011

3. Fürst, J.J., P. Huybrechts, H. Goelzer and O. Rybak: Effects of fast dynamics on

centennial mass loss of the Greenland Ice Sheet.

Glaciology course, University Centre in Svalbard, Longyearbyen (Norway), 14 March 2011

4. Fürst, J.J., P. Huybrechts, H. Goelzer and O. Rybak: Effects of fast dynamics on centennial mass loss of the Greenland Ice Sheet.

ice2sea Open Forum Meeting, Copenhagen (Denmark), 16-18 March 2011

5. Goelzer, H., J.J. Fürst and P. Huybrechts: Set-up of a 3D model to investigate the centennial mass loss of the Greenland Ice Sheet.

European Geosciences Union General Assembly, Vienna (Austria), 3-8 April 2011

6. Fürst, J.J., H. Goelzer, O. Rybak and P. Huybrechts: Effect of fast dynamics on the centennial mass loss of the Greenland Ice Sheet.
7. Goelzer, H., P. Huybrechts, S. Raper, M.-F. Loutre, H. Goosse, and T. Fichefet: Ensemble ice and sea-level change projections with the Earth system model of intermediate complexity LOVECLIM.
8. Goelzer, H., I. Janssens, J. Nemec and P. Huybrechts: A dynamic continental runoff routing model applied to the last Northern Hemisphere deglaciation.
9. Mathiot, P., C. Konig Beatty, H. Goosse, T. Fichefet and F. Massonet: Assimilation of sea ice freeboard and concentration data in a coupled ice-ocean mode
10. Vancoppenolle, M., C. Bitz, T. Fichefet, H. Goosse, C. Lancelot and J.-L. Tison: Sensitivity of a one-dimensional, multi-layer, sea ice-microalgae model
11. Massonet, F., T. Fichefet, H. Goosse, M. Vancoppenolle, Mathiot P. and C. Konig Beatty: Importance of physics in global hindcast simulations of sea ice with NEMO-LIM
12. Goelzer, H., P. Huybrechts, S. Raper, M.-F. Loutre, H. Goosse and T. Fichefet: Ensemble ice and sea-level change projections with the Earth system model of intermediate complexity LOVECLIM

Summer School on Modelling of the Arctic Climate System, Faibanks (USA), 22 May - 4 June 2011

13. Lecomte, O., T. Fichefet, M. Vancoppenolle, H. Goosse: Improving the snow representation in the sea-ice component of GCMs.
14. Goosse H., E. Crespin, S. Dubinkina, M.-F. Loutre, M.E. Mann, H. Renssen, Y. Sallaz-Damaz and D. Shindell: The role of the forcing and internal dynamics in explaining the climate of the past millennium.

IUGG XXV General Assembly. Earth on the Edge: Science for a Sustainable Planet, Melbourne (Australia), 27 June - 8 July 2011

15. Goelzer, H., P. Huybrechts, S. Raper, M.-F. Loutre, H. Goosse, and T. Fichefet: Ensemble ice and sea-level change projections with the Earth system model of intermediate complexity LOVECLIM.

XVII INQUA, Bern (Switzerland), 21-27 July 2011

16. Goelzer, H., I. Janssens, J. Nemec and P. Huybrechts: A dynamic continental runoff routing model applied to the last Northern Hemisphere deglaciation.
17. Loutre, M.-F., H. Goosse and A. Mairesse: Studying climate changes during the Holocene using climate model simulations with data assimilation.
18. Loutre, M.-F., H. Goosse, X. Crosta, P. Mathiot, S. Dubinkina, Y. Sallaz-Damaz and A. Mairesse: How does data assimilation in the Southern Hemisphere affect the representation of climate during the Holocene climate optimum?
19. Goosse, H., J. Guiot, M.E. Mann, S. Dubinkina and Y. Sallaz-Damaz: The medieval climate anomaly in Europe: comparison of the summer and annual mean signals in two reconstructions and in simulations with data assimilation.
20. Goosse, H., E. Crespin, S. Dubinkina, M.-F. Loutre, M.E. Mann, H. Renssen and Y. Sallaz-Damaz: The Medieval Climate Anomaly in simulations with data assimilation.

WCRP Open Science Conference, Denver (USA), 24-28 October 2011

21. Goelzer, H. P. Huybrechts, M.-F. Loutre, H. Goosse, T. Fichefet, and A. Mouchet: Impact of Greenland and Antarctic ice sheet interactions on climate sensitivity.
22. Goosse, H., E. Crespin, S. Dubinkina, A. Mairesse, P. Mathiot, Y. Sallaz-Damaz and V. Zunz: Seamless reanalysis: from paleoclimates to the 21st century.
23. Goosse, H., E. Crespin, S. Dubinkina, Y. Sallaz-Damaz: Cryosphere-related amplification of climate variations over the past millennium.

CERFACS, Toulouse (France), 24 Novembre 2011

24. Goosse, H.: The climate of the past millennium in simulations with data assimilation.

AGU Fall Meeting, San Francisco (USA), 5-9 December 2011

25. Goelzer, H., J.J. Fürst and P. Huybrechts: Ensemble projections of the Greenland ice sheet contribution to future sea-level rise.
26. Fürst, J.J., H. Goelzer and P. Huybrechts: Effects from fast dynamics: the crux for assessing Greenland's centennial mass loss?
27. Zekollari, H., J.J. Fürst, H. Goelzer, O. Rybak and P. Huybrechts: 3D Higher-Order modelling of Vadret da Morteratsch, Switzerland.
28. H. Goosse, E. Crespin, S. Dubinkina, G. Guiot, M.-F. Loutre, H. Renssen, A. Mairesse, M.E. Mann, Y. Sallaz-Damaz and D. Shindell: How the past millennium could contribute to better climate projections ?
29. Goosse H., E. Crespin, S. Dubinkina, M.-F. Loutre, M.E. Mann, H. Renssen, Y. Sallaz-Damaz and D. Shindell: The Role of Forcing and Internal Dynamics in Explaining the Medieval Climate Anomaly.

30. Philippon-Berthier, G., T. Fichefet, H. Goosse, F. Massonnet: Evolution of the Arctic and Antarctic sea ice over the 20th and 21st centuries as simulated by CMIP5 models.
31. Lecomte, O., M. Vancoppenolle, T. Fichefet and F. Massonnet: On the representation of snow in large scale sea-ice models.
32. Lecomte, O.: A first evaluation of the role of wave-ice interactions on the global sea ice volume.

2012

16th Alpine Glaciology Meeting, Zürich (Switzerland), 2-3 February 2012

33. Goelzer, H., J.J. Fürst and P. Huybrechts: Ensemble projections of the Greenland ice sheet contribution to future sea-level rise.
34. Zekollari, H., J.J. Fürst, H. Goelzer, O. Rybak and P. Huybrechts: 3D Higher-Order modelling of Vadret da Morteratsch, Switzerland.

ice2sea Open Forum Meeting, Amsterdam (Netherlands), 14-16 February 2012

35. Fürst, J.J., H. Goelzer and P. Huybrechts: Influence of direct inland stress transmission on the centennial response of the Greenland Ice Sheet.
36. Huybrechts, P., H. Goelzer and J.J. Fürst: Projections of the Greenland ice sheet contribution to future sea-level rise: sensitivity to model formulations.

WCRP Workshop on CMIP5 Climate Model Analysis, University f Hawaii, Honolulu (USA), 5-9 March 2012

37. Fichefet, T., F. Massonnet, G. Philippon-Berthier, C. Bitz, M. Holland, H. Goosse and P.-Y. Barriat: The 21st century changes in the Arctic sea ice cover as a function of its present state: What can we learn from CMIP5 models?

European Geosciences Union General Assembly, Vienna (Austria), 22-27 April 2012

38. Goelzer, H., J.J. Fürst and P. Huybrechts: Ensemble projections of the Greenland ice sheet contribution to future sea-level rise.
39. Fürst, J.J., H. Goelzer and P. Huybrechts: Future Response of the Greenland Ice Sheet to Climatically Induced Changes in Ice Dynamics and Surface Mass Balance.
40. Bazin, L., A. Landais, B. Lemieux-Dudon, H. Toyé Mahamadou Kele, T. Blunier, E. Capron, J. Chappellaz, H. Fischer, M. Leuenberger, V. Lipenkov, M.-F. Loutre, P. Martinerie, F. Parrenin, F. Prié, D. Raynaud, D. Veres, and E. Wolff: Toward an integrated ice core chronology using relative and orbital tie points.
41. Raynaud, D. V. Lipenkov, M-F. Loutre, A. Landais, and E. Capron: Dating the 800 ka long EPICA ice core by tuning the air content and δO2/N2 records on local summer insolation.

42. Loutre, M.-F., T. Fichefet, H. Goosse, P.-Y. Barriat, Y. Sallaz-Damaz, A. Timmermann, A. Laurian and A. Barthélemy: The 6 and 130 kyr BP climates as simulated by an updated version of LOVECLIM1.2
43. Barth, A., P. Mathiot, and H. Goosse: Estimation of the uncertainty of a clilmate model using an ensemble simulation.
44. A. Barthélemy, H. Goosse, P. Mathiot and T. Fichefet: Inclusion of a katabatic wind parameterization in a coarse-resolution global coupled climate model.

PAGES Sea Ice Proxy (SIP) Working Group: The Basis of Sea Ice Proxies, Montréal (Canada) 7-10 March 2012

45. Goosse H., D.M. Roche, A. Mairesse, F Klein, A de Vernal: Sea-ice data assimilation and modelling.

Final HOLOCLIP meeting, Trieste (Italy), 8-9 May 2012

46. Goosse H., M. Braida, X. Crosta, A. Mairesse, V. Masson-Delmotte, P. Mathiot, R. Neukom, H. Oeter, G. Philippon, H. Renssen, B. Stenni, T. van Ommen, E. Verleyen: Temperature changes at high southern latitudes during the lat 1000 years: evaluation of simuations and reconstructions.

MeteoClim PhD symposium 2012, Université de Liège, Liège (Belgium), 1 June 2012

47. Fürst, J.J., H. Goelzer and P. Huybrechts: Future projections of Greenland's ice loss accounting for changes in surface mass balance and dynamic discharge.

NSE PhD day, Vrije Universiteit Brussel, Brussels (Belgium), 8 June 2012

48. Fürst, J.J., H. Goelzer and P. Huybrechts: Future projections of Greenland's ice loss accounting for changes in surface mass balance and dynamic discharge.

4th International Geologica Belgica Meeting 2012, Brussels (Belgium), 11-14 September 2012

49. Goelzer, H. and P. Huybrechts: Committed future sea-level contribution from the Greenland ice sheet.
50. Fürst, J.J., H. Goelzer and P. Huybrechts: Ice-dynamic projections of the Greenland ice sheet to future atmospheric and oceanic warming.

Third International Conference on Earth System Modelling, Hamburg (Germany), 17-21 September 2012

51. Goosse H., M. Braida, X. Crosta, A. Mairesse, V. Masson-Delmotte, P. Mathiot, R. Neukom, H. Oeter, G. Philippon, H. Renssen, B. Stenni, T. van Ommen, E. Verleyen: Antarctic temperature changes during the last millennium: evaluation of simulations and reconstructions.

APECS BENELUX science event, Ghent (Belgium), 11 October 2012

52. Fürst, J.J., H. Goelzer and P. Huybrechts: Ice-dynamic projections of the Greenland ice sheet to future atmospheric and oceanic warming.

Arctic Climate Scenario Assessement: An AMAP Workshop, Pacific Marine and Environmental Laboratory, Seattle (USA), 16-18 October 2012

53. Fichefet, T.: Constraining projections of summer Arctic sea ice.

Earth Observation and Cryosphere Science Conference, Frascati (Italy), 13-16 November 2012

54. Edwards, T.L., X. Fettweis, F. Gillet-Chaulet, H. Goelzer, P. Huybrechts, A.J. Payne and J.C. Rougier: A new SMB-elevation feedback parameterisation for Greenland.

AGU Fall Meeting, San Francisco (USA), 3-7 December 2012

55. Goelzer, H., P. Huybrechts, J.J. Fürst, M.L. Andersen, T.L. Edwards, X. Fettweis, F.M. Nick, A.J. Payne and S. Shannon: Sensitivity of Greenland ice sheet projections to model formulations.
56. Fürst, J.J., H. Goelzer and P. Huybrechts: Ice-dynamic projections of the Greenland ice sheet to future atmospheric and oceanic warming.
57. Zekollari, H., J. J. Fürst, P. Huybrechts: Modelling the dynamics of Vadret da Morteratsch (Switzerland) since the Little Ice Age and its future evolution in a warming climate.
58. Lecavalier, B.S., G.A. Milne, L. Wake, S. Marshall, M.J.R. Simpson, and P. Huybrechts: Sensitivity of the Greenland ice sheet to the Holocene thermal maximum.

2013

European Geosciences Union General Assembly, Vienna (Austria), 7-12 April 2013

59. Goelzer, H., P. Huybrechts, J.J. Fürst, M.L. Andersen, T.L. Edwards, X. Fettweis, F.M. Nick, A.J. Payne, and S. Shannon: Sensitivity of Greenland ice sheet projections to model formulations.
60. Goelzer, H., P. Huybrechts, M.-F. Loutre and T. Fichefet: Evolution of the polar ice sheets during the Last Interglacial from coupled ice sheet-climate experiments with LOVECLIM.
61. Robinson, A., H. Goelzer and P. Huybrechts: A correction factor for positive degree-day modeling of ice sheet surface melt under changing orbital configurations.
62. Fürst, J.J., H. Goelzer and P. Huybrechts: Ice-dynamic projections of the Greenland ice sheet to future atmospheric and oceanic warming.
63. Loutre, M.-F., T. Fichefet, H. Goosse, H. Goelzer and P. Huybrechts: Towards a fully coupled climate–ice sheet model for simulating the climate of the Last Interglacial.
64. Loutre, M.-F., T. Fichefet, H. Goosse, H. Goelzer and P. Huybrechts:

Simulating an abrupt climate change during the Last Interglacial.

65. Loutre, M.-F., T. Fichefet, H. Goosse, H. Goelzer and P. Huybrechts: Evolution of the polar ice sheets during the Last Interglacial from coupled ice sheet-climate experiments with LOVECLIM
66. Edwards, T.L., X. Fettweis, O. Gagliardini, F. Gillet-Chaulet, H. Goelzer, J. Gregory, M. Hoffman, P. Huybrechts, A.J. Payne, M. Perego, S. Price, A. Quiquet and C. Ritz: Effect of uncertainty in surface mass balance elevation feedback on projections of the future sea level contribution of the Greenland ice sheet.
67. Payne, A.J., S. Shannon, I. Bartholomew, M. van den Broeke, T. Edwards, X. Fettweis, O. Gagliardini, F. Gillet-Chaulet, H. Goelzer, M. Hoffman, P. Huybrechts, D. Mair, P. Nienow, M. Perego, S. Price, P. Smeets, A. Sole, R. van de Wal and T. Zwinger: Enhanced basal lubrication and the contribution of the Greenland ice sheet to future sea level rise.

ice2sea Open Forum Meeting, London (UK), 14-16 May 2013

68. Goelzer, H., P. Huybrechts, J.J. Fürst, F.M. Nick, M.L. Andersen, T.L. Edwards, X. Fettweis, A.J. Payne, and S. Shannon: Sensitivity of Greenland ice sheet projections to model formulations.
69. Fürst, J.J., H. Goelzer and P. Huybrechts: Ice-dynamic projections of the Greenland ice sheet to future atmospheric and oceanic warming.

Davos Atmosphere and Cryosphere Assembly DACA-13, 8-12 July 2013

70. Goelzer, H., P. Huybrechts, M.-F. Loutre and T. Fichefet: Coupled ice sheet-climate interactions during the Last Interglacial simulated with LOVECLIM.
71. Zekollari, H., H. Goelzer, J.J. Fürst, P. Huybrechts: Vadret da Morteratsch (Switzerland) between 1864 and 2100: dynamics, geometry and mass balance.
72. Fürst, J.J., H. Goelzer and P. Huybrechts: Ice-dynamic projections of the Greenland ice sheet to future atmospheric and oceanic warming.

IGS International Symposium on Changes in Glaciers and Ice Sheets: observations, modelling and environmental interactions, Beijing (China), 28 July - 2 August 2013

73. Huybrechts, P., J.J. Fürst, and H. Goelzer: The role of ice dynamics in projections of the centennial mass evolution of the Greenland ice sheet

Ice sheet-climate model coupling workshop, Reading (UK), 30 September-2 October 2013

74. Goelzer, H., I. Janssens, J. Nemec and P. Huybrechts: A dynamic continental runoff routing model applied to the last Northern Hemisphere deglaciation.

PALSEA2 2013 Workshop, Rome (Italy), 21-24 October 2013

75. Goelzer, H., P. Huybrechts, M.-F. Loutre and T. Fichefet: Coupled ice sheet-climate interactions during the Last Interglacial simulated with LOVECLIM.

AGU Fall Meeting, San Francisco (USA), 9-13 December 2013

76. Goelzer, H., P. Huybrechts, M.-F. Loutre and T. Fichefet: Coupled ice sheet-climate interactions during the Last Interglacial simulated with LOVECLIM.

2014

18th Alpine Glaciology Meeting (AGM, Innsbruck (Austria), 27-28 February 2014

77. Zekollari, H. and Huybrechts, P.: 3-D ice flow modelling of Vadret da Morteratsch (Switzerland) based on 13 years of fieldwork.

BELQUA Annual Scientific Meeting 2014, Brussels (Belgium), 5 March 2014

78. Goelzer, H., P. Huybrechts, M.-F. Loutre and T. Fichefet: Coupled ice sheet-climate interactions during the Last Interglacial simulated with LOVECLIM.

International Symposium on Sea Ice in a Changing Environment, 10–14 March 2014, Hobart, Tasmania, Australia

79. Lecomte, O., T. Fichefet, M. Vancoppenolle, F. Domine, F. Massonnet, P. Mathiot, S. Morin, and P.-Y. Barriat: On the formulation of snow thermal conductivity in large-scale sea-ice models.
80. Massonnet, F., T. Fichefet, H. Goosse, C. Bitz, M. Holland, G. Philippon-Berthier, and P.-Y. Barriat: Constraining projections of summer Arctic sea ice.
81. Massonnet, F., P. Mathiot, T. Fichefet, H. Goosse, M. Vancoppenolle, C. König Beatty, and T. Lavergne: A model reconstruction of Antarctic sea-ice thickness and volume changes over the past decades using data assimilation.
82. Vancoppenolle, M., T. Fichefet, S. Ackley, H. Shen, F. Massonnet, P. Mathiot, and O. Lecomte: A first evaluation of wave-ice interactions on the global mass balance.
83. Lecomte, O., T. Fichefet, M. Vancoppenolle, and F. Massonnet: Interactions between snow and melt ponds in sea-ice models.

European Geosciences Union General Assembly, Vienna (Austria), 27 April - 02 May 2014

84. Goelzer, H., P. Huybrechts, M.-F. Loutre and T. Fichefet: Coupled ice sheet-climate interactions during the Last Interglacial simulated with LOVECLIM.
85. Robinson A. and H. Goelzer: The Importance of Insolation Changes for Paleo Ice Sheet Modeling.
86. de Boer, B., A.M. Dolan, E. Gasson, N.R. Golledge, J. Bernales, I. Rogozhina, H. Goelzer, P. Huybrechts, J. Sutter and R.S.W. van de Wal: Simulating the Antarctic ice sheet in the Late-Pliocene warm period: PLISMIP-ANT, an ice-sheet model intercomparison project.
87. Loutre, M.-F., T. Fichefet, H. Goosse, P. Huybrechts, H. Goelzer and E. Capron: Factors controlling the last interglacial climate as simulated by

LOVECLIM1.3.

88. Yin, Q., A. Berger, A. Ganopolski, H. Goelzer, Z. Guo and P. Huybrechts: Ice sheets, insolation and CO2 during the interglacial MIS-13.
89. Capron, E., E. Stone, A. Govin, M.-F. Loutre, V. Masson-Delmotte, S. Mulitza, B. Otto-Bliesner, L. Sime, C. Waelbroeck, E. W. Wolff: High latitude temperature evolution across the Last Interglacial: a model-data comparison
90. Massonnet, F., T. Fichefet, and H. Goosse: Calibration of sea ice dynamic parameters in an ocean–sea ice model using an ensemble Kalman filter
91. Massonnet, F., T. Fichefet, H. Goosse, and V. Zunz: Prospects for better seasonal Arctic sea ice predictions from multivariate initialization.
92. Lecomte, O., T. Fichefet, D. Flocco, D. Schroeder, and M. Vancoppenolle: Interactions between snow and melt ponds in sea ice models
93. Zekollari, H., and P. Huybrechts: Correlating the surface mass balance on the Morteratsch glacier (Switzerland) with data from nearby meteorological stations.
94. Zekollari, H. and P. Huybrechts: On the climate-geometry imbalance of Vadret da Morteratsch (Switzerland) and its response time: insights from numerical 3-D flow simulations.

MOCA Joint Model-data workshop for the Late Pleistocene evolution of the Greenland and Antarctic ice sheets, Chamonix (France), 22-24 May 2014

95. Lecavalier, B.S., G.A. Milne, M.J.R. Simpson, L. Wake, P. Huybrechts, L. Tarasov, K.K. Kjeldsen, S. Funder, A.J. Long, S. Woodroffe, A. Dyke, N.K. Larsen: Sea-level contribution from the Greenland ice sheet deglaciation based on a data-constrained modelling methodology.

iCLIPS user committee meeting, Brussels (Belgium), 23 May 2014

96. Goelzer, H., P. Huybrechts, M.-F. Loutre and T. Fichefet: Coupled ice sheet-climate interactions during the Last Interglacial simulated with LOVECLIM.
97. Fürst, J., H. Goelzer, and P. Huybrechts: Ice-dynamic projections of the Greenland ice sheet in response to future atmospheric and oceanic warming.
98. Loutre, M.-F., T. Fichefet, H. Goosse, P. Huybrechts, H. Goelzer, E. Capron: Factors controlling the last interglacial climate as simulated by LOVECLIM1.3

IGS Symposium on the Contribution of Glaciers and Ice Sheets to Sea Level Change, Chamonix (France), 26-30 May 2014

99. Lecavalier, B.S., G.A. Milne, M.J.R. Simpson, L. Wake, P. Huybrechts, L. Tarasov, K.K. Kjeldsen, S. Funder, A.J. Long, S. Woodroffe, A. Dyke, N.K. Larsen: Sea-level contribution from the Greenland ice sheet deglaciation based on a data-constrained modelling methodology.
100. Cowton, T., A. Sole, P. Nienow, D. Slater, P. Christoffersen, E. Hanna, D. Wilton, P. Huybrechts, A. Jowett: Examining the role of submarine melting in

the retreat of Greenland's tidewater glaciers

101. Zekollari, H., and P. Huybrechts: On the climate-geometry imbalance of Vadret da Morteratsch (Switzerland) and its response time: insights from numerical 3-D flow simulations.
102. Zekollari, H., and P. Huybrechts: Correlating the surface mass balance on the Morteratsch glacier (Switzerland) with data from nearby meteorological stations.

PMIP Meeting, Namur (Belgium), 25-30 May 2014

103. Goelzer, H., P. Huybrechts, M.-F. Loutre and T. Fichefet: Coupled ice sheet-climate interactions during the Last Interglacial.
104. Loutre, M.-F., T. Fichefet, H. Goosse, P. Huybrechts, H. Goelzer and E. Capron: Factors controlling the last interglacial climate as simulated by LOVECLIM1.3.
105. de Boer, B., A.M. Dolan and the PLISMIP-ANT participants (including H. Goelzer and P. Huybrechts). The Antarctic ice sheet in the Late-Pliocene warm period: PLISMIP-ANT.

SCAR Open Science Conference, Auckland (New Zealand) 23 August - 3 September 2014

106. de Boer, B., A.M. Dolan and the PLISMIP-ANT participants (including H. Goelzer and P. Huybrechts). The Antarctic ice sheet in the Late-Pliocene warm period: PLISMIP-ANT.

AGU Fall Meeting, San Francisco (USA), 15-19 December 2014

107. Goelzer, H. and A. Robinson: The Importance of Insolation Changes for Paleo Ice Sheet Modeling.

2015

European Geosciences Union General Assembly, Vienna (Austria), 12-17 April 2015

108. Goelzer, H., P. Huybrechts, M.-F. Loutre and T. Fichefet: Impact of ice sheet changes on the climate evolution at the onset of the Last Interglacial.
109. Goelzer, H., P. Huybrechts, M.-F. Loutre and T. Fichefet: Future rates of sea-level rise from long-term coupled climate-ice sheet projections.
110. Van Breedam, J., P. Huybrechts, H. Goelzer, M.-F. Loutre and T. Fichefet: Global sea-level change during the next 10,000 years: the end of an icehouse?
111. Nowicki, S., T. Payne, E. Larour, A. Abe Ouchi, H. Goelzer, J. Gregory, W. Lipscomb, H. Seroussi and A. Shepherd: ISMIP6: Ice Sheet Model Intercomparison Project for CMIP6.
112. Loutre, M.-F., P.-Y. Barriat, M. Crucifix and T. Fichefet: Sensitivity of transient paleoclimate simulation results to season definition.

113. de Boer, B., A.M. Dolan, J. Bernales, E. Gasson, H. Goelzer, N.R. Golledge, J. Sutter, P. Huybrechts, G. Lohmann, I. Rogozhina, A. Abe Ouchi, F. Saito and R.S.W. van de Wal: Simulating the Antarctic ice sheet in the Late-Pliocene warm period: PLISMIP-ANT, an ice-sheet model intercomparison project.
114. Zekollari, H. and P. Huybrechts: On the Holocene evolution of Hans Tausen Iskappe (Greenland).
115. Jowett, A., E. Hanna, P. Huybrechts and F. Ng: Greenland surface mass balance 1870-2013 based on an improved/optimised runoff model.
116. Zekollari, H. and P. Huybrechts: On the climate-geometry imbalance, response time and volume-area scaling of an alpine glacier: insights from a 3-D flow model applied to Vadret da Morteratsch.

IUGG 26th General Assembly, Prague (Czech Republic), 22-29 June 2015

117. Huybrechts, P.: Contribution of the Antarctic and Greenland ice sheets to sea-level change from observations and glaciological modelling (keynote lecture)
118. H. Zekollari and P. Huybrechts: Thresholds for growth and decay of Hans Tausen Iskappe (Greenland).

PALSEA2 Meeting: Data-Model Integration and Comparison, Tokyo (Japan), 22-24 July 2015

119. Goelzer, H., P. Huybrechts, M.-F. Loutre and T. Fichefet: Impact of ice sheet changes on the climate evolution at the onset of the Last Interglacial.
120. Lecavalier, B.S., D. Fisher, G. Milne, B. Vinther, L. Tarasov, P. Huybrechts, D. Lacelle, B. Main, J. Zhen, J. Bourgeois and A. Dyke: A high Arctic Holocene climate record.

XIX INQUA Congress, Nagoya (Japan) 26 July - 2 August 2015

121. Goelzer, H., P. Huybrechts, M.-F. Loutre and T. Fichefet: Climate, ice sheet and sea--- level changes during the Last Interglacial.
122. Yin, Q.Z., A. Berger, A. Ganopolski, H. Goelzer, Z.T. Guo and P. Huybrechts: Modelling the Northern Hemisphere ice sheets during the interglacial MIS-13.
123. B.S. Lecavalier, D. Fisher, G.A. Milne, B. Vinther, L. Tarasov, P. Huybrechts, D. Lacelle, B. Main, J. Zheng, J. Bourgeois, A. Dyke: A warmer High Arctic Holocene Thermal Maximum and its implications for North Greenland.

5. PUBLICATIONS

5.1. Publications of the teams

5.1.1. Peer review

VUB-ESSC

de Boer, B., Dolan, A. M., Bernales, J., Gasson, E., Goelzer, H., Golledge, N. R., Sutter, J., Huybrechts, P., Lohmann, G., Rogozhina, I., Abe-Ouchi, A., Saito, F., and Van De Wal, R. S. W. (2015): Simulating the Antarctic ice sheet in the late-Pliocene warm period: PLISMIP-ANT, an ice-sheet model intercomparison project, The Cryosphere, 9, 881-903, doi:10.5194/tc-9-881-2015

Edwards, T. L., Fettweis, X., Gagliardini, O., Gillet-Chaulet, F., Goelzer, H., Gregory, J. M., Hoffman, M., Huybrechts, P., Payne, A. J., Perego, M., Price, S., Quiquet, A., and Ritz, C. (2014a): Effect of uncertainty in surface mass balance–elevation feedback on projections of the future sea level contribution of the Greenland ice sheet, The Cryosphere, 8, 195-208, doi:10.5194/tc-8-195-2014

Edwards, T. L., Fettweis, X., Gagliardini, O., Gillet-Chaulet, F., Goelzer, H., Gregory, J. M., Hoffman, M., Huybrechts, P., Payne, A. J., Perego, M., Price, S., Quiquet, A., and Ritz, C. (2014b): Probabilistic parameterisation of the surface mass balance–elevation feedback in regional climate model simulations of the Greenland ice sheet, The Cryosphere, 8, 181-194, doi:10.5194/tc-8-181-2014

Fürst, J., Rybak, O., Goelzer, H., De Smedt, B., de Groen, P., and Huybrechts, P. (2011): Improved convergence and stability properties in a three-dimensional higher-order ice sheet model, Geosci. Model Dev., 4, 1133-1149, doi:10.5194/gmd-4-1133-2011

Fürst, J. J., Goelzer, H., and Huybrechts, P. (2013): Effect of higher-order stress gradients on the centennial mass evolution of the Greenland ice sheet, The Cryosphere, 7, 183-199, doi:10.5194/tc-7-183-2013

Fürst, J. J., Goelzer, H., and Huybrechts, P. (2015): Ice-dynamic projections of the Greenland ice sheet in response to atmospheric and oceanic warming (2015): The Cryosphere, 9, 1039-1062, doi:10.5194/tc-9-1039-2015

Goelzer, H., Janssens, I., Nemec, J., and Huybrechts, P. (2012b): A dynamic continental runoff routing model applied to the last Northern Hemisphere deglaciation, Geosci. Model Dev., 5, 599-609, doi:10.5194/gmd-5-599-2012

Goelzer, H., Huybrechts, P., Fürst, J. J., Andersen, M. L., Edwards, T. L., Fettweis, X., Nick, F. M., Payne, A. J., and Shannon, S. R. (2013): Sensitivity of Greenland ice sheet projections to model formulations, J. Glaciol., 59, 733–749, doi:10.3189/2013JoG12J182

Gregory, J. M., White, N. J., Church, J. A., Bierkens, M. F. P., Box, J. E., van den Broeke, M. R., Cogley, J. G., Fettweis, X., Hanna, E., Huybrechts, P., Konikow, L. F., Leclercq, P. W., Marzeion, B., Oerlemans, J., Tamisiea, M. E., Wada, Y., Wake, L. M., and van de Wal, R. S. W. (2012): Twentieth-century global-mean sea-level rise: is the whole greater than the sum of the parts?, J. Clim., 26, 4476–4499, doi:10.1175/jcli-d-12-00319.1

Hanna, E., Huybrechts, P., Cappelen, J., Steffen, K., Bales, R. C., Burgess, E., McConnell, J., Steffensen, J. P., van den Broeke, M., Wake, L. M., Bigg, G., Griffiths, M., and Savas, D. (2013): Greenland ice sheet surface mass balance 1870 to 2010 based on twentieth century reanalysis, and links with global climate forcing, J. Geophys. Res., 116, doi:10.1029/2011jd016387

Hanna, E., Jones, J. M., Cappelen, J., Mernild, S. H., Wood, L., Steffen, K., and Huybrechts, P. (2012): The influence of North Atlantic atmospheric and oceanic forcing effects on 1900–2010 Greenland summer climate and ice melt/runoff, Int. J. Climatol., 33, 862–880, doi:10.1002/joc.3475

Larsen, N. K., Kjær, K. H., Lecavalier, B., Bjørk, A. A., Colding, S., Huybrechts, P., Jakobsen, K. E., Kjeldsen, K. K., Knudsen, K.-L., Odgaard, B. V., and Olsen, J. (2015): The response of the southern Greenland ice sheet to the Holocene thermal maximum, Geology, doi:10.1130/g36476.1

Lecavalier, B. S., Milne, G. A., Simpson, M. J. R., Wake, L., Huybrechts, P., Tarasov, L., Kjeldsen, K. K., Funder, S., Long, A. J., Woodroffe, S., Dyke, A. S., and Larsen, N. K. (2014): A model of Greenland ice sheet deglaciation constrained by observations of relative sea level and ice extent, Quat. Sci. Rev., 102, 54-84, doi:10.1016/j.quascirev.2014.07.018

NEEM community members including P. Huybrechts (2013): Eemian interglacial reconstructed from a Greenland folded ice core, Nature, 493, 489-494, doi:10.1038/nature11789

Robinson, A., and Goelzer, H. (2014): The importance of insolation changes for paleo ice sheet modeling, The Cryosphere Discuss., 8, 337-362, doi:10.5194/tcd-8-337-2014

Shannon, S. R., Payne, A. J., Bartholomew, I. D., van den Broeke, M. R., Edwards, T. L., Fettweis, X., Gagliardini, O., Gillet-Chaulet, F., Goelzer, H., Hoffman, M. J., Huybrechts, P., Mair, D., Nienow, P., Perego, M., Price, S. F., Smeets, C. J. P. P., Sole, A. J., Van De Wal, R. S. W., and Zwinger, T. (2013): Enhanced basal lubrication and the contribution of the Greenland ice sheet to future sea level rise, Proc. Nat. Acad. Sci. U.S.A., 110, 14156–14161, doi:10.1073/pnas.1212647110

Sundal, A. V., Shepherd, A., Nienow, P., Hanna, E., Palmer, S., and Huybrechts, P. (2011): Melt-induced speed-up of Greenland ice sheet offset by efficient subglacial drainage, Nature, 469, 521-524, doi:10.1038/nature09740

Vernon, C. L., Bamber, J. L., Box, J. E., Van Den Broeke, M. R., Fettweis, X., Hanna, E., and Huybrechts, P. (2013): Surface mass balance model intercomparison for the Greenland ice sheet, The Cryosphere, 7, 599-614, doi:10.5194/tc-7-599-2013

Wake, L. M., Milne, G. A., Long, A. J., Woodroffe, S. A., Simpson, M. J. R., and Huybrechts, P. (2012): Century-scale relative sea-level changes in West Greenland — A plausibility study to assess contributions from the cryosphere and the ocean, Earth Planet. Sci. Lett., 315–316, 86-93, doi:10.1016/j.epsl.2011.09.029

Zekollari, H., Huybrechts, P., Fürst, J. J., Rybak, O., and Eisen, O. (2013): Calibration of a higher-order 3-D ice-flow model of the Morteratsch glacier complex, Engadin, Switzerland, Ann. Glaciol., 54, 343-351, doi:10.3189/2013AoG63A434

Zekollari, H., Fürst, J. J., and Huybrechts, P. (2014): Modelling the evolution of Vadret da Morteratsch, Switzerland, since the Little Ice Age and into the future, J. Glaciol., 60, 1155-1168, doi:10.3189/2014JoG14J053

UCL-TECLIM

Barthélemy, A., Goosse, H., Mathiot, P., and Fichefet, T. (2012): Inclusion of a katabatic wind correction in a coarse-resolution global coupled climate model., Ocean Modell., 48, 45–54, doi:10.1016/j.ocemod.2012.03.002

Bazin, L., Landais, A., Lemieux-Dudon, B., Toyé Mahamadou Kele, H., Veres, D., Parrenin, F., Martinerie, P., Ritz, C., Capron, E., Lipenkov, V., Loutre, M. F., Raynaud, D., Vinther, B., Svensson, A., Rasmussen, S. O., Severi, M., Blunier, T., Leuenberger, M., Fischer, H., Masson-Delmotte, V., Chappellaz, J., and Wolff, E. (2013): An optimized multi-proxy, multi-site Antarctic ice and gas orbital chronology (AICC2012): 120–800 ka, Clim. Past, 9, 1715-1731, doi:10.5194/cp-9-1715-2013

Berger, A., Loutre, M.-F., and Yin, Q. (2013): Astronomical theory of paleoclmates, in: The Encyclopedia of Quaternary Science, Elsevier, Amsterdam, 136-141.

Collins, M., Knutti, R., Arblaster, J. M., Dufresne, J.-L., Fichefet, T., Friedlingstein, P., Gao, X., Gutowski, W. J., Johns, T., Krinner, G., Shongwe, M., Tebaldi, C., Weaver, A. J., and Wehner, M. (2013): Long-term Climate Change: Projections, Commitments and Irreversibility., in: Climate Change 2013: The Physical Science Basis. Contribution of Working Group I to the Fifth Assessment Report of the Intergovernmental Panel on Climate Change, edited by: Stocker, T. F., Qin, D., Plattner, G.-K., Tignor, M., Allen, S. K., Boschung, J., Nauels, A., Xia, Y., Bex, V., and Midgley, P. M., Cambridge University Press, Cambridge, United Kingdom and New York, NY, USA.

Crespin, E., Goosse, H., Fichefet, T., Mairesse, A., and Sallaz-Damaz, Y. (2012): Arctic climate over the past millennium: Annual and seasonal response to external forcings, The Holocene, 23, 321–329, doi:10.1177/0959683612463095

Eby, M., Weaver, A. J., Alexander, K., Zickfeld, K., Abe-Ouchi, A., Cimatoribus, A. A., Crespin, E., Drijfhout, S. S., Edwards, N. R., Eliseev, A. V., Feulner, G., Fichefet, T., Forest, C. E., Goosse, H., Holden, P. B., Joos, F., Kawamiya, M., Kicklighter, D., Kienert, H., Matsumoto, K., Mokhov, I. I., Monier, E., Olsen, S. M., Pedersen, J. O. P., Perrette, M., Philippon-Berthier, G., Ridgwell, A., Schlosser, A., Schneider von Deimling, T., Shaffer, G., Smith, R. S., Spahni, R., Sokolov, A. P., Steinacher, M., Tachiiri, K., Tokos, K., Yoshimori, M., Zeng, N., and Zhao, F. (2013): Historical and idealized climate model experiments: an intercomparison of Earth system models of intermediate complexity, Clim. Past., 9, 1111-1140, doi:10.5194/cp-9-1111-2013

Goosse, H., Crespin, E., Dubinkina, S., Loutre, M. F., Mann, M. E., Renssen, H., Sallaz-Damaz, Y., and Shindell, D. (2012): The role of forcing and internal dynamics in explaining the "Medieval Climate Anomaly", Clim. Dyn., 39, 2847-2866, doi:10.1007/S00382-012-1297-0

Hezel, P. J., Fichefet, T., and Massonnet, F. (2014): Modeled Arctic sea ice evolution through 2300 in CMIP5 extended RCPs, The Cryosphere, 8, 1195-1204, doi:10.5194/tc-8-1195-2014

Landais, A., Dreyfus, G., Capron, E., Pol, K., Loutre, M. F., Raynaud, D., Lipenkov, V. Y., Arnaud, L., Masson-Delmotte, V., Paillard, D., Jouzel, J., and Leuenberger, M. (2012): Towards orbital dating of the EPICA Dome C ice core using δO2/N2, Clim. Past., 8, 191-203, doi:10.5194/cp-8-191-2012

Massonnet, F., Fichefet, T., Goosse, H., Bitz, C. M., Philippon-Berthier, G., Holland, M. M., and Barriat, P. Y. (2012): Constraining projections of summer Arctic sea ice, The Cryosphere, 6, 1383-1394, doi:10.5194/tc-6-1383-2012

Thierens, M., Browning, E., Pirlet, H., Loutre, M. F., Dorschel, B., Huvenne, V. A. I., Titschack, J., Colin, C., Foubert, A., and Wheeler, A. J. (2013): Cold-water coral carbonate mounds as unique palaeo-archives: the Plio-Pleistocene Challenger Mound record (NE Atlantic), Quat. Sci. Rev., 73, 14-30, doi:10.1016/j.quascirev.2013.05.006

Weaver, A. J., Sedláček, J., Eby, M., Alexander, K., Crespin, E., Fichefet, T., Philippon-Berthier, G., Joos, F., Kawamiya, M., Matsumoto, K., Steinacher, M., Tachiiri, K., Tokos, K., Yoshimori, M., and Zickfeld, K. (2012): Stability of the Atlantic meridional overturning circulation: A model intercomparison, Geophys. Res. Lett., 39, doi:10.1029/2012gl053763

Zickfeld, K., Eby, M., Weaver, A. J., Crespin, E., Fichefet, T., Goosse, H., Philippon-Berthier, G., Edwards, N. R., Holden, P., Eliseev, A., Mokhov, I., Feulner, G., Kienert, H., Perrette, M., Deimling, T. S. v., Forest, C., Joos, F., Spahini, R., Steinacher, M., Kawamiya, M., Tachiiri, K., Kicklighter, D., Monier, E., Schlosser, A., Sokolov, A., Matsumoto, K., Tokos, K., Olsen, S. M., Pedersen, J. O. P., Shaffer, G., Ridgewell, A., Zeng, N., and Zhao, F. (2013): Long-term climate change commitment and

reversibility : An EMIC intercomparison, J. Clim., 26, 5782–5809, doi:10.1175/JCLI-D-12-00584.1

5.2. Co-publications

5.2.1. Peer review

Goelzer, H., Huybrechts, P., Loutre, M. F., Goosse, H., Fichefet, T., and Mouchet, A. (2011): Impact of Greenland and Antarctic ice sheet interactions on climate sensitivity, Clim. Dyn., 37, 1005-1018, doi:10.1007/s00382-010-0885-0

Goelzer, H., Huybrechts, P., Raper, S. C. B., Loutre, M. F., Goosse, H., and Fichefet, T. (2012a): Millennial total sea level commitments projected with the Earth system model of intermediate complexity LOVECLIM Environ. Res. Lett., 7, doi:10.1088/1748-9326/7/4/045401

Goelzer, H., Huybrechts, P., Loutre, M.-F., and Fichefet, T. (2016a): Impact of ice sheet meltwater fluxes on the climate evolution at the onset of the Last Interglacial, *Clim. Past,* 12, 1721–1737, doi:10.5194/cp-12-1721-2016

Goelzer, H., Huybrechts, P., Loutre, M.-F., and Fichefet, T. (2016b): Last Interglacial climate and sea-level evolution from a coupled ice sheet-climate model, *Clim. Past*, 12, 2195-2213, doi: 10.5194/cp-12-2195-2016

Goosse, H., Brovkin, V., Fichefet, T., Haarsma, R., Huybrechts, P., Jongma, J., Mouchet, A., Selten, F., Barriat, P.-Y., Campin, J.-M., Deleersnijder, E., Driesschaert, E., Goelzer, H., Janssens, I., Loutre, M.-F., Morales Maqueda, M., Opsteegh, T., Mathieu, P.-P., Munhoven, G., Pettersson, E., Renssen, H., Roche, D., Schaeffer, M., Tartinville, B., Timmermann, A., and Weber, S. (2010): Description of the Earth system model of intermediate complexity LOVECLIM version 1.2, Geosci. Model Dev., 3, 603–633, doi:10.5194/gmd-3-603-2010

Huybrechts, P., Goelzer, H., Janssens, I., Driesschaert, E., Fichefet, T., Goosse, H., and Loutre, M. F. (2011): Response of the Greenland and Antarctic Ice Sheets to Multi-Millennial Greenhouse Warming in the Earth System Model of Intermediate Complexity LOVECLIM, Surv. Geophys., 32, 397-416, doi:10.1007/s10712-011-9131-5

Loutre, M. F., Mouchet, A., Fichefet, T., Goosse, H., Goelzer, H., and Huybrechts, P. (2011): Evaluating climate model performance with various parameter sets using observations over the recent past, Clim. Past., 7, 511-526, doi:10.5194/cp-7-511-2011

Loutre, M. F., Fichefet, T., Goosse, H., Huybrechts, P., Goelzer, H., and Capron, E. (2014): Factors controlling the last interglacial climate as simulated by LOVECLIM1.3, Clim. Past, 10, 1541-1565, doi:10.5194/cp-10-1541-2014

6. ACKNOWLEDGEMENTS

Computational resources have been provided by the supercomputing facilities of the Université catholique de Louvain (CISM/UCL) and the Consortium des Equipements de Calcul Intensif en Fédération Wallonie Bruxelles (CECI) funded by the Fond de la Recherche Scientifique de Belgique (FRS-FNRS).

7. REFERENCES

Ahn, J., and Brook, E. (2008): Atmospheric CO2 and climate on millennial time scales during the last glacial period, Science, 322, 83-85, doi:10.1126/science.1160832

Bakker, P., Stone, E. J., Charbit, S., Gröger, M., Krebs-Kanzow, U., Ritz, S. P., Varma, V., Khon, V., Lunt, D. J., Mikolajewicz, U., Prange, M., Renssen, H., Schneider, B., and Schulz, M. (2013): Last interglacial temperature evolution - a model inter-comparison, Clim. Past., 9, 605-619, doi:10.5194/cp-9-605-2013

Bamber, J. L., Griggs, J. A., Hurkmans, R. T. W. L., Dowdeswell, J. A., Gogineni, S. P., Howat, I., Mouginot, J., Paden, J., Palmer, S., Rignot, E., and Steinhage, D. (2013): A new bed elevation dataset for Greenland, Cryosphere, 7, 499-510, doi:10.5194/tc-7-499-2013

Barker, S., Knorr, G., Edwards, R. L., Parrenin, F., Putnam, A. E., Skinner, L. C., Wolff, E., and Ziegler, M. (2011): 800,000 Years of Abrupt Climate Variability, Science, 334, 347-351, doi:10.1126/science.1203580

Barthélemy, A., Goosse, H., Mathiot, P., and Fichefet, T. (2012): Inclusion of a katabatic wind correction in a coarse-resolution global coupled climate model., Ocean Modell., 48, 45–54, doi:10.1016/j.ocemod.2012.03.002

Bauch, H. A., Kandiano, E. S., and Helmke, J. P. (2012): Contrasting ocean changes between the subpolar and polar North Atlantic during the past 135 ka, Geophys. Res. Lett., 39, L11604, doi:10.1029/2012GL051800

Bazin, L., Landais, A., Lemieux-Dudon, B., Toyé Mahamadou Kele, H., Veres, D., Parrenin, F., Martinerie, P., Ritz, C., Capron, E., Lipenkov, V., Loutre, M. F., Raynaud, D., Vinther, B., Svensson, A., Rasmussen, S. O., Severi, M., Blunier, T., Leuenberger, M., Fischer, H., Masson-Delmotte, V., Chappellaz, J., and Wolff, E. (2013): An optimized multi-proxy, multi-site Antarctic ice and gas orbital chronology (AICC2012): 120-800 ka, Clim. Past, 9, 1715-1731, doi:10.5194/cp-9-1715-2013

Beckmann, A., and Goosse, H. (2003): A parameterization of ice shelf-ocean interaction for climate models, Ocean Modell., 5, 157-170, doi:10.1016/S1463-5003(02)00019-7

Berger, A. (1978): Long-term variations of daily insolation and Quaternary climatic changes, Journal of Atmospheric Sciences, 35, 2362-2367, doi:10.1175/1520-0469(1978)035<2362:LTVODI>2.0.CO;2

Bianchi, C., and Gersonde, R. (2002): The Southern Ocean surface between Marine Isotope Stages 6 and 5d: Shape and timing of climate changes, Palaeogeography, Palaeoclimatology, Palaeoecology, 187, 151-177, doi:10.1016/S0031-0182(02)00516-3

Bigg, G. R., Wadley, M. R., Stevens, D. P., and Johnson, J. A. (1996): Prediction of iceberg trajectories for the North Atlantic and Arctic Oceans, Geophys. Res. Lett., 23, 3587-3590, doi:10.1029/96GL03369

Bigg, G. R., Wadley, M. R., Stevens, D. P., and Johnson, J. A. (1997): Modelling the dynamics and thermodynamics of icebergs, Cold Regions Sci. Tech., 26, 113-135, doi:10.1016/S0165-232X(97)00012-8

Böhm, E., Lippold, J., Gutjahr, M., Frank, M., Blaser, P., Antz, B., Fohlmeister, J., Frank, N., Andersen, M. B., and Deininger, M. (2015): Strong and deep Atlantic meridional overturning circulation during the last glacial cycle, Nature, 517, 73–76 doi:10.1038/nature14059

Born, A., and Nisancioglu, K. H. (2012): Melting of Northern Greenland during the last interglaciation, Cryosphere, 6, 1239-1250, doi:10.5194/tc-6-1239-2012

Braithwaite, R. J. (2002): Glacier mass balance: the first 50 years of international monitoring, Prog. Phys. Geog., 26, 76-95, doi:10.1191/0309133302pp326ra

Brovkin, V., Bendtsen, J., Claussen, M., Ganopolski, A., Kubatzki, C., Petoukhov, V., and Andreev, A. (2002): Carbon cycle, vegetation, and climate dynamics in the Holocene: Experiments with the CLIMBER-2 model, Global Biogeochem. Cycles, 16, 86-81-86-20, doi:10.1029/2001GB001662

Campin, J., and Goosse, H. (1999): A parameterization of dense overflow in large-scale ocean models in z coordinate, Tellus. Section A, Dynamic meteorology and oceanography, 51, 412-430, doi:10.1034/j.1600-0870.1999.t01-3-00006.x

Capron, E., Govin, A., Stone, E. J., Masson-Delmotte, V., Mulitza, S., Otto-Bliesner, B., Rasmussen, T. L., Sime, L. C., Waelbroeck, C., and Wolff, E. W. (2014): Temporal and spatial structure of multi-millennial temperature changes at high latitudes during the Last Interglacial, Quat. Sci. Rev., 103, 116-133, doi:10.1016/j.quascirev.2014.08.018

Chapman, M. R., and Shackleton, N. J. (1998): Millennial-scale fluctuations in North Atlantic heat flux during the last 150,000 years, Earth Planet. Sci. Lett., 159, 57-70, doi:10.1016/S0012-821X(98)00068-5

Chou, C., and Neelin, J. D. (1996): Linearization of a longwave radiation scheme for intermediate tropical atmospheric models, Journal of Geophysical Research: Atmospheres, 101, 15129-15145, doi:10.1029/96JD01015

Church, J. A., Clark, P. U., Cazenave, A., Gregory, J. M., Jevrejeva, S., Levermann, A., Merrifield, M. A., Milne, G. A., Nerem, R. S., Nunn, P. D., Payne, A. J., Pfeffer, W. T., Stammer, D., and Unnikrishnan, A. S. (2013): Sea Level Change, in: Climate Change 2013: The Physical Science Basis. Contribution of Working Group I to the Fifth Assessment Report of the Intergovernmental Panel on Climate Change, edited by: Stocker, T. F., Qin, D., Plattner, G.-K., Tignor, M., Allen, S. K., Boschung, J., Nauels,

A., Xia, Y., Bex, V., and Midgley, P. M., Cambridge University Press, Cambridge, United Kingdom and New York, NY, USA, 1137-1216.

Clark, P., Marshall, S., Clarke, G., Hostetler, S., Licciardi, J., and Teller, J. (2001): Freshwater forcing of abrupt climate change during the last glaciation, Science, 293, 283-287, doi:10.1126/science.1062517

CLIMAP project members (1981): Seasonal reconstruction of the earth's surface at the last glacial maximum, Geol.Soc.Am.Map Chart Ser., MC-36.

Colville, E. J., Carlson, A. E., Beard, B. L., Hatfield, R. G., Stoner, J. S., Reyes, A. V., and Ullman, D. J. (2011): Sr-Nd-Pb Isotope Evidence for Ice-Sheet Presence on Southern Greenland During the Last Interglacial, Science, 333, 620-623, doi:10.1126/science.1204673

Cortese, G., and Abelmann, A. (2002): Radiolarian-based paleotemperatures during the last 160 kyr at ODP Site 1089 (Southern Ocean, Atlantic Sector), Palaeogeography, Palaeoclimatology, Palaeoecology, 182, 259-286, doi:10.1016/S0031-0182(01)00499-0

Cortijo, E. (1995): La variabilité climatique rapide dans l'Atlantique Nord depuis 128 000 ans: relations entre les calottes de glace et l'océan de surface, Paris-Sud, Orsay.

Cortijo, E., Duplessy, J. C., Labeyrie, L., Leclaire, H., Duprat, J., and van Weering, T. C. E (1994): Eemian cooling in the Norwegian Sea and North Atlantic ocean preceding continental ice-sheet growth, Nature, 372, 446-449, doi:10.1038/372446a0

Crowley, T. J. (1992): North Atlantic Deep Water cools the southern hemisphere, Paleoceanography, 7, 489-497, doi:10.1029/92PA01058

Dansgaard, W., Clausen, H. B., Gundestrup, N., Hammer, C. U., Johnsen, S. F., Kristinsdottir, P. M., and Reeh, N. (1982): A New Greenland Deep Ice Core, Science, 218, 1273-1277, doi:10.1126/science.218.4579.1273

de Boer, B., Dolan, A. M., Bernales, J., Gasson, E., Goelzer, H., Golledge, N. R., Sutter, J., Huybrechts, P., Lohmann, G., Rogozhina, I., Abe-Ouchi, A., Saito, F., and Van De Wal, R. S. W. (2015): Simulating the Antarctic ice sheet in the late-Pliocene warm period: PLISMIP-ANT, an ice-sheet model intercomparison project, The Cryosphere, 9, 881-903, doi:10.5194/tc-9-881-2015

Deleersnijder, E., and Campin, J. M. (1995): On the computation of the barotropic mode of a free-surface world ocean model, Ann. Geophys., 13, 675-688, doi:10.1007/s00585-995-0675-x

Depoorter, M. A., Bamber, J. L., Griggs, J. A., Lenaerts, J. T. M., Ligtenberg, S. R. M., van den Broeke, M. R., and Moholdt, G. (2013): Calving fluxes and basal melt rates of Antarctic ice shelves, Nature, 502, 89-+, doi:10.1038/nature12567

Driesschaert, E. (2005): Climate change over the next millennia using LOVECLIM, a new Earth system model including the polar ice sheets, PhD thesis, Univ. Catholique de Louvain, Louvain-la-Neuve, Belgium, 214 pp.

EPICA community members (2004): Eight glacial cycles from an Antarctic ice core, Nature, 429, 623-628, doi:10.1038/Nature02599

Fichefet, T., and Maqueda, M. A. M. (1997): Sensitivity of a global sea ice model to the treatment of ice thermodynamics and dynamics, J. Geophys. Res., 102, 12609-12646, doi:10.1029/97JC00480

Fox Maule, C., Purucker, M. E., Olsen, N., and Mosegaard, K. (2005): Heat flux anomalies in Antarctica revealed by satellite magnetic data, Science, 309, 464-467, doi: 10.1126/science.1106888

Fretwell, P., Pritchard, H. D., Vaughan, D. G., Bamber, J. L., Barrand, N. E., Bell, R., Bianchi, C., Bingham, R. G., Blankenship, D. D., Casassa, G., Catania, G., Callens, D., Conway, H., Cook, A. J., Corr, H. F. J., Damaske, D., Damm, V., Ferraccioli, F., Forsberg, R., Fujita, S., Gim, Y., Gogineni, P., Griggs, J. A., Hindmarsh, R. C. A., Holmlund, P., Holt, J. W., Jacobel, R. W., Jenkins, A., Jokat, W., Jordan, T., King, E. C., Kohler, J., Krabill, W., Riger-Kusk, M., Langley, K. A., Leitchenkov, G., Leuschen, C., Luyendyk, B. P., Matsuoka, K., Mouginot, J., Nitsche, F. O., Nogi, Y., Nost, O. A., Popov, S. V., Rignot, E., Rippin, D. M., Rivera, A., Roberts, J., Ross, N., Siegert, M. J., Smith, A. M., Steinhage, D., Studinger, M., Sun, B., Tinto, B. K., Welch, B. C., Wilson, D., Young, D. A., Xiangbin, C., and Zirizzotti, A. (2013): Bedmap2: improved ice bed, surface and thickness datasets for Antarctica, Cryosphere, 7, 375-393, doi:10.5194/tc-7-375-2013

Fürst, J. J., Goelzer, H., and Huybrechts, P. (2013): Effect of higher-order stress gradients on the centennial mass evolution of the Greenland ice sheet, The Cryosphere, 7, 183-199, doi:10.5194/tc-7-183-2013

Fürst, J. J., Goelzer, H., and Huybrechts, P. (2015): Ice-dynamic projections of the Greenland ice sheet in response to atmospheric and oceanic warming, The Cryosphere, 9, 1039-1062, doi:10.5194/tc-9-1039-2015

Gent, P. R., and McWilliams, J. C. (1990): Isopycnal mixing in ocean circulation models, J. Phys. Oceanogr., 20, 150-155, doi:10.1175/1520-0485(1990)020<0150:IMIOCM>2.0.CO;2

Gladstone, R. M., Bigg, G. R., and Nicholls, K. W. (2001): Iceberg trajectory modeling and meltwater injection in the Southern Ocean, J. Geophys. Res. [Oceans], 106, 19903-19915, doi:10.1029/2000JC000347

Golledge, N. R., Menviel, L., Carter, L., Fogwill, C. J., England, M. H., Cortese, G., and Levy, R. H. (2014): Antarctic contribution to meltwater pulse 1A from reduced Southern Ocean overturning, Nature Communications, 5, doi:10.1038/ncomms6107

Goosse, H., Deleersnijder, E., Fichefet, T., and England, M. H. (1999): Sensitivity of a global coupled ocean-sea ice model to the parameterization of vertical mixing, J. Geophys. Res., 104, 13681-13695, doi:10.1029/1999JC900099

Goosse, H., Driesschaert, E., Fichefet, T., and Loutre, M. F. (2007): Information on the early Holocene climate constrains the summer sea ice projections for the 21st century, Clim. Past, 3, 683-692, doi:10.5194/cp-3-683-2007

Goosse, H., and Fichefet, T. (1999): Importance of ice-ocean interactions for the global ocean circulation: A model study, J. Geophys. Res., 104, 23337-23355, doi:10.1029/1999JC900215

Goosse, H., and Renssen, H. (2001): A two-phase response of the Southern Ocean to an increase in greenhouse gas concentrations, Geophys. Res. Lett., 28, 3469-3472, doi:10.1029/2001GL013525

Goosse, H., Selten, F. M., Haarsma, R. J., and Opsteegh, J. D. (2001): Decadal variability in high northern latitudes as simulated by an intermediate-complexity climate model, Ann. Glaciol., 33, 525-532, doi:10.3189/172756401781818482

Goublomme, V., and Decerf, B. (2007): La fonte de l'inlandsis du Groenland au cours des prochains millénaires est-elle irréversible?, MSs thesis, Unversité catholique de Louvain, Louvain-la-Neuve, Belgium.

Govin, A., Braconnot, P., Capron, E., Cortijo, E., Duplessy, J. C., Jansen, E., Labeyrie, L., Landais, A., Marti, O., Michel, E., Mosquet, E., Risebrobakken, B., Swingedouw, D., and Waelbroeck, C. (2012): Persistent influence of ice sheet melting on high northern latitude climate during the early Last Interglacial, Clim. Past., 8, 483-507, doi:10.5194/cp-8-483-2012

Grant, K. M., Rohling, E. J., Bar-Matthews, M., Ayalon, A., Medina-Elizalde, M., Ramsey, C. B., Satow, C., and Roberts, A. P. (2012): Rapid coupling between ice volume and polar temperature over the past 150,000 years, Nature, 1-4, doi:10.1038/nature11593

Gregory, J. M., and Oerlemans, J. (1998): Simulated future sea-level rise due to glacier melt based on regionally and seasonally resolved temperature changes, Nature, 391, 474-476, doi:10.1038/35119

Greve, R. (2001): Glacial isostasy: models for the response of the earth to varying ice loads, in: Continuum mechanics and applications in geophysics and the environment, edited by: Straughan, B., Greve, R., Ehrentraut, H., and Wang, Y., Springer-Verlag, Berlin Heidelberg New York, 307-325.

Hillaire-Marcel, C., de Vernal, A., Bilodeau, G., and Weaver, A. J. (2001): Absence of deep-water formation in the Labrador Sea during the last interglacial period, Nature, 410, 1073-1077, doi:10.1038/35074059

Hodell, D. A., Charles, C. D., Curtis, J. H., Mortyn, P. G., Ninnemann, U. S., and Venz, K.A. (2003): Data report: oxygen isotope stratigraphy of ODP Leg 177 Sites 1088, 1089, 1090, 1093, and 1094, in: ODP, Sci. Results, edited by: Gersonde, R., Hodell, D. A., and Blum, P., (Ocean Drilling Program),, College Station, TX, 1–26.

Huybrechts, P. (1990): The Antarctic ice sheet during the last glacial-interglacial cycle: a three dimensional experiment, Ann. Glaciol., 11, 52-59.

Huybrechts, P. (2002): Sea-level changes at the LGM from ice-dynamic reconstructions of the Greenland and Antarctic ice sheets during the glacial cycles, Quat. Sci. Rev., 21, 203-231, doi:10.1016/S0277-3791(01)00082-8

Jongma, J. I., Driesschaert, E., Fichefet, T., Goosse, H., and Renssen, H. (2009): The effect of dynamic-thermodynamic icebergs on the Southern Ocean climate in a three-dimensional model, Ocean Modell., 26, 104-113, doi:10.1016/j.ocemod.2008.09.007

Kandiano, E. S., Bauch, H. A., and Müller, A. (2004): Sea surface temperature variability in the North Atlantic during the last two glacial–interglacial cycles: comparison of faunal, oxygen isotopic, and Mg/Ca-derived records, Palaeogeography, Palaeoclimatology, Palaeoecology, 204, 145-164, doi:10.1016/S0031-0182(03)00728-4

Kleiven, H. F., and Jansen, E. (2003): Data report: early–mid-Pleistocene oxygen isotope stratigraphy from the Atlantic sector of the Southern Ocean: ODP Leg 177 Sites 1094 and 1091, in: ODP, Sci. Results, edited by: Gersonde, R., Hodell, D. A., and Blum, P., (Ocean Drilling Program),, College Station, TX, 1-20.

Kopp, R. E., Simons, F. J., Mitrovica, J. X., Maloof, A. C., and Oppenheimer, M. (2009): Probabilistic assessment of sea level during the last interglacial stage, Nature, 462, 863-867, doi:10.1038/nature08686

Kopp, R. E., Simons, F. J., Mitrovica, J. X., Maloof, A. C., and Oppenheimer, M. (2013): A probabilistic assessment of sea level variations within the last interglacial stage, Geophys. J. Int., 193, 711-716, doi:10.1093/gji/ggt029

Langebroek, P. M., and Nisancioglu, K. H. (2014): Simulating last interglacial climate with NorESM: role of insolation and greenhouse gases in the timing of peak warmth, Clim. Past., 10, 1305-1318, doi:10.5194/cp-10-1305-2014

Letreguilly, A., Huybrechts, P., and Reeh, N. (1991): Steady-state characteristics of the Greenland ice sheet under different climates, J. Glaciol., 37, 149-157

Lisiecki, L. E., and Raymo, M. E. (2005): A Pliocene-Pleistocene stack of 57 globally distributed benthic delta O-18 records, Paleoceanography, 20, 17, doi:10.1029/2004pa001071

Løset, S. (1993): Thermal energy conservation in icebergs and tracking by temperature, Journal of Geophysical Research: Oceans, 98, 10001-10012, doi:10.1029/93JC00138

Loulergue, L., Schilt, A., Spahni, R., Masson-Delmotte, V., Blunier, T., Lemieux, B., Barnola, J.-M., D. Raynaud, Stocker, T. F., and Chappellaz, J. (2008): Orbital and millennial-scale features of atmospheric CH4 over the past 800,000 years, Nature, 453, 383-386, doi:10.1038/nature06950

Lunt, D. J., Abe-Ouchi, A., Bakker, P., Berger, A., Braconnot, P., Charbit, S., Fischer, N., Herold, N., Jungclaus, J. H., Khon, V. C., Krebs-Kanzow, U., Langebroek, P. M., Lohmann, G., Nisancioglu, K., Otto-Bliesner, B., Park, W., Pfeiffer, M., Phipps, S. J., Prange, M., Rachmayani, R., Renssen, H., Rosenbloom, N., Schneider, B., Stone, E. J., Takahashi, K., Wei, W., Yin, Q., and Zhang, Z. S. (2013): A multi-model assessment of last interglacial temperatures, Clim. Past., 9, 699-717, doi:10.5194/cp-9-699-2013

MacGregor, J. A., and Fahnestock, M. A. (2015): Radiostratigraphy and age structure of the Greenland Ice Sheet, J Geophys Res-Earth, doi:10.1002/2014JF003215

Masson-Delmotte, V., Buiron, D., Ekaykin, A., Frezzotti, M., Gallée, H., Jouzel, J., Krinner, G., Landais, A., Motoyama, H., Oerter, H., Pol, K., Pollard, D., Ritz, C., Schlosser, E., Sime, L. C., Sodemann, H., Stenni, B., Uemura, R., and Vimeux, F. (2011): A comparison of the present and last interglacial periods in six Antarctic ice cores, Clim. Past., 7, 397-423, doi:10.5194/cp-7-397-2011

Masson-Delmotte, V., Schulz, M., Abe-Ouchi, A., Beer, J., Ganopolski, A., González Rouco, J., Jansen, E., Lambeck, K., Luterbacher, J., Naish, T., Osborn, T., Otto-Bliesner, B., T. Quinn, R. R., M. Rojas, X. S., and Timmermann, A. (2013): Information from paleoclimate archives, in: Climate Change 2013: The Physical Science Basis. Contribution of Working Group I to the Fifth Assessment Report of the Intergovernmental Panel on Climate Change, edited by: Stocker, T. F., Qin, D., Plattner, G.-K., Tignor, M., Allen, S. K., Boschung, J., Nauels, A., Xia, Y., Bex, V., and Midgley, P. M., Cambridge University Press, Cambridge, United Kingdom and New York, NY, USA, 383-464.

Mengel, M., and Levermann, A. (2014): Ice plug prevents irreversible discharge from East Antarctica, Nature Climate Change, 4, 451-455, doi:10.1038/nclimate2226

Merz, N., Born, A., Raible, C. C., Fischer, H., and Stocker, T. F. (2014): Dependence of Eemian Greenland temperature reconstructions on the ice sheet topography, Clim. Past, 10, 1221-1238, doi:10.5194/cp-10-1221-2014

Mix, A. C., and Fairbanks, R. G. (1985): North Atlantic surface-ocean control for Pleistocene deep-ocean circulation. Earth Planet, Science, 73, 231-243, doi:10.1016/0012-821X(85)90072-X

Moss, R. H., Edmonds, J. A., Hibbard, K. A., Manning, M. R., Rose, S. K., van Vuuren, D. P., Carter, T. R., Emori, S., Kainuma, M., Kram, T., Meehl, G. A., Mitchell, J. F. B., Nakicenovic, N., Riahi, K., Smith, S. J., Stouffer, R. J., Thomson, A. M., Weyant, J. P., and Wilbanks, T. J. (2010): The next generation of scenarios for climate change research and assessment, Nature, 463, 747-756, doi:10.1038/nature08823

NEEM community members (2013): Eemian interglacial reconstructed from a Greenland folded ice core, Nature, 493, 489-494, doi:10.1038/nature11789

Oppo, D. W., McManus, J. F., and Cullen, J. L. (2006): Evolution and demise of the Last Interglacial warmth in the subpolar North Atlantic, Quat. Sci. Rev., 25, 3268-3277, doi:10.1016/j.quascirev.2006.07.006

Opsteegh, J. D., Haarsma, R. J., Selten, F. M., and Kattenberg, A. (1998): ECBILT: a dynamic alternative to mixed boundary conditions in ocean models, Tellus, 50, 348-367, doi:10.1034/j.1600-0870.1998.t01-1-00007.x

Pepin, L., Raynaud, D., Barnola, J. M., and Loutre, M. F. (2001): Hemispheric roles of climate forcings during glacial-interglacial transitions as deduced from the Vostok record and LLN-2D model experiments, J. Geophys. Res. [Atmos.], 106, 31885-31892, doi:10.1029/2001jd900117

Petit, J.-R., Jouzel, J., Raynaud, D., Barkov, N. I., Barnola, J.-M., Basile, I., Bender, M., Chappellaz, J., Davis, M. E., Delaygue, G., Delmotte, M., Kotlyakov, V. M., Legrand, M., Lipenkov, V. Y., Lorius, C., Pepin, L., Ritz, C., Saltzman, E., and Stievenard, M. (1999): Climate and atmospheric history of the past 420,000 years from the Vostok ice core, Antarctica, Nature, 399, 429-436, doi:10.1038/20859

Pollard, D., DeConto, R. M., and Alley, R. B. (2015): Potential Antarctic Ice Sheet retreat driven by hydrofracturing and ice cliff failure, Earth Planet. Sci. Lett., 412, 112-121, doi:10.1016/j.epsl.2014.12.035

Raper, S., and Braithwaite, R. (2006): Low sea level rise projections from mountain glaciers and icecaps under global warming, Nature, 439, 311-313, doi:10.1038/nature04448

Rasmussen, T. L., Oppo, D. W., Thomsen, E., and Lehman, S. J. (2003): Deep sea records from the southeast Labrador Sea: Ocean circulation changes and ice-rafting events during the last 160,000 years, Paleoceanography, 18, doi:10.1029/2001PA000736

Rasmussen, T. L., Thomsen, E., Kuijpers, A., and Wastegard, S. (2003): Late warming and early cooling of the sea surface in the Nordic seas during MIS 5e (Eemian Interglacial), Quat. Sci. Rev., 22, 809-821, doi:10.1016/S0277-3791(02)00254-8

Raynaud, D., Barnola, J. M., Souchez, R., Lorrain, R., Petit, J. R., Duval, P., and Lipenkov, V. Y. (2005): Palaeoclimatology - The record for marine isotopic stage 11, Nature, 436, 39-40, doi:10.1038/43639b

Redi, M. H. (1982): Oceanic Isopycnal Mixing by Coordinate Rotation, J. Phys. Oceanogr., 12, 1154-1158, doi:10.1175/1520-0485(1982)012<1154:OIMBCR>2.0.CO;2

Renssen, H., Goosse, H., and Fichefet, T. (2005): Contrasting trends in North Atlantic deep-water formation in the Labrador Sea and Nordic seas during the Holocene, Geophys. Res. Lett., 32, doi:10.1029/2005GL022462

Ritz, S. P., Stocker, T. F., and Joos, F. (2011): A Coupled Dynamical Ocean–Energy Balance Atmosphere Model for Paleoclimate Studies, J. Clim., 24, 349-375, doi:10.1175/2010JCLI3351.1

Robinson, A., Calov, R., and Ganopolski, A. (2011): Greenland ice sheet model parameters constrained using simulations of the Eemian Interglacial, Clim. Past., 7, 381-396, doi:10.5194/cp-7-381-2011

Rossow, W. B., Walker, A. W., Beuschel, D. E., and Roiter, M. D. (1996): International satellite cloud climatology project (ISCCP) documentation of new cloud datasets, World Meteorological Organisation.

Sanchez Goni, M. F., Bakker, P., Desprat, S., Carlson, A. E., Van Meerbeeck, C. J., Peyron, O., Naughton, F., Fletcher, W. J., Eynaud, F., Rossignol, L., and Renssen, H. (2012): European climate optimum and enhanced Greenland melt during the Last Interglacial, Geology, 40, 627-630, doi:10.1130/G32908.1

Shannon, S. R., Payne, A. J., Bartholomew, I. D., van den Broeke, M. R., Edwards, T. L., Fettweis, X., Gagliardini, O., Gillet-Chaulet, F., Goelzer, H., Hoffman, M. J., Huybrechts, P., Mair, D., Nienow, P., Perego, M., Price, S. F., Smeets, C. J. P. P., Sole, A. J., Van De Wal, R. S. W., and Zwinger, T. (2013): Enhanced basal lubrication and the contribution of the Greenland ice sheet to future sea level rise, Proc. Nat. Acad. Sci. U.S.A., 110, 14156–14161, doi:10.1073/pnas.1212647110

Shapiro, N. M., and Ritzwoller, M. H. (2004): Inferring surface heat flux distributions guided by a global seismic model: particular application to Antarctica, Earth Planet. Sci. Lett., 223, 213-224, doi:10.1016/j.epsl.2004.04.011

Simpson, M. J. R., Milne, G. A., Huybrechts, P., and Long, A. J. (2009): Calibrating a glaciological model of the Greenland ice sheet from the Last Glacial Maximum to present-day using field observations of relative sea level and ice extent, Quat. Sci. Rev., 28, 1631-1657, doi:10.1016/j.quascirev.2009.03.004

Sjolte, J., and Hoffmann, G. (2014): Modelling stable water isotopes in monsoon precipitation during the previous interglacial, Quat. Sci. Rev., 85, 119-135, doi:10.1016/j.quascirev.2013.12.006

Smith, S. D. (1993): Hindcasting Iceberg Drift Using Current Profiles and Winds, Cold Regions Sci. Tech., 22, 33-45, doi:10.1016/0165-232X(93)90044-9

Smith, S. D., and Banke, E. G. (1983): The Influence of Winds, Currents and Towing Forces on the Drift of Icebergs, Cold Regions Sci. Tech., 6, 241-255, doi:10.1016/0165-232X(83)90045-9

Spahni, R., Chappellaz, J., Stocker, T. F., Loulergе, L., Hausammann, G., Kawamura, K., Flückiger, J., Schwander, J., Raynaud, D., Masson-Delmotte, V., and Jouzel, J. (2005): Atmospheric methane and nitrous oxide of the late Pleistocene from Antarctic ice cores, Science, 310, 1317-1321, doi:10.1126/science.1120132

Steen-Larsen, H. C., Masson-Delmotte, V., Hirabayashi, M., Winkler, R., Satow, K., Prié, F., Bayou, N., Brun, E., Cuffey, K. M., Dahl-Jensen, D., Dumont, M., Guillevic, M., Kipfstuhl, S., Landais, A., Popp, T., Risi, C., Steffen, K., Stenni, B., and Sveinbjörnsdottír, A. E. (2014): What controls the isotopic composition of Greenland surface snow?, Clim. Past., 10, 377-392, doi:10.5194/cp-10-377-2014

Stocker, T. F. (1998): The Seesaw Effect, Science, 282, 61-62, doi:10.1126/science.282.5386.61

Stocker, T. F., Wright, D. G., and Broecker, W. S. (1992): The influence of high-latitude surface forcing on the global thermohaline circulation, Paleoceanography, 7, 529-541, doi:10.1029/92PA01695

Stone, E. J., Lunt, D. J., Annan, J. D., and Hargreaves, J. C. (2013): Quantification of the Greenland ice sheet contribution to Last Interglacial sea level rise, Clim. Past., 9, 621-639, doi:10.5194/cp-9-621-2013

Sundal, A. V., Shepherd, A., Nienow, P., Hanna, E., Palmer, S., and Huybrechts, P. (2011): Melt-induced speed-up of Greenland ice sheet offset by efficient subglacial drainage, Nature, 469, 521-524, doi:10.1038/nature09740

Tartinville, B., Campin, J. M., Fichefet, T., and Goosse, H. (2001): Realistic representation of the surface freshwater flux in an ice–ocean general circulation model, Ocean Modell., 3, 95-108, doi:10.1016/S1463-5003(01)00003-8

van de Berg, W. J., van den Broeke, M. R., van Meijgaard, E., and Kaspar, F. (2013): Importance of precipitation seasonality for the interpretation of Eemian ice core isotope records from Greenland, Clim. Past., 9, 1589-1600, doi:10.5194/cp-9-1589-2013

van de Wal, R., and Wild, M. (2001): Modelling the response of glaciers to climate change by applying volume-area scaling in combination with a high resolution GCM, Clim. Dyn., 18, 359-366, doi:10.1007/s003820100184

Winsor, K., Carlson, A. E., Klinkhammer, G. P., Stoner, J. S., and Hatfield, R. G. (2012): Evolution of the northeast Labrador Sea during the last interglaciation, Geochemistry Geophysics Geosystems, 13, doi:10.1029/2012gc004263

Zielinski, U., Gersonde, R., Sieger, R., and Fütterer, D. (1998): Quaternary surface water temperature estimations: Calibration of a diatom transfer function for the Southern Ocean, Paleoceanography, 13, 365-383, doi:10.1029/98PA01320

Zwally, H., Abdalati, W., Herring, T., Larson, K., Saba, J., and Steffen, K. (2002): Surface melt-induced acceleration of Greenland ice-sheet flow, Science, 297, 218-222, doi:10.1126/science.1072708

Zweck, C., and Huybrechts, P. (2005): Modeling of the northern hemisphere ice sheets during the last glacial cycle and glaciological sensitivity, J. Geophys. Res, 110, D07103, doi:10.1029/2004JD005489

All information on our website:

http://www.belspo.be/belspo/SSD/science/pr_climate_en.stm